

UNCLASSIFIED

AD NUMBER	
AD231946	
CLASSIFICATION CHANGES	
TO:	UNCLASSIFIED
FROM:	CONFIDENTIAL
LIMITATION CHANGES	
TO: Approved for public release; distribution is unlimited.	
FROM: Distribution authorized to U.S. Gov't. agencies and their contractors; Administrative/Operational Use; 26 AUG 1959. Other requests shall be referred to Rome Air Development Center, Griffiss AFB, NY.	
AUTHORITY	
RADC ltr 15 Jun 1983 ; RADC ltr 15 Jun 1983	

THIS PAGE IS UNCLASSIFIED

THIS REPORT HAS BEEN DELIMITED
AND CLEARED FOR PUBLIC RELEASE
UNDER DOD DIRECTIVE 5200.20 AND
NO RESTRICTIONS ARE IMPOSED UPON
ITS USE AND DISCLOSURE.

DISTRIBUTION STATEMENT A

APPROVED FOR PUBLIC RELEASE;
DISTRIBUTION UNLIMITED.

UNCLASSIFIED

AD 231946

CLASSIFICATION CHANGED

TO: UNCLASSIFIED

FROM: CONFIDENTIAL

AUTHORITY: ST-A (NTIS) RADDC
17, 15 Jan 83



UNCLASSIFIED

UNCLASSIFIED

AD

2	3	1		9	4	6
---	---	---	--	---	---	---

Reproduced

Armed Services Technical Information Agency

ARLINGTON HALL STATION; ARLINGTON 12 VIRGINIA

NOTE: WHEN GOVERNMENT OR OTHER DRAWINGS, SPECIFICATIONS OR OTHER DATA ARE USED FOR ANY PURPOSE OTHER THAN IN CONNECTION WITH A DEFINITELY RELATED GOVERNMENT PROCUREMENT OPERATION, THE U. S. GOVERNMENT THEREBY INCURS NO RESPONSIBILITY, NOR ANY LIABILITY WHATSOEVER; AND THE FACT THAT THE GOVERNMENT MAY HAVE FORMULATED, FURNISHED, OR IN ANY WAY SUPPLIED THE SAID DRAWINGS, SPECIFICATIONS, OR OTHER DATA IS NOT TO BE REGARDED BY ANY OTHER PERSON OR CORPORATION, OR CONVEYING ANY RIGHTS OR PERMISSION TO MANUFACTURE, USE OR SELL ANY PATENTED INVENTION MAY IN ANY WAY BE RELATED THERETO.

UNCLASSIFIED

UNCLASSIFIED

10

MASSACHUSETTS INSTITUTE OF TECHNOLOGY

LINCOLN LABORATORY

EXPERIMENTAL INVESTIGATION OF WIND-INDUCED

VIBRATIONS IN ANTENNA MEMBERS

William Weaver, Jr.

Approved

William J. Theriault

Group Report No. 75-4

August 26, 1959

FILE COPY

Return to

ASTIA

ARLINGTON HALL STATION

ARLINGTON 12, VIRGINIA

ATTN: TISS

The research reported in this document was supported jointly by the Department of the Army, the Department of the Navy, and the Department of the Air Force under Air Force Contract No. AF19(604)-5200

LEXINGTON

MASSACHUSETTS

UNCLASSIFIED

TABLE OF CONTENTS

	<u>Page</u>
I. SUMMARY.....	1
II. INTRODUCTION.....	2
2.1 Origin and Background of the Problem.....	2
2.2 Object.....	4
2.3 Scope.....	4
2.4 Notation.....	6
III. AERODYNAMIC ASPECTS.....	10
3.1 Fundamental Considerations.....	10
3.2 Circular Cylinder in a Fluid Stream.....	11
3.3 The Fluctuating Lift and Drag Forces.....	11
3.4 Effect of Vibration on Lift Forces.....	15
3.5 Effect of Protuberances.....	17
IV. VIBRATION ASPECTS.....	17
4.1 Preliminary Considerations.....	17
4.2 Natural Frequencies of a Prismatical Member with Elastic End Connections.....	20
4.3 Response of an Elastic System to Vortex Forces.....	20
4.4 Self-Amplification of Vibrations.....	23
V. TEST PROGRAM AND DESIGN OF COMPONENTS.....	28
5.1 Basic Assumptions.....	28
5.2 Phases of Test Program.....	29
5.3 Design of Test Members and Support Systems.....	29
VI. MATERIALS AND APPARATUS.....	31
6.1 Materials.....	31
6.2 Test Apparatus.....	31
VII. TESTING PROCEDURES.....	36
7.1 Tests on Stationary Cylinders.....	36
7.2 Tests on Spring-Supported Cylinders.....	36
7.3 Tests on Flexural Members.....	37
VIII. TEST RESULTS.....	37
8.1 General.....	37
8.2 Results of Tests on Stationary Cylinders.....	37
8.3 Results of Tests on Spring-Supported Cylinders.....	38
8.4 Results of Tests on Flexural Members.....	39
8.5 Correlation among the Results of the Three Phases and Comparisons with Previously Published Information.....	39

TABLE OF CONTENTS

	<u>Page</u>
IX. DESIGN CRITERIA, PROCEDURES, AND APPLICATIONS.....	43
9.1 General.....	43
9.2 Design Criteria.....	44
9.3 Analysis Charts.....	44
9.4 Procedure for Design against Lateral Vibrations.....	57
9.5 Analysis of Existing Structures.....	57
X. DISCUSSION.....	61
10.1 Validity of Initial Assumptions.....	61
10.2 Vibrations in Subcritical Range.....	62
10.3 Vibrations in Supercritical Range.....	62
10.4 Discussion on Use of Spoilers.....	62
XI. CONCLUSIONS AND RECOMMENDATIONS.....	63
11.1 Conclusions.....	63
11.2 Recommendations.....	63
11.3 Recommendations for Further Research.....	64
BIBLIOGRAPHY.....	65

APPENDICES

A. Phase A Test Results.....	67
B. Phase B Test Results.....	78
C. Phase C Test Results.....	89

LIST OF ILLUSTRATIONS

<u>FIGURES</u>		<u>Page</u>
3.1	Flow for Very Low N_R	12
3.2	Flow for $N_R < 40$	12
3.3	Flow for $40 < N_R < 3 \times 10^5$	12
3.4	Flow for $3 \times 10^5 < N_R$	12
3.5	Variation of Drag Coefficient and Strouhal Number with Reynolds Number for a Circular Cylinder.....	13
3.6	Vortex Geometry Behind Cylinder.....	14
3.7	Dimensional Increase in Vortex Street Due to Vibration.....	16
4.1	Fundamental Frequencies of Various Members in Terms of Frequency of Pinned Member.....	19
8.1	Comparison of Results of Present Values of C_K with Previously Reported Experimental Values of C_K for Stationary Cylinders....	40
8.2	Comparison of N_s Curves with Published Values.....	42
9.1	Schematic Diagram of G.C.I. Antenna.....	59
A-1	Transducer Calibration - Sanborn Oscillograph.....	68
A-2	Oscillograph Record for Stationary 5" ϕ Bare Cylinder (Subcritical Reynolds Number).....	68
A-3	Oscillograph Record for Stationary 5" ϕ Cylinder with 8 Windings	69
A-4	Oscillograph Record for Stationary 5" ϕ Cylinder with Spoilers..	69
A-5	Oscillograph Record for Stationary 10" ϕ Bare Cylinder (Supercritical Reynolds Number).....	70
A-6	Oscillograph Record for Stationary 10" ϕ Cylinder with 16 Windings.....	70
A-7	Values of C_K for Bare Cylinders and with Spoilers.....	71
A-8	Summary of C_K curves.....	72
A-9	Combined Values of N_s for Bare Cylinders.....	73
A-10	Values of N_s for Cylinders with 8 and 16 Windings.....	74
A-11	Influence of Number of Windings on Spoiler Effectiveness - 3" ϕ Cylinder.....	75
A-12	Influence of Winding Diameter on Spoiler Effectiveness - 3" ϕ Cylinder.....	76
A-13	Influence of Pitch on Spoiler Effectiveness - 6" ϕ Cylinder.....	77
B-1	Oscillograph Record of Decay Curve for 6" ϕ Spring-Supported Cylinder.....	79

LIST OF ILLUSTRATIONS

<u>FIGURES</u>		<u>Page</u>
B-2	Oscillograph Record for 6" ϕ Spring-Supported Bare Cylinder.....	80
B-3	Oscillograph Record for 6" ϕ Spring-Supported Cylinder with 8 Windings.....	81
B-4	Oscillograph Record for 6" ϕ Spring-Supported Cylinder with Spoilers.....	82
B-5	Response of 5" ϕ Cylinder - $k_c = 201$ lb/in.....	83
B-6	Values of Standard \bar{C}_K - Bare Cylinders.....	84
B-7	Values of Standard \bar{C}_K - Cylinders with Numerous Windings.....	85
B-8	Values of N_s - Bare Cylinders.....	86
B-9	Values of N_s - Cylinders with Numerous Windings.....	87
B-10	Incremental Load Factors for Oscillating Cylinders.....	88
C-1	Oscillograph Record of Decay Curve for Member M4b1.....	90
C-2	Oscillograph Record for M4b1 (Bare).....	90
C-3	Oscillograph Record for M4b1 (with Spoilers over 100% of Length).....	91
C-4	Oscillograph Record for M4b1 (with Spoilers over 40% of Length).....	91
C-5	Response of Member M2c.....	92
C-6	Values of Standard \bar{C}_K - Bare Members.....	93
C-7	Values of N_s for First Mode - Phase C.....	94
C-8	(ILF) for Vibrating Members.....	95
<u>PHOTOGRAPHS</u>		
2.1	28 ft. Kennedy Paraboloid Reflector.....	3
5.1	Base Layout - Phase A (3" ϕ Cylinder in Place).....	30
5.2	4" ϕ Spring-Supported Cylinder.....	32
5.3	Members M1.....	33
5.4	Member M1b - End Connection EC-1.....	34
9.1	120' x 30' G.C.I. Antenna Structure.....	58
<u>ANALYSIS CHARTS</u>		
AC-a1	Maximum Flexural Stress at Ends of Fixed Aluminum Tube Due to Vibration.....	45
AC-a2	Maximum Flexural Stress at Ends of Semi-Fixed ($f=2.10 f_p$) Tube Due to Vibration.....	46
AC-a3	Maximum Flexural Stress at Center of Pinned Aluminum Tube Due to Vibration.....	47
AC-a4	Maximum Flexural Stress in Cantilever Aluminum Tube Due to Vibration.....	48
AC-b1 and 2	(IDF) for Fixed Members.....	51
AC-b3	(IDF) for Pinned Members.....	52
AC-b4	(IDF) for Cantilever Members.....	53

I. SUMMARY

Steady wind flow acting upon a structural member induces lateral vibrations in the member due to the generation of lift forces associated with the shedding of vortices from alternating sides. When the frequency of vortex shedding is approximately equal to the natural frequency of the member, resonant vibrations result which are amplified to a certain extent by the self-exciting nature of the oscillations. Stresses caused by severe and frequent vibrations have resulted in failures in a variety of types of structures.

The present investigation deals with the generation and suppression of wind-induced vibrations in the circular aluminum tubular members of large radar antenna space frames. Failures and undesirable vibrations have occurred in individual members of this type of facility, and a means of analyzing and reducing their response is required.

The experimental portion of the investigation consists of wind tunnel tests on stationary cylinders, oscillating cylinders, and vibrating flexural members. The significant results of the test program are the following: (1) a continuous curve for the RMS value of the Kármán lift coefficient was obtained for the range of Reynolds numbers of interest in this investigation, (2) a curve expressing the extent of the self-amplification characteristics of members was determined, (3) a system of aerodynamic spoilers was tested and optimized, and (4) non-dimensional Strouhal frequencies were evaluated and compared with established values.

Experimental results are combined with theoretical developments to give a semi-empirical solution to the response problem in the form of graphical analysis charts. Design and analysis procedures are outlined, and the use of optimized spoilers is recommended for applicable cases.

Field tests are recommended for the purpose of obtaining information on damping in existing structures and for the advantage of studying vibration phenomena under atmospheric conditions.

II. INTRODUCTION

2.1 Origin and Background of the Problem

A steady wind flow acting upon a cylindrical structural member induces lateral vibrations in the member due to the formation of vortices on alternating sides of the member. These vortices are formed and shed from opposite sides of the member at a regular frequency, depending upon the velocity of the wind, and as a result alternating lateral forces are exerted upon the member by the fluid motion. When the frequency of vortex shedding (and hence, the frequency of the alternating forces) is approximately equal to the frequency of one of the normal modes of vibration of the member, a condition of resonance results. If the structural damping and the stiffness of the member are small and the wind remains steady, large amplitudes of vibration will be developed.

These vibrations possess the ability of self-amplification and for this reason may be considered to be self-exciting for a limited range of wind velocities at and around the resonant, or "critical", wind velocity. This self-amplification has an upper limit of vibrational stability, however, so that the vibrations produced by the wind are not catastrophic in nature. Oscillation persists for a certain range of wind speed above the critical velocity and reaches a maximum amplitude near the top of the range.

There are several methods by which vibrations of this type can be suppressed.

- a) By increasing the flexural stiffness of the member so that its critical velocity is above the range of moderate winds.
- b) By reducing the effective length of the member through the introduction of intermediate struts.
- c) By use of damping devices to restrict the amplitude of vibration.
- d) By attaching "spoilers" to the member which serve to disrupt the flow near the surface and to interfere with the regular formation of vortices, thereby destroying the cause of the vibrations.

In the past, the first three methods of suppressing wind-induced vibrations have been used repeatedly. The solution to this problem by the method of applying spoilers to the surface of the member has not, in general, been attempted in civil engineering structures because of a lack of information concerning their design and their effectiveness.

This investigation deals with the specific problem of wind-induced vibrations in individual members of large radar antenna space frames. The problem arose at the M.I.T. Lincoln Laboratory when a slender member on a 28-foot diameter paraboloid reflector failed. This type of reflector is shown in Photograph 2.1, and the type of member which failed is indicated thereon. Failures have also occurred in members of the much larger 84-foot diameter reflector. Vibrations were also observed in the 120' x 30' G.C.I. Antenna at the Boston Hill site in North Andover, Massachusetts, during the process of erecting that structure. The G.C.I. Antenna is shown in Photograph 9.1.

In all of the cases cited above, studies were conducted (Refs. 1 and 29), and it was ascertained that the cause of the failures was wind-induced vibrations



Photograph 2.1; 28 ft. Kennedy Paraboloid Reflector

due to von Kármán vortex forces. The failures occurred in slender tubular members subjected to moderate winds, and they appeared to be fatigue type failures in weld-heated areas at points of maximum flexural stress. In each case the problem was remedied by adding additional bracing pieces for the purpose of restraining lateral vibrations in the more flexible members of the structures.

A preliminary wind tunnel test was carried out (Ref. 30) on a small diameter flexural specimen of the type in which failures have occurred. The purposes of the pilot experiment were to test the effectiveness of an arbitrary arrangement of spiral spoilers and to determine the feasibility of conducting a more extensive wind tunnel investigation of this nature. As a result of the preliminary test, the present experimental project was initiated. A fully detailed report of this investigation was presented in the form of an Sc. D. thesis (Ref. 31) in the Department of Civil and Sanitary Engineering at M.I.T., and the present report represents a condensed summary of that thesis.

2.2 Object

One of the primary objectives in the current investigation is to evaluate an experimental curve for the variation of the Kármán coefficient, C_K , with Reynolds number. The range of Reynolds numbers of interest in this experiment is approximately from 10^4 to 10^6 . A continuous curve for C_K in the region of interest is a basic necessity for the establishment of design criteria for wind-induced vibrations.

A second objective of this project is to study the self-amplification aspect which characterizes wind-induced vibrations of this type. With sufficient experimental data, involving variations in all of the parameters affecting the semi-empirical solution to the problem can be developed.

Strouhal numbers are evaluated in this investigation for the purpose of comparing with well-established values previously published in engineering and scientific literature. The extent of agreement of Strouhal numbers with published values may be considered to be a measure of the validity of other aspects of these experiments.

Another primary purpose for these experiments is to test and optimize a system of spoilers attached to the surfaces of a variety of member sizes. The function of these spoilers is to interfere with the periodic circulation and formation of vortices around the periphery of a circular cylinder. The measure of their effectiveness is the ratio of the Kármán coefficient for the cylinder with spoilers to the Kármán coefficient for the bare member.

$$\text{Spoiler effectiveness} = C_{KS}/C_{KB}$$

Finally, the ultimate objective in this project is to evolve design criteria and procedures for analysis of antenna structures with respect to the danger of severe and frequent vibrations due to wind. Optimum spoiler designs are specified, and their application to members of new and existing structures is delineated. It is intended that the criteria and procedures developed in this paper shall be applicable for all or most of the practical member sizes which are used in the design of antenna space frames.

2.3 Scope

This investigation is limited to a study of tubular aluminum members in the

form of circular cylinders. The types of test members considered are as follows:

- a) Stationary rigid body cylinders.
- b) Spring-supported rigid body cylinders.
- c) End-supported flexural members - fixed.
- d) End-supported flexural members - partially fixed.
- e) End-supported flexural members - pinned.
- f) Cantilever flexural members.

The cylinder and member diameters range from $1\frac{1}{2}$ " ϕ to 10" ϕ .

The spoiler configuration selected for these experiments consists of small diameter tubing attached to the surface of the member and wound in a helical pattern over all or part of the length of the member. This particular configuration was chosen because of the ease with which windings can be installed on a cylindrical member and because of the fact that a helical pattern of spoilers is not sensitive to the direction of the wind. The variable parameters for optimization of spoilers of this kind were the following:

- a) Number of windings.
- b) Size of windings.
- c) Pitch of windings.
- d) Portion of length over which windings are applied.

The appropriate range of Reynolds numbers was obtained by means of subjecting standard diameter test members and cylinders to the full range of wind speeds in a wind tunnel with a velocity range of 10 to 100 mph.

In tests on vibrating members, stiffnesses and structural damping were varied in such a manner that the effects of these parameters upon the response may be evaluated.

The test program was divided into three main phases. Phase A consisted of tests on stationary cylinders mounted in the wind tunnel with a sensitive transducer built into the supports in such a manner that direct measurements of the lift forces on the cylinders were obtained. Spoiler optimization was carried out on the stationary cylinders. Phase B dealt with the response of spring-supported cylinders oscillating as rigid bodies in the wind stream. The third phase was a study of the response of flexural members vibrating in bending modes under the influence of a steady wind. Each of these phases contributed information on the lift coefficient, the self-amplification phenomenon, the Strouhal number, and the spoiler optimization.

2.4 Notationa) Notation - English

<u>Symbol</u>	<u>Definition</u>	<u>Units</u>
A	= Cross-sectional area.	in ²
A _p	= Projected area = LD.	ft ²
a	= Radius of cylinder.	L
a'	= A convenient constant = $\frac{EIg}{A\beta}$	in ² /sec.
a _o	= Maximum acceleration due to vibration.	in/sec ² .
b	= Radial distance from center of cylinder to center of a vortex in the wake.	L
b, α	= Polar coordinates for location of a vortex in the wake. (b = na.)	
C	= A constant.	
C _D	= Dimensionless drag coefficient = $\frac{F_D}{q A_p}$	
C' _D	= Fluctuating component of the drag coefficient.	
C _L	= Fluctuating lift coefficient = $\frac{F_L}{q A_p}$	
C _K	= Kármán coefficient, or the maximum value of the lift coefficient.	
\bar{C}_K	= "Standard C _K ", or the RMS value of C _K , or the standard deviation of C _K .	
\bar{C}'_{Kc}	= Self-amplified standard Kármán coefficient for a spring-supported cylinder.	
\bar{C}'_{Km}	= Self-amplified standard Kármán coefficient for a vibrating flexural member.	
c	= Damping coefficient for viscous damping = damping force per unit linear velocity.	lb-sec/in
c _c	= Critical damping coefficient = (Spring const.)πf	lb-sec/in
$\frac{c}{c_c}$	= Damping ratio = $\frac{\delta}{2\pi}$ = rate of damping per radian.	
D	= Diameter of cylinder or member, in feet.	ft
d	= Diameter of cylinder or member, in inches.	in
E	= Modulus of elasticity of material.	lb/in ²
e	= Distance between two vortices in the same row.	in
e'	= Increased distance between vortices in same row.	in
F	= Force.	lb

<u>Symbol</u>	<u>Definition</u>	<u>Units</u>
F_D	= Drag force = $C_D q A_p$	lb
F_L	= Lift force = $C_L q A_p$	lb
F_K	= Kármán force = $C_K q A_p$	lb
f	= Frequency of vibration	cps
f_c	= Natural frequency of vibration of a spring-supported cylinder.	cps
f_m	= Natural frequency of vibration of a flexural member.	cps
f_n	= Natural undamped frequency of an elastic system.	
f_1	= Natural frequency of the fundamental mode.	cps
f_j	= Natural frequency of the j th mode.	cps
f_v	= Frequency of shedding vortex pairs.	cps
g	= Acceleration due to a gravity = 386.	in/sec ²
h	= Width between the centers of two rows of eddies behind a non-oscillating circular cylinder. $h \sim 1.3d$.	in
h'	= Increased width of vortex street.	in
i	= Complex operator = $\sqrt{-1}$.	
J	= Number in a series.	
K	= Moment for unit rotation.	in-lb.
k	= A convenient constant = $\sqrt{\frac{\omega}{a'}}$.	1/in
k_c	= Spring constant of a spring-supported cylinder with respect to a uniform loading = the total load, $w\ell$, which produces a deflection of unity. $k_c = w\ell$.	lb/in
k_m	= Spring constant of a member with respect to a uniform loading = the total load, $w\ell$, which produces a maximum static deflection, Δ_m , of unity.	lb/in
k_o	= Spring constant of an elastic system.	lb/in
L	= Length, in feet.	ft
ℓ	= Length, in inches.	in
M	= Total mass.	lb-sec ² /in
m	= Mass per unit length.	lb-sec ² /in ²

<u>Symbol</u>	<u>Definition</u>	<u>Units</u>
m_c	= Mass per unit length of a spring-supported cylinder.	$\text{lb-sec}^2/\text{in}^2$
m_m	= Mass per unit length of a flexural member.	$\text{lb-sec}^2/\text{in}^2$
N_R	= Reynolds number = $\frac{VD}{\nu} = 780 \text{ vd}$.	
N_s	= Strouhal number = $\frac{fD}{V} = \frac{fd}{17.6v}$.	
N'_s	= Self-reduced Strouhal number.	
n	= A dimensional ratio.	
P	= Concentrated load.	lb
p	= Gage pressure = air pressure above or below atmospheric pressure acting on a surface or a projected area.	lb/ft^2
q	= Stagnation pressure = $\frac{1}{2} \rho_a v^2$.	lb/ft^2
r	= Modulus of the complex number $re^{i\theta}$.	L
r, θ	= Polar coordinates of any point in a region.	
t	= Time.	sec
V	= Uniform velocity of undisturbed flow.	fps
v	= Velocity in miles per hour.	mph
v_{cr}	= Critical wind velocity.	mph
v_p	= Velocity corresponding to peak amplitude of vibration.	mph
v_v	= Velocity of vortices in street.	LT^{-1}
W_c	= Weight of spring-supported cylinder.	lb
w	= Load per unit length.	lb/in
w'	= w magnified by (DLF) at resonance.	lb/in
w_o	= Effective lateral loading per unit length due to vortex shedding on a stationary cylinder with $v = v_p$.	lb/in
y	= Orthogonal coordinate denoting deflection at any point, x , along a member	in
y_o	= Amplitude of vibration.	in
y_m	= Amplitude of vibration at point of maximum deflection on a flexural member.	in

<u>Symbol</u>	<u>Definition</u>	<u>Units</u>
y_{mp}	= Value of y_m when $v = v_p$, including the effect of self-amplification.	in
$Z(i\omega)$	= Mechanical impedance of an elastic system.	
z	= Complex coordinate of any point.	L

b) Abbreviations

(ASF)	=	Aeroelastic Suppression Factor.
(DLF)	=	Dynamic Load Factor.
(ILF)	=	Incremental Load Factor.
(IDF)	=	Incremental Deflection Factor.
(NDD)	=	Non-Dimensional Deflection = $\frac{y_m}{d}$.
(RF)	=	Reduction Factor.

c) Notation - Greek

<u>Symbol</u>	<u>Definition</u>	<u>Units</u>
α	= Polar coordinate for location of a vortex in the wake.	
Γ	= Strength of a vortex.	$L^2 T^{-1}$
γ	= Unit weight of structural material.	lb/in ³
ρ_a	= Mass density of air at standard temperature (15°C) and pressure (760 mm of mercury) = 0.0765.	lb/ft ³
Δ	= Deflection under static loading.	in
Δ_m	= Maximum deflection of a member under static loading.	in
δ	= Logarithmic damping decrement, or rate of decay.	
θ	= Argument of the complex number $re^{i\theta}$.	
μ	= Viscosity of fluid.	$ML^{-1} T^{-1}$
μ_a	= Viscosity of air at standard temperature and pressure.	lb-sec/ft ²
ν	= Kinematic viscosity of fluid.	$L^2 T^{-1}$
ν_a	= Kinematic viscosity of air at standard temperature and pressure $\nu_a = \frac{\mu_a}{\rho_a} = 1.564 \times 10^{-4}$	ft ² /sec
ρ	= Mass density of fluid.	ML^{-3}
ρ_a	= Mass density of air at standard temperature and pressure = 0.00238.	lb-sec ² /ft ⁴
σ	= Unit stress.	lb/in ²
$\phi()$	= Denotes "a function of" the term inside the parentheses.	
Ω	= Ratio of frequency of forcing function to natural frequency.	
ω	= Circular frequency of vibration.	Rad/sec

III. AERODYNAMIC ASPECTS

3.1 Fundamental Considerations

a) Definitions

Lift and drag forces on a bluff obstacle may be defined in terms of the "stagnation" pressure, q , which represents the velocity pressure head in the free stream.

$$q = \frac{1}{2} \rho V^2$$

Form factors, called non-dimensional lift and drag coefficients, relate the lift and drag forces acting on the body to the stagnation pressure and the surface area (or a projected area) of the body.

$$\text{Non-dimensional drag coefficient} = C_D = \frac{F_D}{qA_p}$$

$$\text{Non-dimensional lift coefficient} = C_L = \frac{F_L}{qA_p}$$

The Reynolds number is a dimensionless number expressing the ratio, or relative importance, of the inertial forces (or velocity pressure forces) to the frictional forces which a fluid stream exerts upon a body.

$$\text{Reynolds number} = N_R = \frac{VD}{\nu}$$

The Strouhal number is a dimensionless number which represents the fact that a flow phenomenon is unsteady and periodic in its nature.

$$\text{Strouhal number} = N_S = \frac{fD}{V}$$

b) Dynamic Similarity

The method of dimensional analysis (Ref. 3) may be used to obtain model relationships for the problem of wind-induced vibrations. For a model (denoted by subscript 2) which is geometrically similar to a prototype (denoted by subscript 1) and constructed of the same material, the following expressions may be obtained (Ref. 31):

$L_2 = nL_1$	$F_2 = n^2 F_1$	$a_{o2} = \frac{1}{n} a_{o1}$
$I_2 = n^4 I_1$	$Mom_2 = n^3 Mom_1$	$f_2 = \frac{1}{n} f_1$
$E_2 = E_1$	$m_2 = n^2 m_1$	$\mu_2 = n\mu_1$
$\Delta_2 = n\Delta_1$	$V_2 = V_1$	$\delta_2 = \delta_1$

It is evident that for the conditions determining the foregoing relationships the Strouhal numbers for model and prototype will be the same. The Reynolds number will be the same only if a fluid medium is used which has a kinematic viscosity of

$$\nu_2 = n \nu_1.$$

Therefore, in testing the resonant response of geometrically similar models in air, equal Reynolds numbers cannot be practically attained. "Incomplete dynamic similarity" may be obtained, however, by testing models in air in the range of Reynolds numbers where the Strouhal number is fairly constant and where the value of C_K involved may be corrected for the influence of the Reynolds number.

3.2 Circular Cylinder in a Fluid Stream

The fluid flow in the immediate vicinity of a circular cylinder in the stream takes a variety of forms, depending upon the value of the Reynolds number. At extremely small Reynolds numbers the flow picture is very much like ideal flow, as shown in Figure 3.1. At somewhat higher values, up to $N_R = 40$, the flow separates from the surface, as in Figure 3.2, and forms two symmetrical, stationary vortices (Refs. 11 and 15). Above $N_R = 40$, however, the stationary vortices become distorted and unstable, and an asymmetrical flow condition develops wherein vortices are formed at opposite sides of the cylinder. These vortices grow in strength in the vicinity of the cylinder, are detached from the cylinder, and move down stream with the flow in an alternating pattern. The flow in the vortex street is viscous from $N_R = 40$ to approximately 150, and the vortices decay by viscous diffusion (Ref. 20). The range from $N_R = 150$ to 300 is a transition range in which the flow changes from laminar to turbulent in the free vortex layer which separates from each side of the cylinder (Ref. 20). Above $N_R = 300$, the flow becomes turbulent at the point of separation. In this range, called the irregular range, the vortex shedding is periodic, but the velocities fluctuate in an irregular fashion because of the turbulence in the flow. The result of these fluctuations is that the amplitudes of the lift forces are more or less random, and the randomness becomes more pronounced with increasing Reynolds numbers.

The vortex street behind a cylinder is commonly idealized as in Figure 3.3, which incorporates the stability criteria derived by Th. von Kármán (Ref. 13). This configuration is applicable from $N_R = 40$ to approximately $N_R = 3 \times 10^5$. At or near the latter Reynolds number the flow in the boundary layer on the forward portion of the cylinder changes from laminar to turbulent, and the separation points move rearward on the cylinder. There follows an abrupt drop in the drag coefficient, a sharp rise in the Strouhal number, and the wake becomes narrower and apparently aperiodic. Regular vortex formation is no longer visible, and the flow is highly turbulent. The flow picture is indicated in Figure 3.4, and the variations in the drag coefficient and the Strouhal number are shown in Figure 3.5. It is reasonable to suppose that the unknown plot of C_K would also undergo a rapid change in the vicinity of $N_R = 3 \times 10^5$. This value of N_R is referred to as the "critical" Reynolds number. Values of N_R below this number will be called "subcritical Reynolds numbers" in this paper, and those above will be termed "super-critical Reynolds numbers".

3.3 The Fluctuating Lift and Drag Coefficients

Under the assumptions of ideal flow and the vortex geometry behind the cylinder shown in Figure 3.6, it can be shown (Ref. 31) that the perimeter of the cylinder is a streamline and that the pressure distribution at the surface is given by:

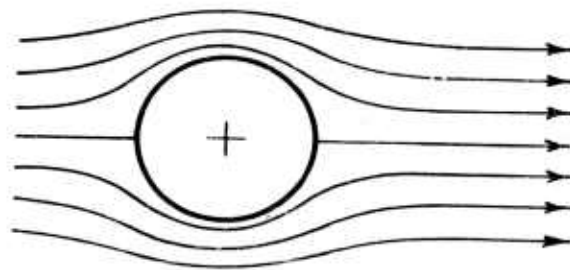


Figure 3.1:

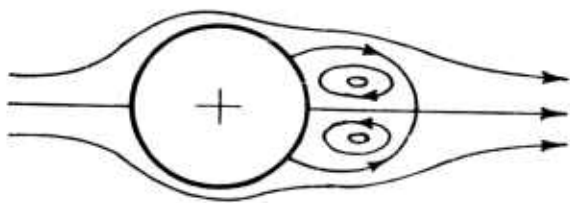
FLOW FOR VERY LOW N_R 

Figure 3.2:

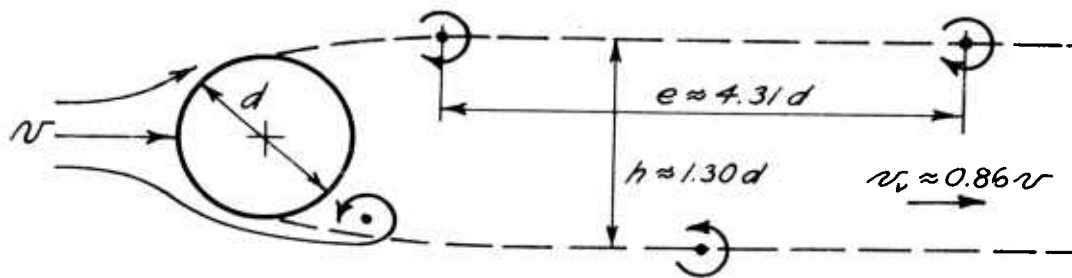
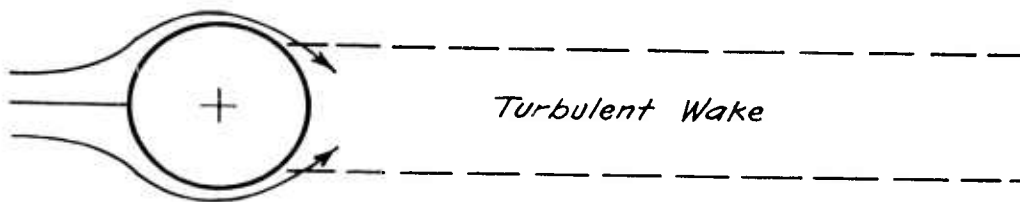
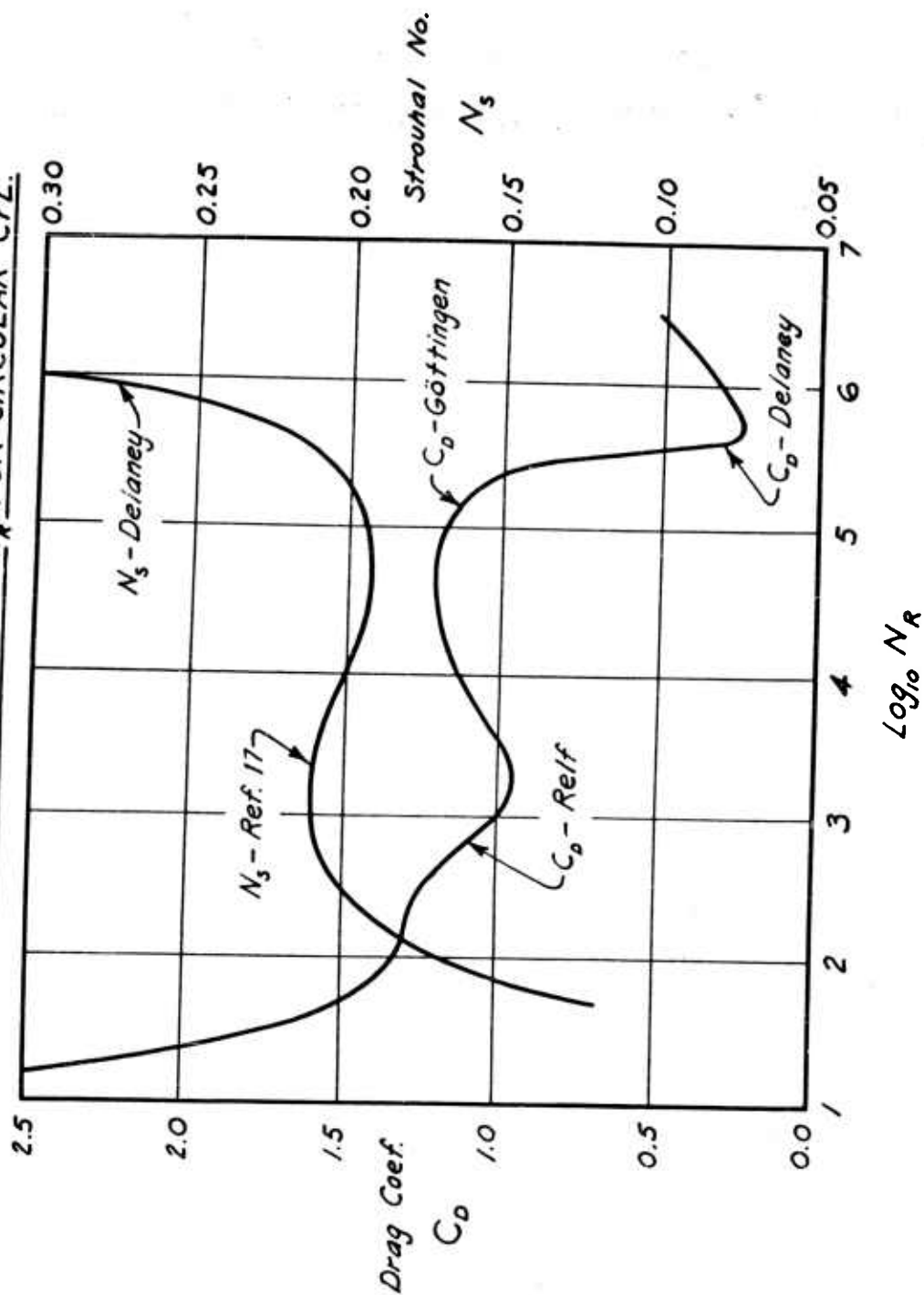
FLOW FOR $N_R < 40$ Figure 3.3: FLOW FOR $40 < N_R < 3 \times 10^5$ Figure 3.4: FLOW FOR $3 \times 10^5 < N_R$

Figure 3.5: VARIATION OF DRAG COEFFICIENT AND STROUHAL NO. WITH N_R FOR CIRCULAR CYL.



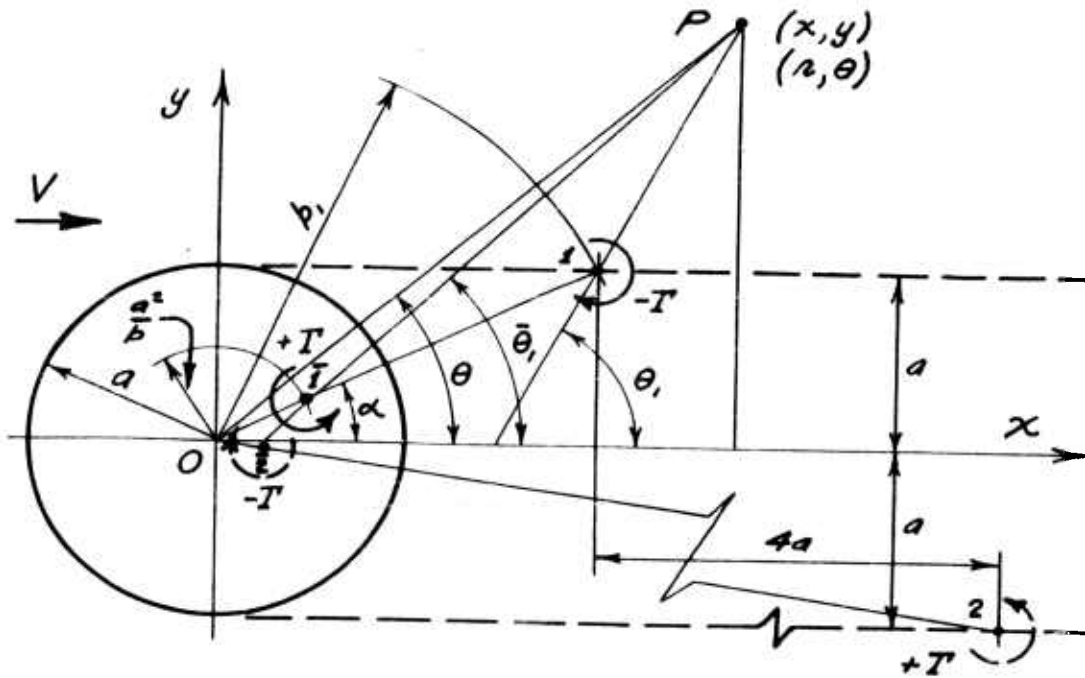


Figure 3.6: VORTEX GEOMETRY BEHIND CYLINDER

$$\alpha = \sin^{-1} \frac{a}{b}$$

$$O-P=r$$

$$1-P=r_1$$

$$2-P=\bar{r}_1$$

$$\theta_1 = \tan^{-1} \left[\frac{r \sin \theta - a}{r \cos \theta - b \cos \alpha} \right]$$

$$\bar{\theta}_1 = \tan^{-1} \left[\frac{r \sin \theta - \frac{a^2}{b^2}}{r \cos \theta - \frac{a^2}{b} \cos \alpha} \right]$$

$$r_1 = \left[(r \sin \theta - a)^2 + (r \cos \theta - b \cos \alpha)^2 \right]^{\frac{1}{2}}$$

$$= \left[r^2 - 2r(a \sin \theta + b \cos \alpha \cos \theta) + b^2 \right]^{\frac{1}{2}}$$

$$\bar{r}_1 = \left[\left(r \sin \theta - \frac{a^2}{b^2} \right)^2 + \left(r \cos \theta - \frac{a^2}{b} \cos \alpha \right)^2 \right]^{\frac{1}{2}}$$

$$= \left[r^2 - 2r \left(\frac{a^2}{b^2} \sin \theta + \frac{a^2}{b} \cos \alpha \cos \theta \right) + \frac{a^4}{b^2} \right]^{\frac{1}{2}}$$

(using $n = b/a$)

$$C = \frac{\rho V^2}{2} \left\{ 1 - \left[-2 \sin \theta + \sum_{j=1}^{\infty} (-1)^j \frac{\Gamma}{4\pi a V} \left(\frac{n_j^2 + 1}{2} - \sin \theta - n_j \cos \alpha_j \cos \theta \right) \right]^2 \right\} \dots (1)$$

This approximate expression is obtained from the Bernoulli equation for steady flow considering an instantaneous equilibrium condition.

The instantaneous lift and drag coefficients are obtained by integrating the lateral and longitudinal components, respectively, of the surface pressure.

$$C_L = \frac{1}{2} \int_0^{2\pi} \left\{ 1 - \left[-2 \sin \theta + \sum_{j=1}^{\infty} (-1)^j \frac{\Gamma}{4\pi a V} \left(\frac{n_j^2 + 1}{2} - \sin \theta - n_j \cos \alpha_j \cos \theta \right) \right]^2 \right\} \sin \theta d\theta \dots (2)$$

$$C_D' = \frac{1}{2} \int_0^{2\pi} \left\{ 1 - \left[-2 \sin \theta + \sum_{j=1}^{\infty} (-1)^j \frac{\Gamma}{4\pi a V} \left(\frac{n_j^2 + 1}{2} - \sin \theta - n_j \cos \alpha_j \cos \theta \right) \right]^2 \right\} \cos \theta d\theta \dots (3)$$

3.4 Effect of Vibration on Lift Forces

When an elastically-supported cylinder or a flexural member is vibrating in resonance with periodic vortex forces, the vibration itself causes an increase in the magnitude of the lift. The additional aerodynamic force is probably associated with a periodic shifting of the points of separation on the cylinder, resulting in increased circulation. At the same time, the vortices created in the wake are larger and stronger than in the case of the stationary cylinder.

D. Steinman (Ref. 24), citing the results of experiments at the David Taylor Model Basin, proposed the hypothesis that if eddies are shed at or near each end of the amplitude range, the normal width of the vortex street is increased by the ratio

$$\frac{h + 2y}{h} = 1 + \frac{2y}{1.3d}$$

For stability, the distances between vortices in each row must also increase in the same ratio. It is assumed that the drag, the circulation, and the lift must all increase by the same ratio. At the same time, the eddy frequency and the Strouhal number are decreased by the reciprocal ratio. Figure 3.7 shows schematically the increased dimensions of the vortex street.

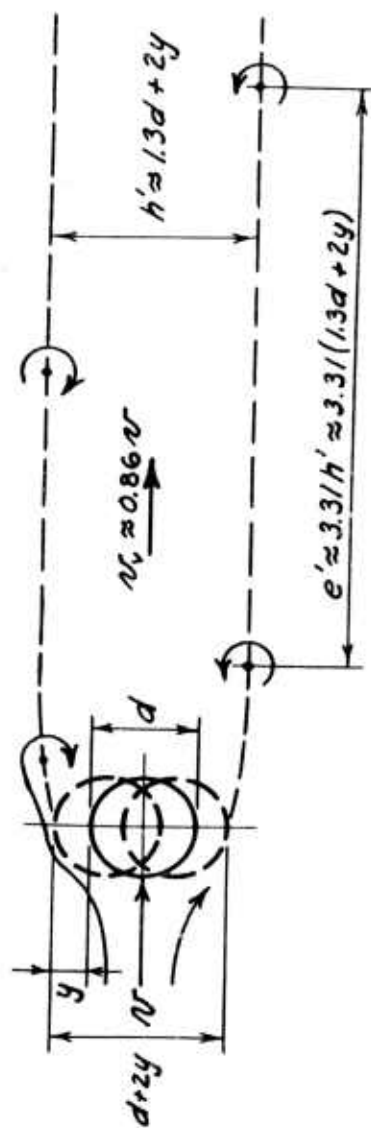


Figure 3.7: DIMENSIONAL INCREASE IN VORTEX STREET DUE TO VIBRATION

It is important to realize that resonant vibrations of large amplitude cannot be attained when the Strouhal frequency for a stationary cylinder exactly equals the natural frequency of an elastic body. In this instance, as soon as oscillation begins, the Strouhal frequency decreases and goes out of phase from the natural frequency. When oscillation occurs at some higher stream velocity, however, the Strouhal frequency decreases to the point where it matches the natural frequency of the body, and the vibration stabilizes at the corresponding amplitude.

There is an upper limit of stream velocity beyond which this self-controlling action cannot occur. At this point the amplitude drops abruptly to a lower value determined by the dynamic load factor of the forcing function. For the case of zero damping, Steinman deduced an upper limit of velocity for peak amplitude of

$$v_p \approx 1.45 v_{cr}$$

The ratio of v_p to v_{cr} must be the same as the ratio of dimensional increase in the vortex street.^p

$$\frac{v_p}{v_{cr}} = \frac{\frac{fd}{N_s'}}{\frac{fd}{N_s}} = \frac{N_s}{N_s'} = 1 + \frac{2y}{1.3d}$$

3.5 Effect of Protuberances

One may expect, from the experiments of Fage and Warsap (Ref. 9), that not only the drag coefficient but also the Strouhal number may become insensitive to Reynolds number for a cylinder with many small windings attached to the surface. Also, the use of a few small diameter spoilers would not serve to reduce lift forces appreciably except in the vicinity of the critical Reynolds number, where the boundary layer may easily be tripped into turbulent flow. It appears more promising to approach the problem from the point of view of disturbing the flow picture drastically through the use of windings which are of significant size compared to the diameter of the cylinder. If the regular formation of vortices can be prevented or interrupted by this means, an irregularity will be imparted to the lift forces which will inhibit the occurrence of resonant vibrations. In addition, if the windings are attached in a helical pattern, their three-dimensional character should be additionally advantageous for the purpose of disturbing a two-dimensional flow.

IV. VIBRATION ASPECTS

4.1 Preliminary Considerations

a) Damped Vibrations

The equation of motion for the forced, damped vibration for a single-degree-of-freedom system having viscous type damping and subjected to a harmonic forcing function of constant amplitude is

$$My + cy + k_0y = F_0 e^{i\omega t} \dots\dots\dots(4)$$

from which the response is found to be

$$y = \frac{F_o e^{i\omega t}}{Z(i\omega)} = \frac{F_o e^{i\omega t}}{\sqrt{(k_o - M\omega^2)^2 + c^2\omega^2}} \dots\dots\dots(5)$$

The real part of equation (5) may be written

$$y = \frac{F/k_o}{(1 - \Omega^2)^2 + (2\zeta_c \Omega)^2} \dots\dots\dots(6)$$

in which, $\Omega = \omega / \omega_n = f/f_n$.

b) Free Lateral Vibration of Members

The natural frequency of any free lateral vibration of a flexural member of constant section may be written (Ref. 28):

$$f = \frac{k_a^2}{2\pi} \dots\dots\dots(7)$$

in which the term k depends upon the conditions of end support and the mode of vibration. The fundamental frequencies for the elementary end conditions pictured in Figure 4.1 are the following:

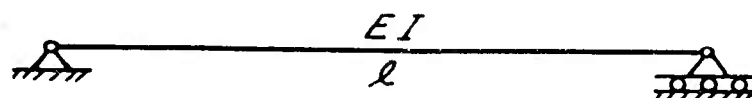
$$\text{Fixed:} \quad f_1 = \frac{3.56}{\ell^2} \sqrt{\frac{EIg}{A\gamma}} = 2.27 f_p \dots\dots\dots(8)$$

$$\text{Partly Fixed:} \quad f_1 = \frac{\pi}{2 \text{ to } 3.56} \sqrt{\frac{EIg}{A\gamma}} = (1.00 \text{ to } 2.27) f_p \dots\dots(9)$$

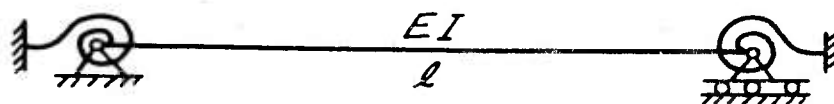
$$\text{Pinned:} \quad f_1 = \frac{\pi}{2\ell^2} \sqrt{\frac{EIg}{A\gamma}} = 1.00 f_p \dots\dots\dots(10)$$

$$\text{Cantilever:} \quad f_1 = \frac{0.560}{\ell^2} \sqrt{\frac{EIg}{A\gamma}} = 0.356 f_p \dots\dots\dots(11)$$

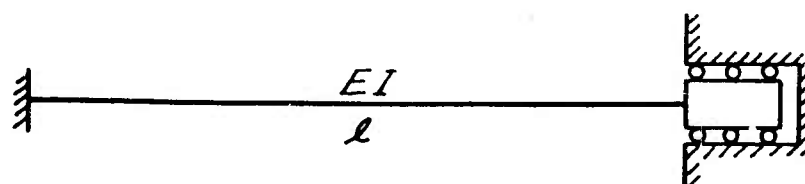
When a vibrating member is carrying an axial load (as in the case of a space frame), the natural frequency of the member is a function of the load as well as the properties of the member. For a member with pinned ends, for example, the expression for the natural frequency of the j th mode differs from that for zero load by the factor (Ref. 28):



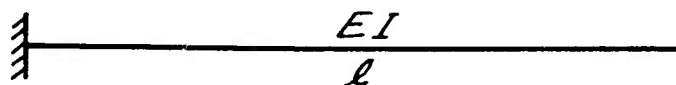
a) Pinned: $f_i = 1.00 f_p$



b) Partly Fixed: $f_i = 1.00 \text{ to } 2.27 f_p$



c) Fixed: $f_i = 2.27 f_p$



d) Cantilever: $f_i = 0.356 f_p$

Figure 4.1: FUNDAMENTAL FREQUENCIES OF
VARIOUS MEMBERS IN TERMS OF
FREQUENCY OF PINNED MEMBER

$$\sqrt{1 \pm \frac{F \ell^2}{J^2 EI \pi^2}}$$

in which the positive sign applies for a tensile load and the negative sign refers to a compression load.

4.2 Natural Frequencies of a Prismatical Member with Elastic End Connections

Actual end-supported members in a practical structure are neither pinned nor fixed. Instead, their end connections are of intermediate fixity, depending upon the manner of joint construction. Consider the member with elastic end connections shown in Figure 4.1a, in which the springs at the ends are weightless and of equal stiffness, K = moment for unit rotation. The frequency equations for the symmetrical and anti-symmetrical modes, respectively, may be shown (Ref. 31) to be:

$$\frac{K}{EIk} (\tanh k\ell/2 + \tan k\ell/2) - 2 = 0 \dots \dots \dots (12)$$

and $\frac{K}{EIk} (\coth k\ell/2 - \cot k\ell/2) - 2 = 0 \dots \dots \dots (13)$

A study of actual and experimental members (Ref. 31) resulted in the conclusion that a value of $(k\ell)^2 = 2.10 \pi^2$ can be used for estimating the fundamental frequencies of individual members in space frames having rigid joints. Natural frequencies of vibration of members having gusset plate connections may be assumed to be pinned with respect to vibrations in a direction normal to the plane of the gusset plates for all practical purposes.

4.3 Response of an Elastic System to Vortex Forces (without self-amplification)

a) Response to a Variable Forcing Function

The magnitude of the Kármán lift force varies with the velocity and the lift coefficient. The dimensionless response of a single-degree-of-freedom system, having viscous damping, to vortex forces at low Reynolds numbers may be written:

$$(NDD) = \frac{y_0}{d} = \frac{c_1 c_K \Omega^2 / k_0}{\sqrt{(1 - \Omega^2)^2 + (2 \frac{c}{c_c} \Omega)^2}} \dots \dots \dots (14)$$

The above expression may also be applied for the case of a flexural member vibrating in its fundamental mode, in which case k_m may be approximated as the total load acting on the member divided by the maximum deflection of the member when that load is applied statically.

b) Response to a Random Forcing Function

(Single-degree-of-freedom elastic system with viscous damping, without self-amplification)

We have discussed thus far only the ideal case of a forcing function having amplitude and frequency which vary with the stream velocity and which are constant for a particular velocity. For this case the response is calculated on the basis of a forcing function which may be assumed to vary sinusoidally with time and which has an unvarying amplitude and a discrete frequency. Equation 15,

$$F = \frac{1}{2} C_K C_a V_p^2 \sin \pi f_v t \dots\dots\dots(15)$$

is the commonly-used expression applied to the vortex shedding phenomenon.

However, for Reynolds numbers above approximately 3×10^2 the amplitude of the lift force is not constant for a given stream velocity but becomes increasingly random as the Reynolds number increases. At a Reynolds number above approximately 3×10^5 the vortex shedding frequency also becomes random as the separation point moves rearward on the cylinder. Therefore, for the purposes of computing the response of an elastic system, there are two important types of forcing functions to be considered: (1) $3 \times 10^2 < N_R < 3 \times 10^5$ sinusoidal forcing function with discrete frequency but random amplitude. (2) $3 \times 10^5 < N_R$ harmonic forcing function with random frequency and random amplitude.

(1) Response at Subcritical Reynolds Numbers

The range of Reynolds numbers below 3×10^5 is of primary interest in this investigation because most practical-sized antenna members subjected to moderate wind velocities fall into this category.

In this case the force amplitude is random with a steady mean value of zero. The response of the system depends upon the energy input from the vortex forces averaged over a period of time. Now, the energy input per cycle is proportional to the product of the force and the amplitude of vibration. But the amplitude itself varies directly with the applied force; so the energy input per cycle varies as the square of the force.

$$\text{Energy input per cycle} \propto F_K \cdot y_o$$

$$\propto F_K^2$$

$$\text{Power input} \propto F_K \cdot y_o \cdot f_v$$

$$\propto F_K^2 \cdot f_v$$

Therefore, the mean square of the force determines the energy input, and the response must be calculated on the basis of the standard deviation from the mean, or the RMS of all of the random deviations. We may define the non-dimensional lift coefficient, \bar{C}_K , as the RMS value of C_K and present the forcing function as

$$F = \frac{1}{2} \bar{C}_K C_a V_p^2 \sin \pi f_v t \dots\dots\dots(16)$$

and compute the response from

$$(NDD) = \frac{y_o}{d} = \frac{c_1 \bar{c}_K \Omega^2 / k_o}{\sqrt{(1 - \Omega^2)^2 + (2 \frac{c}{c_c} \Omega)^2}} \dots\dots\dots(17)$$

(2) Response at Supercritical Reynolds Numbers

Supercritical Reynolds numbers are of secondary interest in this investigation but are of primary interest for structures with large diameters, such as steel stacks and guided missiles.

In this case the force amplitude has a mean value of zero, and both the amplitude and frequency are random. We must, therefore, deal with power input rather than energy input per cycle, because the power depends upon the frequency of the excitation as well as the force amplitude. The power input must be evaluated in terms of the whole spectrum of frequencies involved. In order to do this, some characteristic function for the power with respect to frequency must be either assumed or evaluated experimentally. The resulting plot of power- vs - frequency is called the power spectrum, and the ordinate associated with a particular frequency is referred to as the "power spectral density" for that frequency (Refs. 10, 27, etc.). A frequency of high spectral density will produce a high response at resonance.

For the stochastic process under consideration, if the power spectrum is expressed as a function of the non-dimensional Strouhal frequency, N_s ,

$$(PSD) = \phi(N_s)$$

and is normalized so that

$$\int_0^\infty \phi(N_s) dN_s = 1,$$

then the mean square amplitude of the forcing function may be expressed in terms of the mean square lift coefficient and the integral of the power spectral density (Ref. 10).

$$\bar{F}^2 = (\frac{1}{2} \rho_a V_p^2 A_p) \bar{c}_K^2 \int_0^\infty \phi(N_s) dN_s \dots\dots\dots(18)$$

The mean square value of the response may then be calculated from

$$(NDD)^2 = \left(\frac{y_o}{d}\right)^2 = \frac{c_1^2 \bar{c}_K^2 \Omega^2}{k_o^2} \int_0^\infty \frac{\phi(N_s) dN_s}{(1 - \Omega^2)^2 + (2 \frac{c}{c_c} \Omega)^2} \dots\dots(19)$$

Under the assumption that there are no phase differences along the length of the cylinder, and not considering the effect of self-amplification, equation (19) may be evaluated with respect to the power spectrum in a narrow band width at a frequency corresponding to the natural frequency of the elastic system (Ref. 31).

The mean square response becomes:

$$\bar{y}^2 = \frac{(q A_p)^2 \bar{C}_K^2}{k_o (2 \frac{c}{c_c})} \cdot \frac{\pi}{2} N_s \cdot \phi(N_s) \dots\dots\dots(20)$$

High spectral densities at low Strouhal numbers would indicate the probability of dangerously large oscillations at fairly high wind velocities.

4.4 Self-Amplification of Vibrations

a) Method of Approach to the Problem

In this investigation a means is developed for dealing with the phenomenon of self-amplification of wind-induced vibrations. The general approach to the problem is as follows:

(1) All of the parameters that are known to have an influence on the amount of the self-amplification of either a spring-supported cylinder or a flexural member are lumped into dimensionless numbers which will be called "aeroelastic suppression factors", (ASF). These (ASF)'s are a measure of the relative ability of vibrating systems to amplify their own vibrations.

(2) "Incremental deflection factors", (IDF), are derived for various types of members which represent the degree of self-amplification that can be attained. The (IDF)'s depend, among other things, upon the ratio v/v_{cr} (or its equivalent, the "incremental load factor, ILF). The latter term can be determined by the experiments, and when plotted against the (ASF) for each member tested, yields a useful empirical curve for the purpose of calculating the (IDF) for any member in an antenna structure.

The tools for this semi-empirical solution of the self-amplification problem will be summarized in this section. Plots of (ILF) - vs - (ASF) will be presented in the test results of phases B and C, and the procedure outlined will be applied in Chapter IX of this report to give a combined solution to the problem of self-amplification of vibrations.

b) Aeroelastic Suppression Factors

(1) Spring - Supported Cylinders

The ratio by which v exceeds v_{cr} (as well as the ratio by which \bar{C}_K is increased due to the vibration) depends, in the case of a spring-supported cylinder, upon the following three elements: (1) the damping, (2) the stiffness, and (3) the relative magnitude of the wind forces.

Let us define an "aeroelastic suppression factor", (ASF):

$$(ASF) = \delta \frac{k_c}{F_K} d \dots\dots\dots(a)$$

in which,

δ = non-dimensional logarithmic damping decrement = rate of damping per cycle.

k_c = stiffness of spring supports, lb/in.

d = diameter of cylinder, inches.

F_K = lift force on cylinder, lb.

Note that the inclusion of the diameter, d , serves to render the ratio $\frac{k_c}{F_K}$ dimensionless by changing the spring stiffness, lb. per inch of deflection, to lb. per unit of non-dimensional deflection, (NDD).

Expressing k_c and F_K in terms of m_c , N_s , and \bar{C}_K yields:

$$(\text{ASF}) = 6.86 \times 10^8 \frac{m_c N_s^2 \delta}{\bar{C}_K d^2} \dots\dots\dots (b)$$

(2) Flexural Members

The (ASF) for a flexural member vibrating in its fundamental mode may be expressed in a manner similar to that for a spring-supported cylinder. The stiffness, k , of the flexural member, however, shall be defined as the total uniformly distributed static load which produces a maximum deflection of unity. Accounting for the mode shapes and corresponding member stiffnesses in this manner, the following (ASF)'s are obtained:

<u>Type of Member</u>	<u>(ASF)</u>
Fixed.....	$5.28 \times 10^8 \frac{m_c N_s^2 \delta}{\bar{C}_K d^2} \dots\dots\dots (21)$
Pinned.....	$5.44 \times 10^8 \frac{m_c N_s^2 \delta}{\bar{C}_K d^2} \dots\dots\dots (22)$
Cantilever.....	$4.42 \times 10^8 \frac{m_c N_s^2 \delta}{\bar{C}_K d^2} \dots\dots\dots (23)$
Cylinder.....	$6.86 \times 10^8 \frac{m_c N_s^2 \delta}{\bar{C}_K d^2} \dots\dots\dots (24)$

(c) Incremental Deflection Factors

(1) General

A member vibrating at a fairly large amplitude under the action of von Kármán vortex forces experiences a magnification of lateral forces over and above those acting on a stationary cylinder. Connected with this self-amplification are the facts that the width of the vortex street increases and that the strengths of vortices increase correspondingly. At the same time, the frequency of vortex shedding decreases in the same ratio in order to maintain geometric similarity, and hence, stability in the vortex street. The ratio of the self-amplified lift force per unit length of an oscillating cylinder or flexural member to the lift force per unit length if there were no amplification shall be defined as the "incremental

load factor", (ILF).

$$(\text{ILF}) = 1 + \frac{2\gamma}{1.3d} = 1 + 1.54 (\text{NDD})$$

For an oscillating cylinder the (ILF) is equal to v/v_{cr} . For a vibrating member the (ILF) at the point of maximum deflection is also assumed to be equal to v/v_{cr} .

When a cylinder or a flexural member is vibrating under the influence of a wind velocity somewhat greater than the critical velocity, the aerodynamic forces exceed those acting at the critical velocity for two reasons. First, the forces increase in proportion to the velocity pressure head increase, $(v/v_{cr})^2$. Second, the forces increase due to the self-magnification shown by the increased width of the vortex street. There is an upper limit of amplitude and velocity where the vibration becomes unstable and breaks down abruptly. Thus, the amplitude rises gradually to a peak at a velocity somewhat above the critical velocity and then drops suddenly to a low value.

Let us define a term which will account not only for the increase in forces due to the self-amplification but also for the increase due to the velocity increment. This term shall be called the "incremental deflection factor", (IDF). The (IDF) is the ratio of the peak amplitude to the hypothetical amplitude at the critical velocity. The latter amplitude must be recognized as hypothetical because resonant vibrations of large amplitude cannot be attained when the Strouhal frequency for a stationary cylinder exactly equals the natural frequency of the body. In this instance, as soon as oscillation begins, the Strouhal frequency decreases and goes out of phase from the natural frequency, and a pulsating response results. For the purpose of computing the (IDF), however, we shall imagine that there is no inter-action between the calculated forces and the response at the critical velocity.

For a cylinder oscillating as a rigid body the (ILF) and the (IDF) are determined by the damping, the spring stiffness, and the lift coefficient. For a vibrating flexural member, however, the (ILF) varies along the length of the member, and the (IDF) is a function of the shape of the dynamic deflection curve and the phase relationships of the forces acting over the total length.

D. B. Steinman (Ref. 24) evaluated for a specific case the effect of the self-amplification, (ILF), of an oscillating cylinder, simultaneously with the dynamic amplification equation, (DLF), for an elastic system, by means of a two-part graphical interpretation substituted for the solution of a 6th degree equation. It will be more convenient for design purposes, however, to consider the elastic vibrational amplification, (DLF), and the aerodynamic type of amplification, (IDF), separately.

In this investigation there are two different situations for which amplification implements must be developed:

A. Design or Analysis: Knowing the member characteristics, the damping, the lift coefficient, and the Strouhal number, calculate the maximum possible amplitude of vibration.

B. Wind Tunnel Tests: Having measured the member characteristics, the damping, the maximum amplitude, and the corresponding wind velocity, calculate the lift coefficient and the Strouhal number for a stationary cylinder of the same diameter and at the same wind velocity.

These two approaches will be taken up individually. The factors for the former case have already been defined. The factors for the latter case will be defined simply as the "reduction factors", (RF).

(2) (IDF)'s for Design or Analysis

In the case of design or analysis the member characteristics, the damping, the lift coefficient, and the Strouhal number are known. The problem is to calculate the maximum possible amplitude of vibration. The method to be used is to calculate the hypothetical amplitude of vibration at the critical velocity and then to increase this amplitude by the (IDF). Since the (IDF) is a function of the velocity ratio $v/v_{cr} = (ILF)_{max}$, the latter term must also be known. The experimental curve for $(ILF)_{max}$, obtained from the laboratory tests in this investigation, may be used for this purpose.

The (IDF) will be developed in detail for the case of a simply-supported member. Expressions for the (IDF)'s for other cases of interest will also be written.

For a simply-supported member vibrating under the influence of the wind velocity which causes peak amplitude,

$$y_{mp} = \left[\frac{5}{384} \cdot \frac{w_o l^4}{EI} + \frac{2y_{mp}}{1.3d} w_o \frac{0.01025 l^4}{EI} \right] (DLF) *$$

Solving for y_{mp} ,

$$y_{mp} = \frac{\frac{5}{384} \frac{w_o l^4}{EI} (DLF)}{1 - \frac{2w_o}{1.3d} \frac{0.01025 l^4}{EI} (DLF)} \dots (25)$$

By definition,

$$(IDF) = \frac{y_{mp}}{\frac{5}{384} \frac{w_o l^4}{EI} (DLF)} = \frac{1}{1 - \frac{2w_o}{1.3d} \frac{0.01025 l^4}{EI} (DLF)} \dots (26)$$

But,

$$\begin{aligned} w_o &= \bar{C}_K \left(\frac{1}{2} \rho a_p^2 v^2 \right) \cdot \frac{d}{144} \left(\frac{44}{30} \right)^2 \\ &= 1.779 \times 10^{-5} \bar{C}_K v_p^2 d \dots \dots \dots (lb/in) \dots \dots \dots (a) \end{aligned}$$

* Deflections of all vibrating members are approximated by fourth degree parabolas. The incremental loading on a member will therefore be assumed to vary as a fourth degree parabola.

Also, $v_p = v_{cr} \times (ILF)_{max} \dots\dots\dots(b)$

And, $v_{cr} = \frac{f_1 d}{3.344} = 96,400 \frac{dr}{\ell^2} \dots\dots\dots(c)$

Substituting (a), (b), and (c) into equation (26) and writing similar equations for other types of members results in the following:

A. Pinned Members: (Defl. assumed 4th degree parabola)

$$(IDF) = \frac{1}{1 - 2.41 \times 10^{-4} \bar{C}_K \frac{d^2}{A} (DLF) (ILF)^2} \dots\dots\dots(27a)$$

B. Fixed Members: (Defl. assumed 4th degree parabola)

$$(IDF) = \frac{1}{1 - 2.64 \times 10^{-4} \bar{C}_K \frac{d^2}{A} (DLF) (ILF)^2} \dots\dots\dots(27b)$$

C. Cantilever Members: (Defl. assumed 4th degree parabola)

$$(IDF) = \frac{1}{1 - 2.46 \times 10^{-4} \bar{C}_K \frac{d^2}{A} (DLF) (ILF)^2} \dots\dots\dots(27c)$$

D. Spring-Supported Cylinders: (Defl. uniform)

$$(IDF) = \frac{1}{1 - 2.44 \times 10^{-4} \bar{C}_K \frac{d^2}{A} (DLF) (ILF)^2} \dots\dots\dots(27d)$$

It must be noted that in the derivation of the (IDF)'s a discrepancy arises in the case of a flexural member. At large amplitudes of vibration the vortex shedding in the region of maximum deflection will tend to be slower than in regions of lesser deflection near the supports. The acting forces will tend to lose some phase homogeneity, and a limit of self-amplification will be reached which is less than that indicated by the calculations discussed above. Qualitatively speaking, a flexural member will have less self-amplification than an oscillating cylinder not only because of the mode shape but also because of the phase differences which arise. The experimental plot of (ILF) from the member tests in this investigation will be assumed to account for these phase differences. (It will be seen from the results of the experiments of Phases B and C that the (ILF) curve for members is somewhat lower than that for spring-supported cylinders because of the phase differences discussed here.)

(3) (RF)'s for Reducing Wind Tunnel Tests

The second situation of interest involves the transformation of the wind tunnel test data into useful information. In order to have some basis of comparison, dynamic values of \bar{C}_K' and N_s' must be referred to the case of the stationary cylinder. The experimental values of \bar{C}_K' and N_s' are to be multiplied and divided, respectively, by the appropriate reduction factors, (RF).

In the process of reducing the test data for a flexural member, an "apparent" dynamic \bar{C}_K is computed which refers to a uniformly distributed lateral loading acting on the member. Then the proper reduction factor is calculated by equating the deflection of the member with a statically-applied, uniformly-distributed apparent \bar{C}_K loading to the deflection obtained with a statically-applied "standard" \bar{C}_K loading properly modified by the effect of self-amplification. In this manner, the following expressions for (RF) are obtained:

- A. Pinned Members: (Defl. assumed 4th degree parabola)

$$(RF) = \frac{1}{1 + 1.21 (NDD)} \dots\dots\dots(28a)$$

- B. Fixed Members: (Defl. assumed 4th degree parabola)

$$(RF) = \frac{1}{1 + 1.26 (NDD)} \dots\dots\dots(28b)$$

- C. Cantilever Members: (Defl. assumed 4th degree parabola)

$$(RF) = \frac{1}{1 + 1.09 (NDD)} \dots\dots\dots(28c)$$

- D. Spring-Supported Cylinders: (Defl. uniform)

$$(RF) = \frac{1}{1 + 1.54 (NDD)} \dots\dots\dots(28d)$$

V. TEST PROGRAM AND DESIGN OF COMPONENTS

5.1 Basic Assumptions

The following basic assumptions apply to the wind tunnel experiments in this investigation:

- a) Spanwise correlation is assumed for the vortex-shedding mechanism. That is, the flow picture is assumed to be two-dimensional, and the vortex-shedding is assumed to be in phase at all sections of a cylinder (at sub-critical Reynolds numbers) at all times. Very little experimental evidence exists to support this assumption, but Roshko (Ref. 20) found good spanwise correlation at low Reynolds numbers.
- b) Spoiler configurations optimized on stationary cylinders are assumed to be optimum for vibrating cylinders also. This assumption permits the results of stationary tests to be extrapolated to vibration tests for the purpose of checking spoiler effectiveness without having to repeat the optimization process.
- c) Short, spring-supported cylinders are assumed to simulate the behavior of structural members which are too large to test in the wind tunnel. For this purpose, stiffnesses and mass ratios of cylinders and members must be adjusted.
- d) It is assumed that the fundamental mode of vibration of practical members is of much more common occurrence than the higher modes of vibration. For this reason the design of spoilers for flexural members shall be directed toward suppressing the first mode efficiently, without regard to higher modes.

5.2 Phases of Test Program

The following three phases constituted the test program:

- a) Phase A: The first phase consisted of tests on stationary cylinders mounted vertically in the wind tunnel. These cylinders ranged in size from 3" ϕ to 10" ϕ , in increments of 1 inch. The variation of the lift force on a cylinder, with respect to time, was measured by means of a small force transducer at the lower end of the cylinder. The output of the force transducer provided information for calculating lift coefficients and Strouhal numbers for the range of wind tunnel velocities available as well as for optimizing spoiler designs.
- b) Phase B: The second phase involved mounting the cylinders from Phase A on cantilever spring supports at top and bottom. The response of these spring-supported cylinders to the vortex action of the wind was measured indirectly by accelerometers mounted on each end. These response measurements permit the calculation of the magnitude and frequency of the forcing function for both bare cylinders and cylinders with spoilers and also provide comparisons between the two. A second parameter, the damping coefficient, was not subject to control, but the fact that it varied proved to be useful in the final analysis.
- c) Phase C: In the last phase a series of flexural members was tested. These members were of fairly small diameter (1 $\frac{1}{2}$ " ϕ , 2" ϕ , 3" ϕ , and 4" ϕ) and had various conditions of end support. The members tested were selected on the basis of a feasibility study which determined the sizes and methods of supports which could be used in the wind tunnel available and which could be expected to attain resonance within the speed range of the tunnel. The response of these full-size test members was measured in terms of fiber strains by means of SR-4 gages applied at points of maximum stress. This phase provides: (1) values for the lift coefficient and Strouhal number at lower Reynolds numbers, (2) correlation with spring-supported cylinders, (3) information on the effect of varying the length of spoilers over the length of the member, and (4) verification of model relationships for the vortex shedding phenomenon.

Phases B and C also yield useful information on the degree of self-amplification in vibrating members.

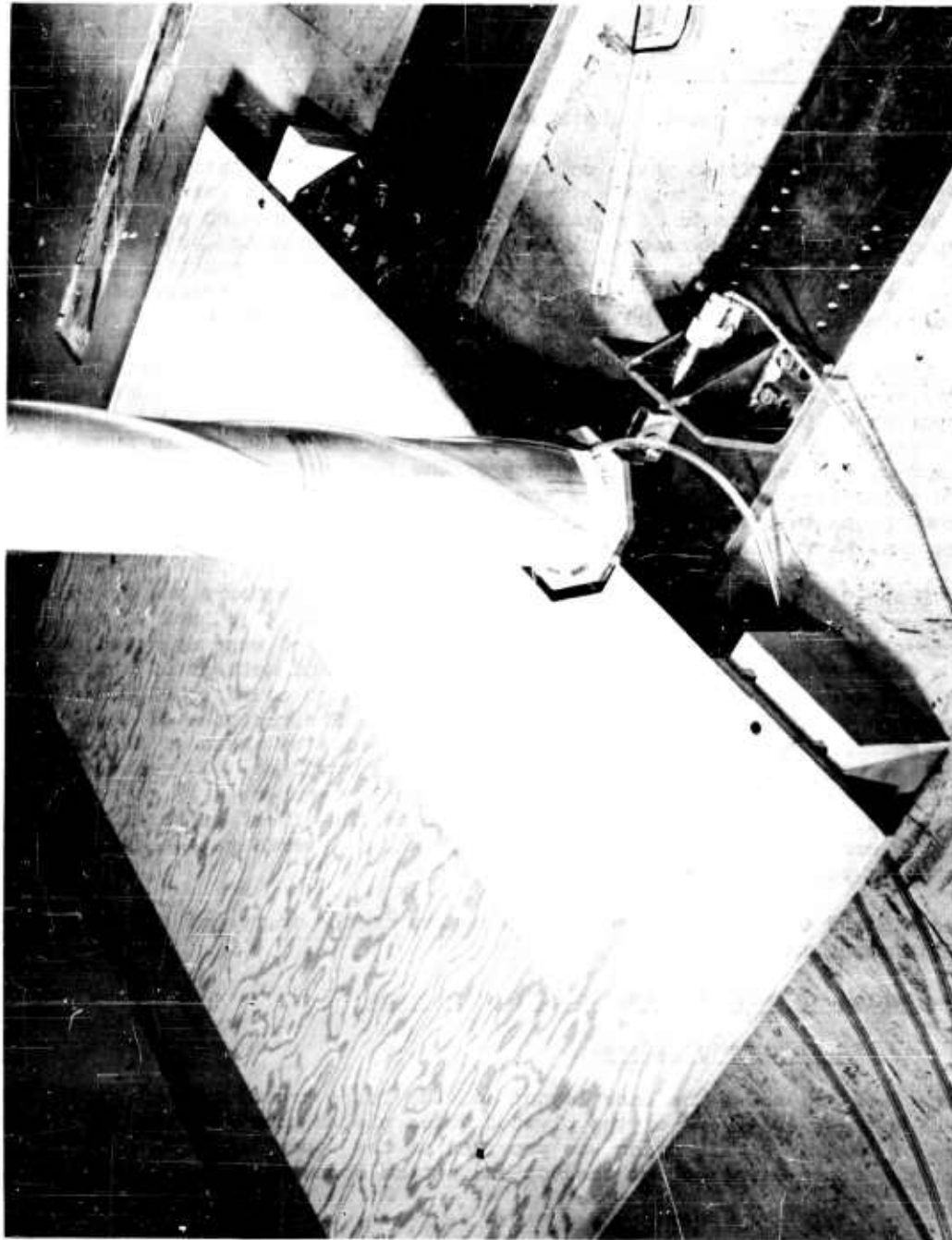
5.3 Design of Test Members and Support Systems

a) Stationary Cylinders

Photograph 5.1 shows the base layout and the force transducer connection for the Phase A tests (with one of the plywood guide plates removed). A "dummy" connection of similar construction was provided at the upper end of the cylinder so that the force reactions at the top and bottom connections would be approximately equal.

b) Spring-Supported Cylinders

The same cylinders were used in Phase B that were used in Phase A. The support system was transformed by removing the lateral restraints top and bottom so that the cylinders could swing freely on their spring supports. Twin accelerometers were attached at both ends of the test cylinder to complete the Phase B set-up. Variable spring constants for the supports were obtained using different lengths and thicknesses of the cantilever support strips. These strips were clamped to



Photograph 5.1 : Base Layout - Phase A (3" ϕ Cylinder in Place)

heavy base plates with rigid connectors and high strength bolts uniformly tensioned with a torque wrench. Photograph 5.2 shows the 4" ϕ spring-supported cylinder of Phase B with optimum spoilers attached.

c) Flexural Members

The types of members tested were the following:

<u>Number</u>	<u>Designation</u>	<u>End Connections</u>	<u>Diameters</u>
3	M1	Fixed	1½" ϕ to 3" ϕ
3	M2	Partly Fixed	1½" ϕ to 3" ϕ
4	M3	Pinned	1½" ϕ to 4" ϕ
6	M4	Cantilever	1½" ϕ to 3" ϕ

Cantilever members with $\ell/d = 30$ and $\ell/d = 20$ were obtained by sawing off one end of the fixed members after the M1 tests had been completed. In this manner a total of 16 different members were tested using only 10 shop specimens.

Photograph 5.3 shows the M1 members as they were fabricated previous to testing, and Photograph 5.4 shows an example end connection for M1 as it was mounted in the wind tunnel. The bolted connections were tightened uniformly with a torque wrench, and the guide plates (one of which is removed) were cut to clear the members by $\frac{1}{8}$ in.

VI MATERIALS AND APPARATUS

6.1 Materials

a) Test Members

All test members were fabricated from structural aluminum stock 6061 T6, which is the material commonly employed for the construction of antenna structures. Support members and stationary connectors were made up from structural grade steel.

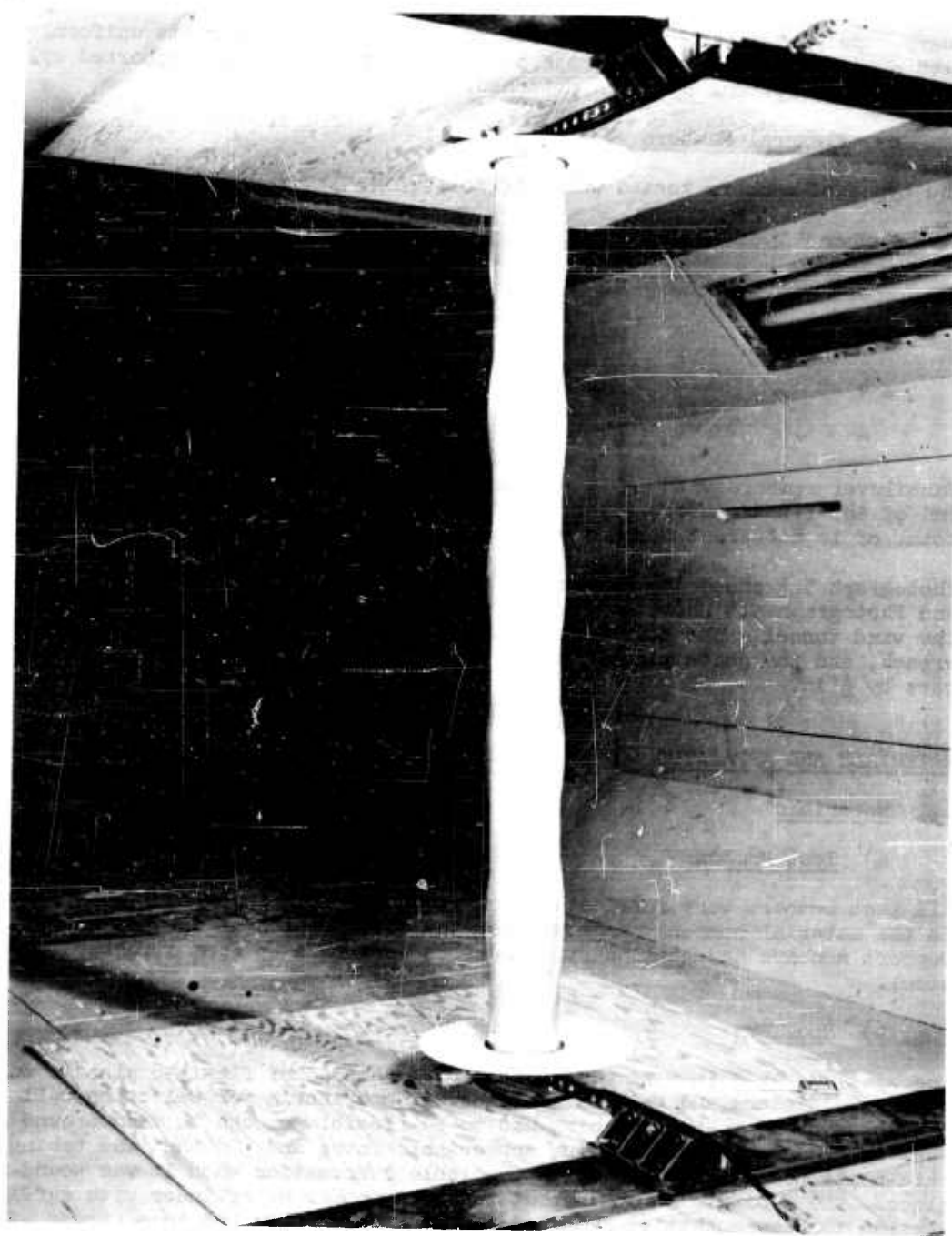
b) Spoilers

The spoilers used in wind tunnel testing consisted of flexible plastic tubing of various diameters and wall thicknesses. The criteria for selecting wall thicknesses were (1) that the tubing had to be flexible enough to wind around the test cylinders without applying appreciable force and (2) that the tubing had to retain its round shape without appreciable deformation when it was wound in place. The tubing was wound about the test member or cylinder with sufficient tension to assure that it remained in place when subjected to a strong wind, and it was fastened at each end with narrow strips of electrical adhesive tape.

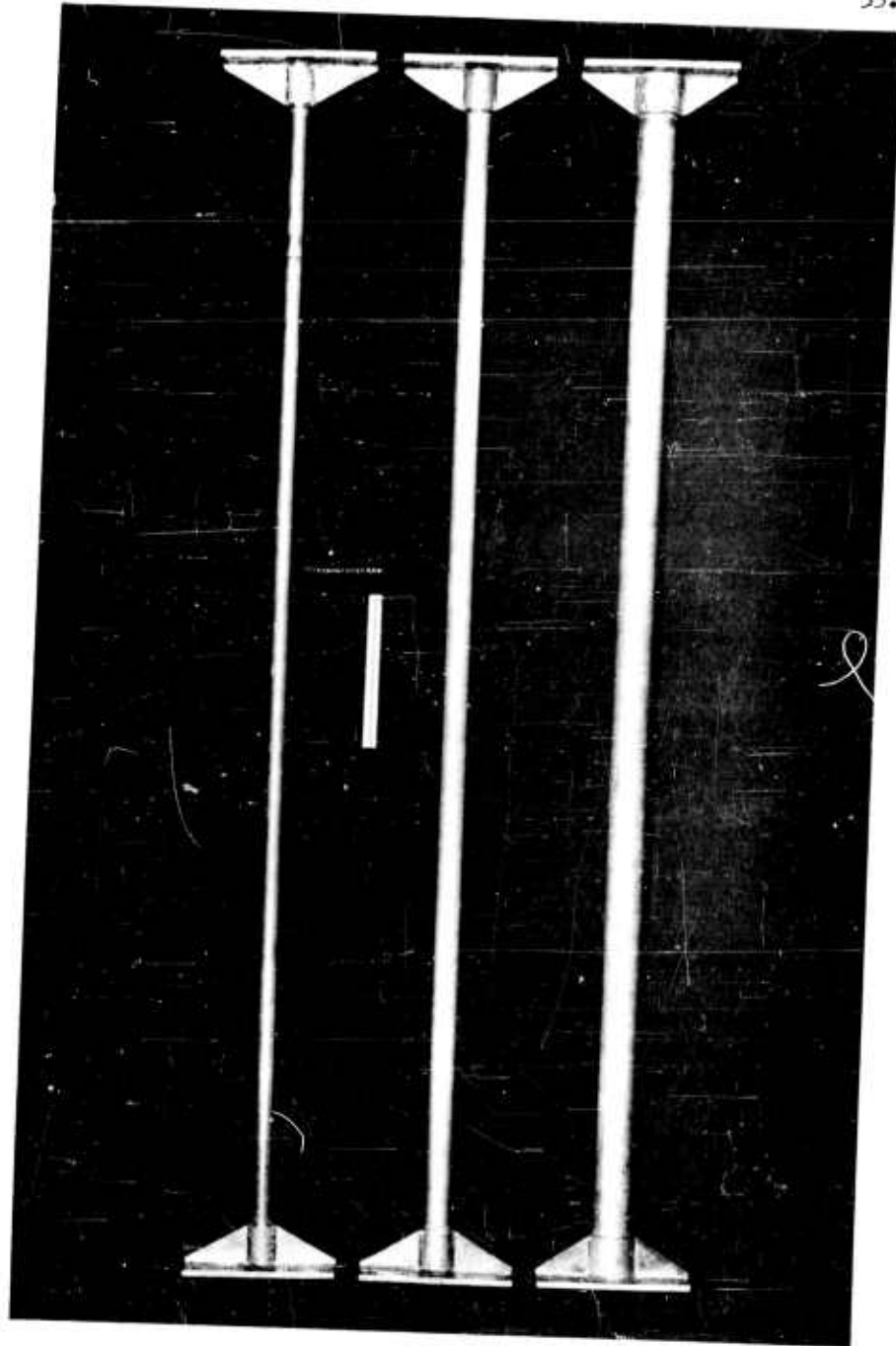
6.2 Test Apparatus

a) Wind Tunnel

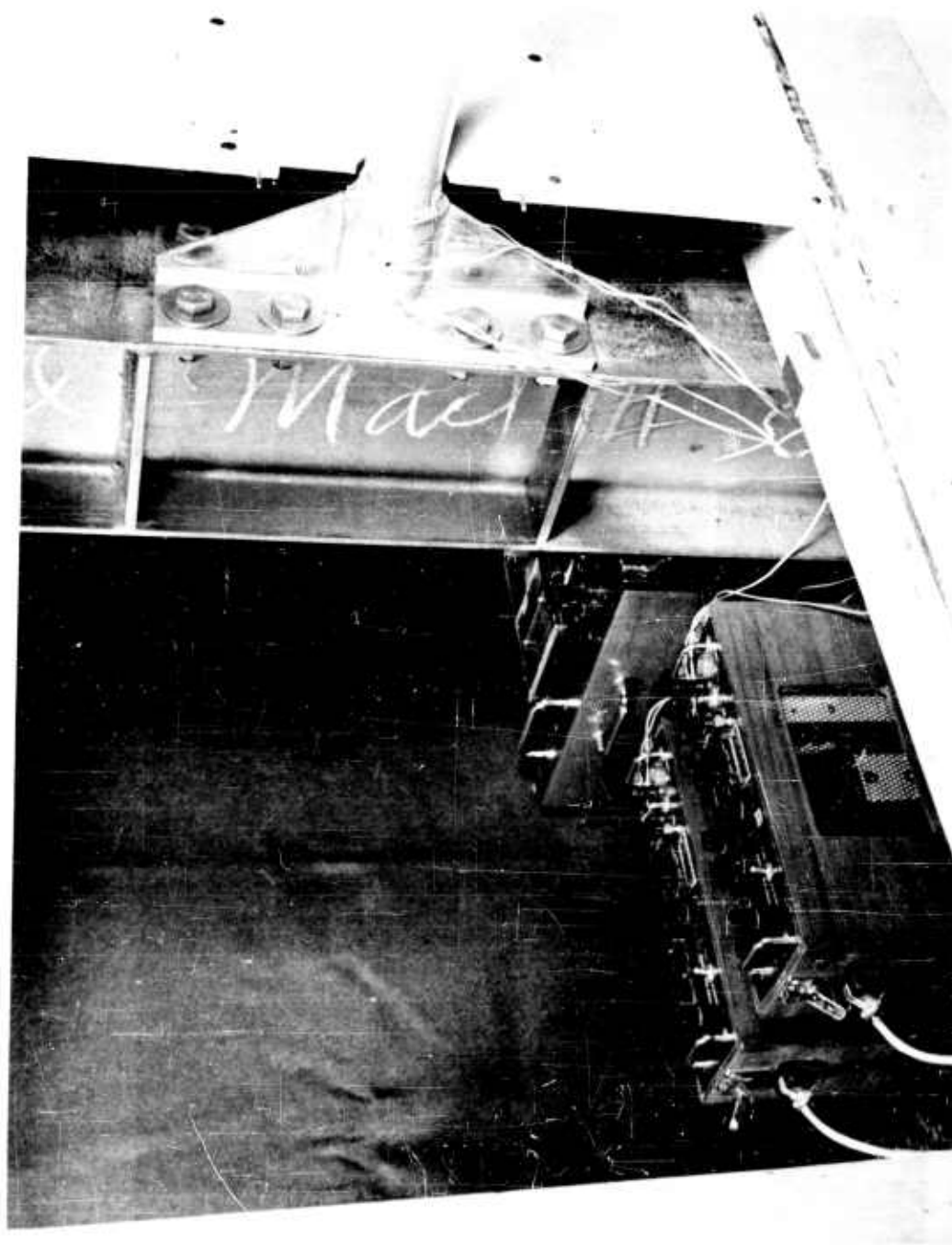
The experiments in this investigation were conducted in the low speed wind tunnel in the Aeroelastic Laboratory of M.I.T. This tunnel is of the closed-circuit



Photograph 5.2 : 4" ϕ Spring-Supported Cylinder (Looking Upstream)



Photograph 5.3 : Members M1



Photograph 5.4 : Member Mlb - End Connection EC-1

type having a $5\frac{1}{2}'$ x $7\frac{1}{2}'$ rectangular test section and a velocity range of 10 to 100 mph. Screens in front of the transition section served to reduce the scale of turbulence at the test section to approximately 0.5%.

b) Pitot-Static Equipment

Pitot-static equipment was used for measuring wind velocities for the purpose of calibrating the tunnel controls and for determining the blockage effects of test members. A Prandtl (Göttingen) type Pitot tube with an instrument coefficient of 1.00 was used in conjunction with an alcohol manometer having vernier divisions of 0.001 inch of alcohol.

c) Oscillographs

Two types of oscillographs were used for recording the signals from the electrical gages in these experiments. A Sanborn oscillograph was used wherever feasible because the traces are immediately available for visual inspection. In cases where the frequencies of the signals exceeded the capacity of the Sanborn, a Heiland oscillograph was used.

d) RMS Equipment

In Phase A a voltmeter analyzer arrangement was used to obtain standard values of \bar{C}_K . This set-up consisted of an AC Ballantine electronic voltmeter in combination with a DC voltmeter shunted across the recording galvanometer. The former meter was used to determine values of \bar{C}_K , and the latter meter provided a means of static load calibration.

e) Force Transducer

The force transducer used in Phase A is basically a compression force load cell with a 25 lb. working range. The load cell was modified for measuring alternating tension and compression forces, however, by precompressing the force resisting element and attaching a suitable adaptor to the force probe. When this was done, the range of the instrument was ± 12.5 lb.

f) Accelerometers

The twin accelerometers used in Phase B tests were ± 50 g units having natural frequencies of 650 cps. Both the accelerometers and the load cell contain four-arm balanced bridges consisting of unbonded strain gages.

g) Bonded Strain Gages

SR-4 Bonded Strain Gages, type A-7, were used in the tests of Phase C to measure vibrational fiber strains. These gages have resistances of 120 ohms \pm and gage factors of 2.0 \pm .

h) Miscellaneous Apparatus

Static load deflections in Phase C were measured with a standard Ames dial with 1/1000 inch divisions and 0.3 inch travel.

A torque wrench having interchangeable sockets and a torque range of ± 150 ft-lb was utilized for tightening bolted connections in Phases B and C.

Joint rotations of fixed-end connections were checked in the static load tests of Phase C using a surveyor's transit and a mirror-scale arrangement for magnifying readings.

VII TESTING PROCEDURES

7.1 Tests on Stationary Cylinders

After calibrating the transducer, the bare cylinders were mounted in the tunnel and subjected to steady wind speeds in 5 mph increments. At each velocity an oscillograph record was taken, examples (below and above the critical N_R) of which are shown in Figures A-2 and A-5 of Appendix A. For certain of the bare cylinders, RMS galvanometer voltages were recorded, using the RMS equipment described previously. These readings were taken simultaneously with the oscillograph traces.

A series of spoiler designs was tested on each of the stationary cylinders. Configurations consisting of 1, 2, 4, 8, and 16 windings were tested using three or more tubing diameters and three or more pitches for each size tubing. It was found that the lift forces were minimized in all cases with a configuration of four medium size windings wound at a fairly large pitch. An oscillograph record for a cylinder with spoilers is shown in Figure A-4.

During the course of spoiler optimization the fact was discovered that configurations of many small diameter windings had the effect of increasing the lift forces on stationary cylinders instead of suppressing them. Moreover, the lift forces were not only larger in magnitude, but they were more regular in frequency and also more uniform in amplitude than for the case of bare cylinders. Furthermore, this force regularity transcended the critical Reynolds number for bare cylinders. The discovery of this phenomenon prompted a study of the effects of numerous small windings in addition to the optimization of useable spoiler configurations. Figures A-3 and A-4 demonstrate the effects of many small windings applied to stationary cylinders. Note the contrasts in the oscillograph traces for Figures A-2 through A-4, which were all recorded for the same size cylinder.

7.2 Tests on Spring-Supported Cylinders

Following the calibration of the accelerometers, decay curves were recorded by displacing the spring-supported cylinders and allowing them to oscillate freely in the fundamental mode of vibration. A typical decay curve obtained in this manner is shown in Figure B-1 of Appendix B.

For each test on each bare cylinder a different spring stiffness factor was obtained by varying the lengths of the cantilever spring supports. Accelerometer readings were recorded for a series of wind speeds, and the resonant wind velocity was carefully adjusted in the critical range so that the peak amplitude of vibration was observed in each case. Figure B-2 represents an example oscillograph trace for a bare cylinder oscillating at maximum amplitude. In this record a lower gain was used on the second amplifier because the Sanborn stylus does not give accurate readings for displacements over 20 mm. Note that the vibration was quite steady at the peak amplitude.

Tests were also conducted with 8 - $3/16$ " ϕ windings attached to the cylinders, an example of which is shown in Figure B-3. Surprisingly, the amplitudes obtained in most cases were not significantly different from those obtained for

the bare cylinders, and the steadiness of the response was also about the same.

Previously optimized spoiler configurations dramatically reduced the response of the spring-supported cylinders. Compare the oscillograph record of Figure B-4 with that of Figure B-2 (the effect is even greater than a first glance indicates because different gains were used for the two records).

7.3 Tests on Flexural Members

Static load tests were carried out on each member in order to check the electrical calibrations of strain gages, to check computed stresses and deflections with actual values, and to identify regions of stress concentrations at the supports.

Decay curves for the fundamental modes of vibration, an example of which is shown in Figure C-1 of Appendix C, were obtained by striking the members and recording the response in terms of gage strains. Because the rate of decay varied with amplitude in some cases, curves were obtained for a series of gain settings in order to assure that the applicable damping coefficient would be available for response calculations in the wind loading tests.

The bare members were subjected to the range of wind velocities as in the previous tests, and fundamental modes of vibration were readily developed at or near the predicted critical wind speeds. Figure C-2 shows the response of a member vibrating at maximum amplitude, the Sanborn record for which was made at two paper speeds. In the more flexible members the second and even the third modes of vibration were developed with similar ease. The layouts of strain gages were oriented to the first mode, however; so no quantitative results are reported for these higher modes.

Optimum spoilers were applied to the members over various portions of their lengths. The length increments tested were 100%, 80%, 60%, 40%, and 20% of the lengths of the members. When the spoiler lengths were less than 100% of the member lengths, they were applied at locations which represented the most efficient regions for suppressing the exciting forces. Figures B-3 and B-4 depict the response of a cantilever with spoilers over 100% and 40% of its length. Note the attenuator setting, compared to Figure B-2.

Because the evaluation of Phase C data required the use of the modulus of elasticity of the material, stress-strain curves were obtained from load tests carried out on cylindrical compression specimens cut from certain of the Phase C members.

VIII TEST RESULTS

8.1 General

Appendices A through C contain the plotted results of the laboratory experiments in this investigation. The test results will be described in this section, making continuous reference to these appendices.

8.2 Results of Tests on Stationary Cylinders

Values of peak C_K for bare cylinders and with spoilers are shown in Figure A-7, and Figure A-8 summarizes all of the C_K curves obtained from Phase A tests. The C_K curves for individual cylinders are typified by a "tail" effect, shown by dashed lines, which lead up to the common curve of C_K - vs - $\log_{10} N_R$ in

Figure A-7. These "tails" are apparently due to the fact that the vortex shedding phenomenon is not strong and stable at low wind velocities.

The C_K curve for optimum spoilers is quite low and fairly flat. On the other hand, the curves for 8 and 16 small windings stand well above the curve for bare cylinders, but all have somewhat similar shapes. The plot of standard \bar{C}_K shown in Figure A-8 appears to level off at approximately 0.10.

Strouhal numbers are plotted for all members in Figures A-9 and A-10. The combined plot of N_S - vs - $\log_{10} N_R$ for bare cylinders is found to rise abruptly at a Reynolds number of approximately 3.6×10^5 . In contrast, the N_S curve for cylinders with numerous windings continues horizontally through the critical region of N_R .

Figure A-11 demonstrates in a general manner the influence of the number of windings on spoiler effectiveness. Configurations with four windings repeatedly gave maximum suppression of lift forces.

Figure A-12 illustrates the influence of winding diameter on spoiler effectiveness for the 3" ϕ cylinder. The knee of this type of curve occurs consistently at a spoiler diameter of roughly $d/12$ to $3d/32$. The curves rise toward $C_{KS}/C_{KB} = 1$ for small diameter windings and appear to rise only slowly for large size windings.

The relative insensitivity of the phenomenon to spoiler pitch is shown in Figure A-13 for the 6" ϕ cylinder. A wide effective range exists from a pitch of approximately $8d$ to about $16d$. The most effective pitch appears to be at about $12d$.

Thus, optimum spoilers may be assumed to be 4 windings of size $d/16$ or larger at a pitch of $12d$.

8.3 Results of Tests on Spring-Supported Cylinders

An example plot of the response of the 5" ϕ cylinder is presented in Figure B-5 in the form of (NDD) - vs - wind velocity. The plot compares the response of the bare cylinder to the response with both spoilers and anti-spoilers attached. In all cases the resonant response was reduced dramatically by the addition of spoilers.

Values of the standard \bar{C}_K at resonance are plotted - vs - $\log_{10} N_R$ for bare cylinders in Figure B-6 and for cylinders with 8 - $3/16$ " ϕ windings in Figure B-7. The resulting plots of \bar{C}_K for these two cases are not significantly different from each other. The curve of \bar{C}_K for bare cylinders is lower than that for C_K in Phase A, and the data is rather scattered. The "tail" effect is again apparent for resonance at low velocities. The general trend of the \bar{C}_K curve is to decrease to a rather low value in the vicinity of the critical Reynolds number of 3.6×10^5 .

Figures B-8 and B-9 represent plots of Strouhal numbers calculated from the resonant response of bare cylinders and of cylinders with numerous windings, respectively. There appears to be no difference between the two plots for the vibrating cylinders. In both cases there does not seem to be a rise in N_S at the critical N_R , but instead, there appears to be some tendency to continue horizontally. There are not enough points at high Reynolds numbers to draw a definite conclusion, but there is at least an indication of a trend. The fact

that the data is more scattered than for the stationary cylinders may be due to the ability of the vibrating cylinders to control the shedding frequencies at resonance to some degree.

The (ILF)'s calculated for the cylinders at resonance are plotted - vs - (ASF) in Figure B-10. A similar curve for v/v_c is practically identical to Figure B-10. Thus, the supposition that $(ILF)^2 = C_F/v_c$ is verified, and the (ASF) proves itself to be a valid basis for determining the degree of self-amplification.

8.4 Results of Tests on Flexural Members

Example response curves for a bare test member and for the member with spoilers over varying portions of its length are exhibited in Figure C-5. For most of the members tested, vibration amplitudes were suppressed to approximately 10% by optimum spoilers wound over portions as short as 20% of the member lengths. A spoiler length of $0.40 \ell_m$ gave the best results in most cases. It must be pointed out, however, that spoilers were not as effective for the small diameter members as for the larger diameter members, and they were not as effective on cantilever members as they were on members supported at both ends. Thus, it appears that the larger the (NDD) the less the effectiveness of the spoilers. Therefore, spoilers should be most efficient on fixed-end members, as shown by the results of the Phase C tests.

Figure C-6 shows calculated values of the standard \bar{C}_K at resonance for bare members. A smooth curve is drawn through the predominant pattern. It is difficult to say whether this curve should continue to drop or whether it should level off in the vicinity of $N_R = 10^5$. The \bar{C}_K at lower Reynolds numbers appears to level off at a value of 0.48.

The Phase C Strouhal numbers appear in Figure C-7. It is readily apparent that these values check very well with the plot of N_S obtained from stationary cylinders in Phase A.

The curve for (ILF) for the vibrating members is shown in Figure C-8. The data is somewhat more scattered, and the curve is definitely lower than for the cylinder tests (shown by dashed lines) discussed above. The latter discrepancy is probably due to phase differences along the lengths of the members which do not arise along the lengths of cylinders oscillating as rigid bodies.

From load tests on compression specimens a value of 10.72 ksi was obtained for the modulus of elasticity of 6061 T6 aluminum tubing.

8.5 Correlations among the Results of the Three Phases and Comparisons with Previously Published Information

In Figure 8.1 all of the C_K and \bar{C}_K curves determined in this investigation are represented by the solid lines. Isolated points and dashed lines denote the values of C_K reported by previous investigators, and Table 8.1 summarizes published values for C_K and notes whether they are experimental or analytical.

Figure 8.1: COMPARISON OF RESULTS OF PRESENT VALUES OF C_K
WITH PREVIOUSLY REPORTED EXPERIMENTAL VALUES OF C_K
FOR STATIONARY CYLINDERS

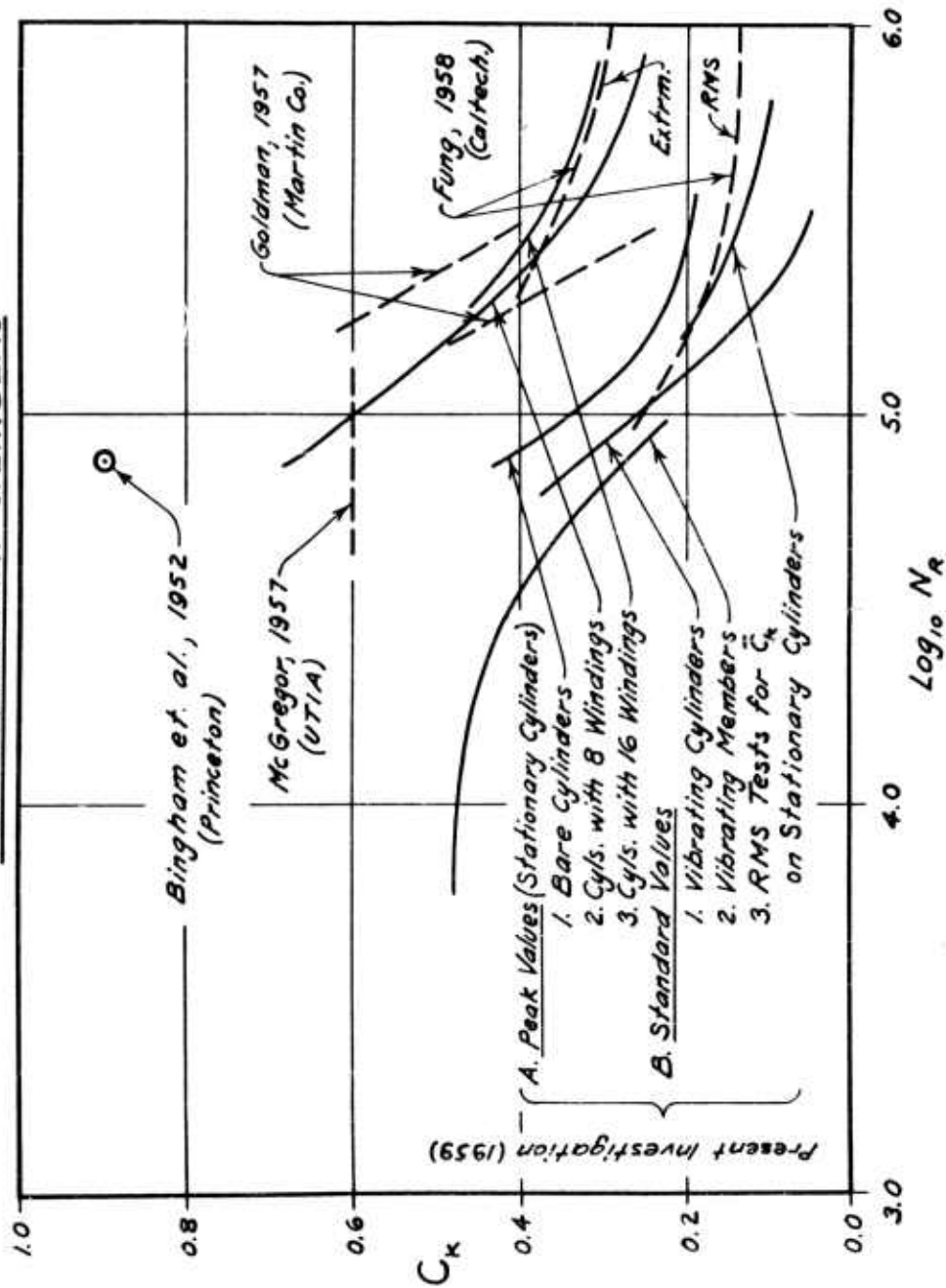


Table 8.1: Previously Published Values for C_K

Date	Source	Ref.	Experimental (E) or Analytical (A)	N_R	C_K
1932	Tyler	-	E	-	0.61 -1.05
1935	Pagon	-	-	9.6×10^5	1.00
1935	Reudy	19	A	-	0.93
1935	Schwabe	21	E	735	0.45
1942	Landweber	-	A	-	3.42
1946	Steinman	24	A	-	1.71
1952	Bingham	2	E	7.6×10^4	0.90
1956	Phillips	-	-	40 -160	0.76
1957	Goldman	12	E	(See Fig. 8.1)	
1957	McGregor	14	E	4.5×10^4 -1.3×10^5	0.60
1958	Fung	11	E	(See Fig. 8.1)	

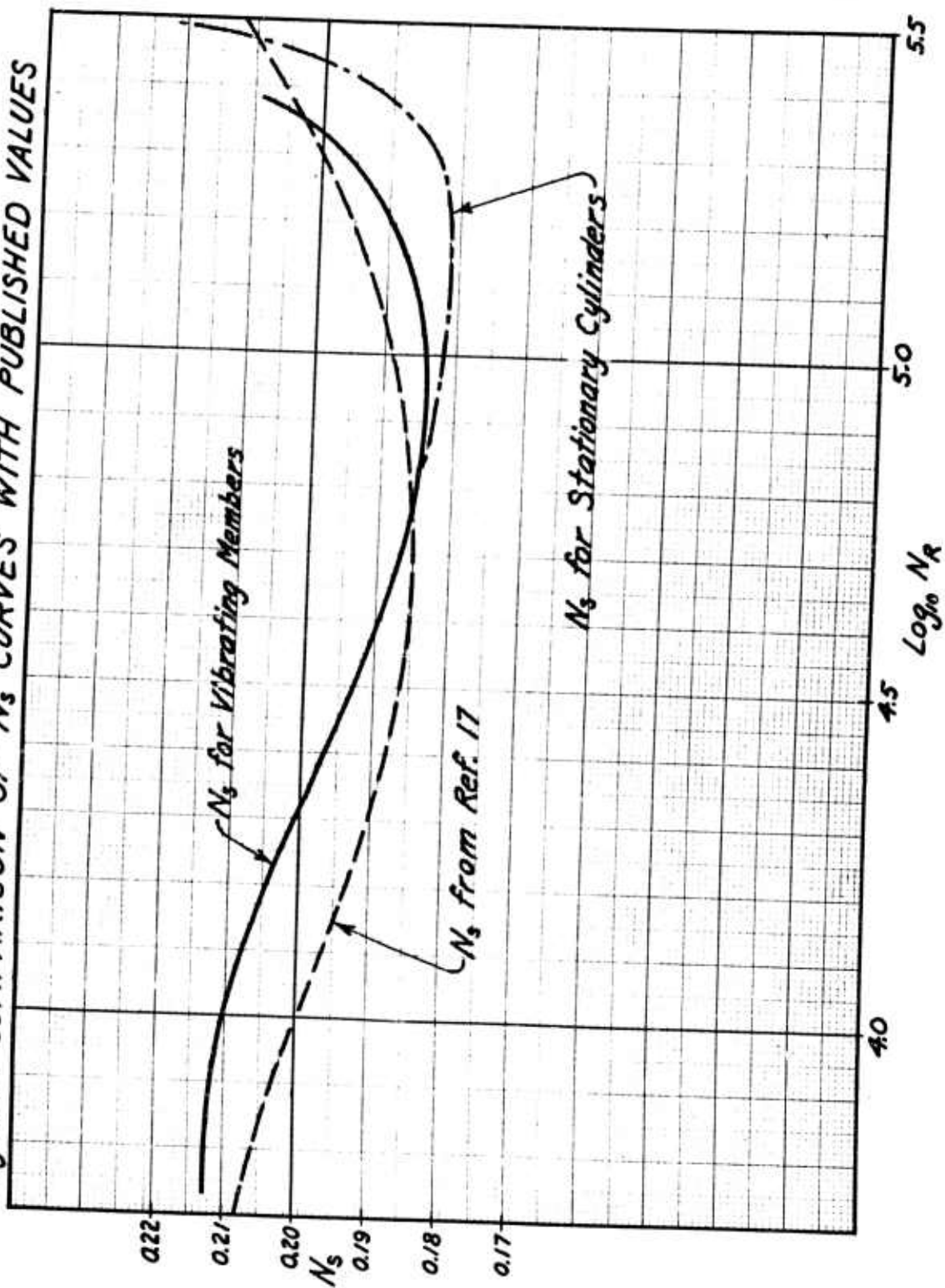
The three curves for standard \bar{C}_K from each of the three phases merge into each other fairly well except where the curve for vibrating cylinders descends to a low value in the vicinity of $N_R \approx 3 \times 10^5$. Moreover, the \bar{C}_K curves show good correlation with Fung's curve for RMS C_K shown in Figure 8.1.

The peak C_K curves for 8 and 16 windings correspond very closely to the values given by McGregor and Goldman and the curve given by Fung for extreme values of C_K . All of these published values are probably extreme values, although McGregor and Goldman do not mention this point. It appears, then, that roughening the surfaces of cylinders in the present investigation has the effect of raising the peak values of C_K to approximately the same values reported by other experimenters. Whether differences in tunnel turbulences has a bearing on this behavior remains an open question. The peak C_K curve for bare cylinders probably depends upon the characteristics of the wind tunnel for its relative location. Neither this curve nor the other peak C_K curves have any practical value for the purpose of calculating the response of a vibrating member. It is the \bar{C}_K curve which assumes great importance in this respect.

Curves for N_s obtained in this investigation are compared in Figure 8.2 with a curve (shown dashed) derived from Ref. 8 which represents a summary of the works of several previous investigators. In general, the curves check fairly well, and the maximum difference in ordinates is approximately 5%.

Considering the results of spoiler optimization, it is interesting to compare the tubular windings with a configuration of spiral fins, or "strakes", tested by

Fig. 8.2: COMPARISON OF N_s CURVES WITH PUBLISHED VALUES



C. Scruton and D. Walshe (Ref. 23). Scruton introduced a design consisting of three helical strakes of height up to $d/8$ and set at a pitch of $15d$. He states that the strakes must be of sufficient height and number and that their helical formation is an essential feature. He further states that their effectiveness increases with size but that they need be no larger than $1/8d$. In addition, he reports that the result is not sensitive to pitch and that a single strake is not effective because of the opposite-side characteristic of vortices. Scruton also states that any number of strakes can be used, but he does not support this remark with experimental evidence. It is apparent that the tubular windings optimized in the present investigation show characteristics similar to Scruton's strakes, with some reservations.

IX DESIGN CRITERIA, PROCEDURES, AND APPLICATIONS

9.1 General

The general approach to presenting design and/or analysis tools for tubular aluminum members of antenna space frames is as follows:

- a) Design criteria, drawn from the results of the laboratory experiments, are summarized and applied.
- b) The members are separated into categories of end fixities - - - pinned, fixed, and selected conditions of intermediate elastic supports.
- c) A specific wall thickness of $1/16$ th of the outside diameter is chosen for each tube size from $2''\phi$ to $8''\phi$ in increments of one inch. This selection of member sizes is representative of proportions used in practical design and has also the convenient property of geometric similarity. The exception to this rule is the $7''\phi \times 3/8''$ tube, which was chosen because the $7/16''$ thickness is not manufactured. The sizes selected, then, are the following:

$2'' \phi \times 1/8''$	$6'' \phi \times 3/8''$
$3'' \phi \times 3/16''$	$7'' \phi \times 3/8''$
$4'' \phi \times 1/4''$	$8'' \phi \times 1/2''$
$5'' \phi \times 5/16''$	

Behavior of members of other diameters and wall thicknesses may also be interpolated from the charts presented herein.

- d) Charts are constructed which can be used to obtain natural frequencies, critical velocities for resonance, Reynolds numbers at resonance, applicable values of \bar{C}_x , and resulting maximum flexural stresses in terms of incremental deflection factors, (IDF), for any practical-sized bare member. The manner of constructing the charts is described, and examples for use of the charts are given.
- e) A second set of charts provide a graphical means of determining the effect of self-amplification due to the vibration itself. These charts give the values for the aeroelastic suppression factor, (ASF), the incremental load factor, (ILF), and the incremental deflection factor, (IDF), for various conditions of end fixity. In addition, the values of (IDF) are applied to the values of $\sigma_{\max} = \phi$ (IDF) obtained from the first set of charts, producing values of maximum flexural stress

in kips per sq. in. as the end result.

f) A recommended method of approach is given for the design of antenna members against lateral vibrations due to wind. The use of spoilers is discussed, and effective configurations are specified.

g) Applications to existing structures are also considered, and an example study of an actual structure is briefly outlined.

9.2 Design Criteria

a) Strouhal Number

The range of Reynolds numbers of interest for the members of antenna structures is approximately from 10^4 to 10^6 . Within this range the Strouhal number varies, but design procedures are simplified somewhat assuming N_s to be constant. The average value of $N_s = 0.19$ will be used as a design criterion in this report (see Figure C-7).

b) Lift Coefficient

A curve for standard Karman lift coefficient, \bar{C}_K , must be specified for design purposes. Of the plots shown in Figure 8.1, the \bar{C}_K curves from the vibration tests of Phases B and C represent the appropriate values. The fact that the Phase B curve descends to a low value in the vicinity of the critical Reynolds numbers conforms to the stochastic response calculations presented previously in Section 4.3. However, Figure C-6 shows some deviation of flexural members from this trend. Therefore, in order to provide conservatism in the design, a combination of the Phase C curve for \bar{C}_K and Fung's RMS curve at super-critical Reynolds numbers will be used in the graphical analysis charts of this section.

c) Self-Amplification

The (ILF) curve from member tests shown in Figure C-8 will be used for predicting the degree of self-amplification of actual structural members. An upper limit of (ILF) = 1.40 will be selected for the case of zero damping. This value is set somewhat below Steinman's limit of 1.45 (see Section 3.4) because of the phase differences discussed previously.

9.3 Analysis Charts

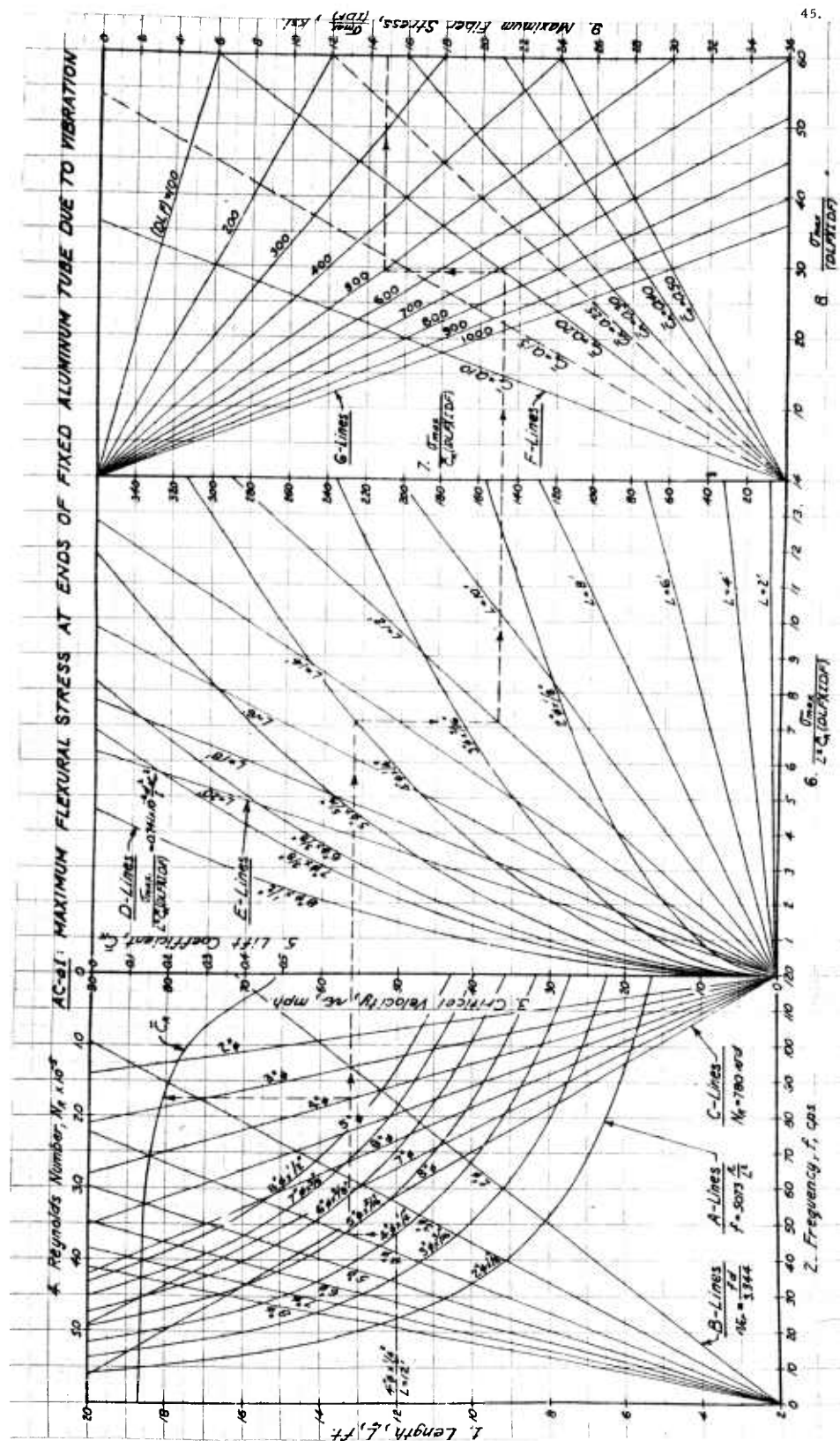
a) Charts for Resonant Frequencies, Velocities, and Stresses (AC-a1 to AC-a4)

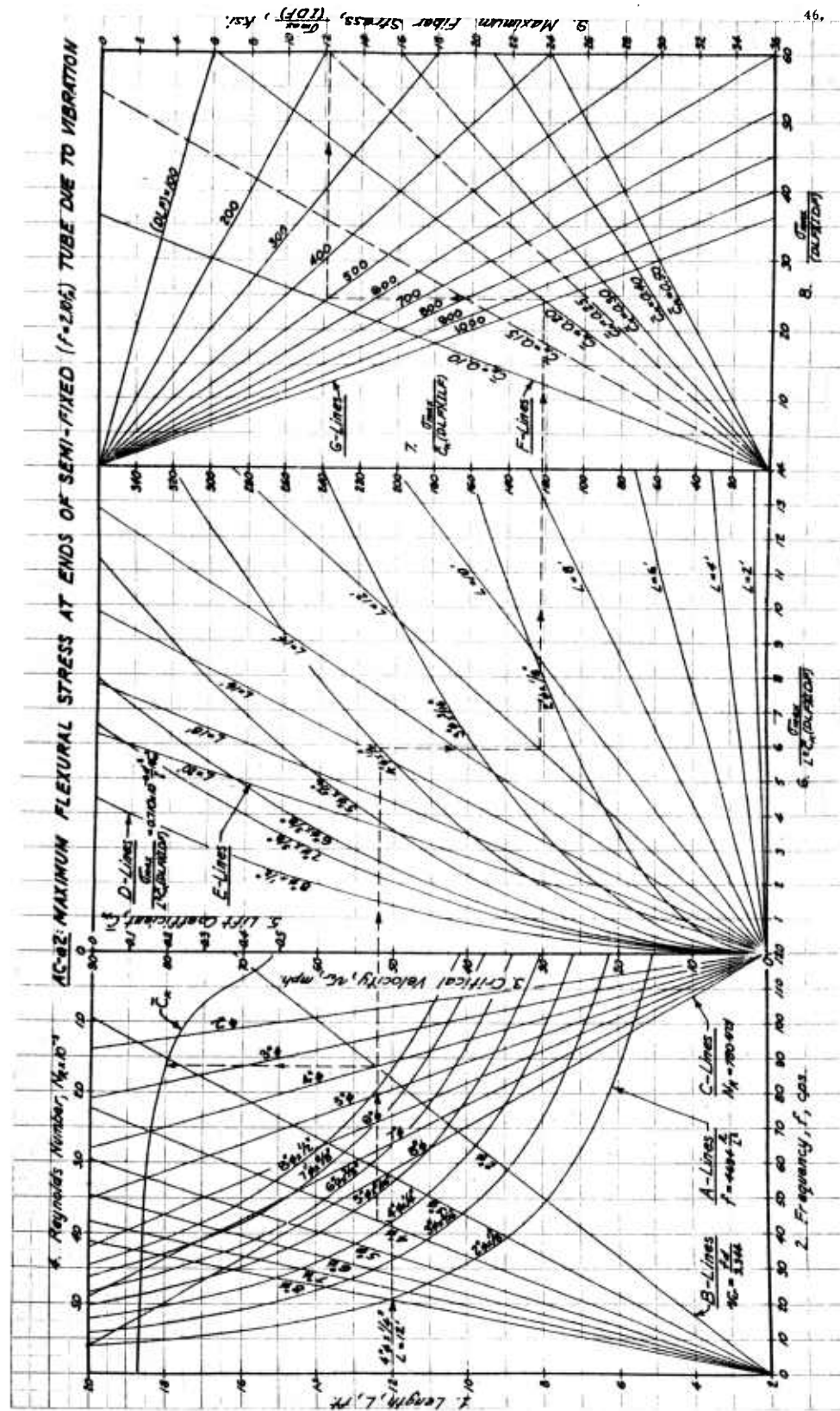
(1) Construction of Charts (AC-a)

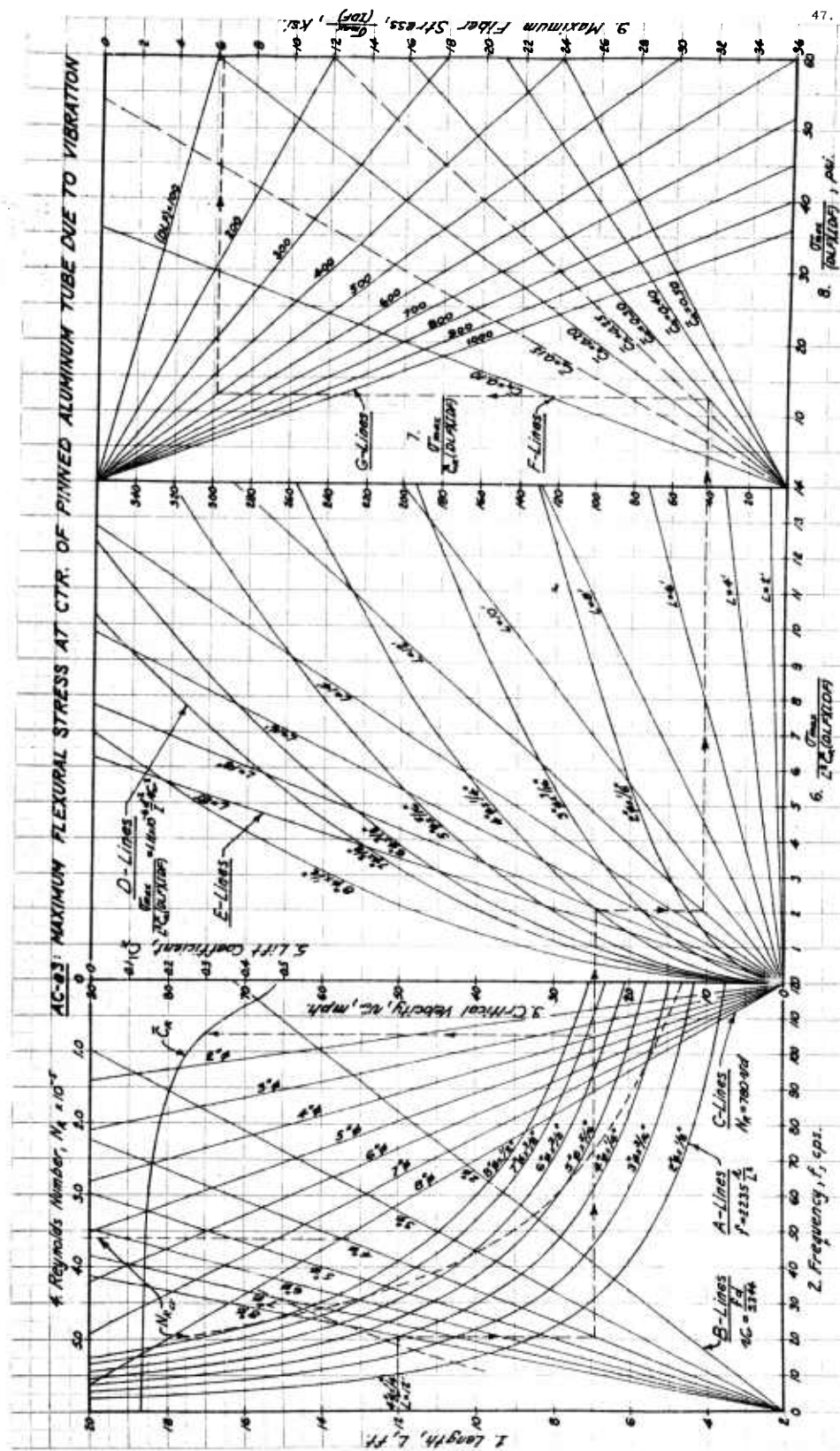
A-Lines are plots of fundamental frequencies of vibration, $f = \phi(r, L)$, - vs - length of member for various member sizes.

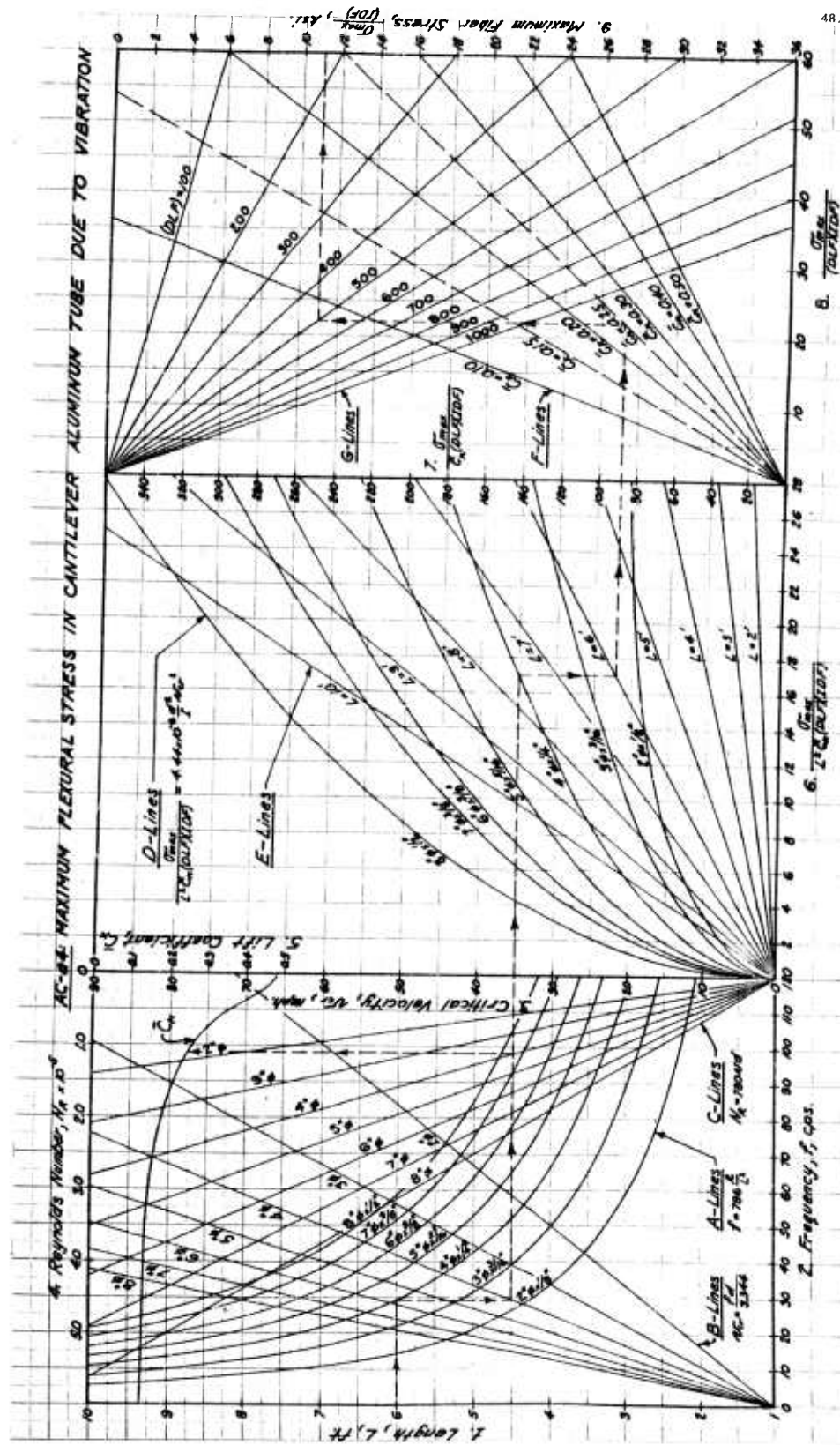
B-Lines are plots of vortex shedding frequencies, $f_v = N_s \frac{V}{D}$, using $N_s = 0.19$ determined from the experiments. The shedding frequencies and natural frequencies are matched on scale 2 to give the critical velocities directly on scale 3.

C-Lines represent the corresponding Reynolds numbers, $N_R = 780 \frac{V}{d}$, at resonance - vs - critical velocities. The experimentally-determined plot of the standard lift coefficient, \bar{C}_K , is plotted - vs - Reynolds numbers with ordinates shown by scale 5.









D-Lines are partial solutions for the maximum fiber stress, in the form of

$$\frac{\sigma_{\max}}{L^2 \bar{C}_K (DLF) (IDF)} = \phi (v_{cr}, d, I), -$$

vs - the critical wind velocity.

E-Lines constitute a multiplication of $\frac{\sigma_{\max}}{L^2 \bar{C}_K (DLF) (IDF)}$ by L^2 for various lengths to obtain the expression $\frac{\sigma_{\max}}{\bar{C}_K (DLF) (IDF)}$.

F-Lines continue the process by multiplying the last expression by various values of \bar{C}_K to obtain $\frac{\sigma_{\max}}{(DLF) (IDF)}$ on scale 9.

G-Lines represent a final graphical multiplication for a variety of dynamic load factors to give $\frac{\sigma_{\max}}{(IDF)}$ on scale 9.

Thus, the charts provide a direct solution for the maximum flexural stress in a member subjected to a critical wind velocity and a semi-automatic solution for the stress in a member subjected to a wind velocity, somewhat greater than the critical, which causes the maximum stable amplitude of vibration. If the member is very stiff, the amplitude will be small, and the two cases will be approximately the same. In general, however, the effect of self-amplification must be evaluated by making use of the second set of charts, (AC-b). The latter charts yield the applicable values of (IDF)'s and increase the output of charts (AC-a) accordingly.

(2) Procedure for Using Charts (AC-a)

In order to use the analysis charts it is necessary to know (or to estimate) the member size, length, condition of support, and the logarithmic damping decrement. The following steps describe the procedure for using the charts:

- a. Select the appropriate chart (depending upon the conditions of support) and enter scale 1 with the member length, in feet. Draw a horizontal line to the A-Line corresponding to the appropriate member size. The abscissa of this point is the natural frequency of the fundamental mode of vibration (scale 2).
- b. Draw a vertical line to intersect the B-Line representing the outside diameter of the member. The critical wind velocity is given by the ordinate of this point (scale 3).
- c. Draw a horizontal line to meet the C-Line also representing the outside diameter. The Reynolds number at resonance may then be read on scale 4, and the corresponding von Kármán lift coefficient may be found by projecting a vertical line to the \bar{C}_K curve and reading the value on scale 5.
- d. Extend the horizontal line of step c to the D-Line for the member size.
- e. Draw a vertical to the E-Line for the known span length. The ordinate of this point is given on scale 7 as the fiber stress for a statically applied load with $\bar{C}_K = 1$.

f. Draw a horizontal line to the F-Line which corresponds to the value of \bar{C}_K found in step c. The abscissa of this point is the fiber stress (scale 8) for a statically applied load determined by the indicated value of \bar{C}_K .

g. Draw a vertical line to the G-Line of the dynamic load factor corresponding to the logarithmic damping decrement for the structure. The ordinate of this point is found on scale 9 to be the maximum flexural stress, magnified by the (DLF), but not yet modified by the incremental deflection factor, (IDF).

h. A separate calculation for the (IDF) may be made for each member in the following manner:

(1) Compute the aeroelastic suppression factor, (ASF), for the member, using the expressions developed previously.

(2) Obtain the $(ILF)_{\max}$ from the experimental plot from member tests.

(3) Compute the (IDF) for the member using the expressions developed for this application.

An alternative procedure for finding the (IDF) is to make use of the second set of charts, (AC-b), constructed for this purpose. The latter charts are explained in the next section.

b) Charts for Determining Effects of Self-Amplification
(AC-b1 to AC-b4)

(1) Construction of Charts (AC-b)

A-Lines represent a partial calculation of the aeroelastic suppression factor, (ASF), for various wall thickness-diameter ratios. The partial product, given on scale 2, does not include the effect of the lift coefficient, \bar{C}_K .

B-Lines serve to divide the abscissae on scale 2 by the indicated values of \bar{C}_K to give (ASF) on scale 3. The experimental plot of the corresponding incremental load factor for a vibrating member then provides (ILF) on scale 4. The (ILF) is then squared graphically as shown by the $(ILF)^2$ curve and scale 5.

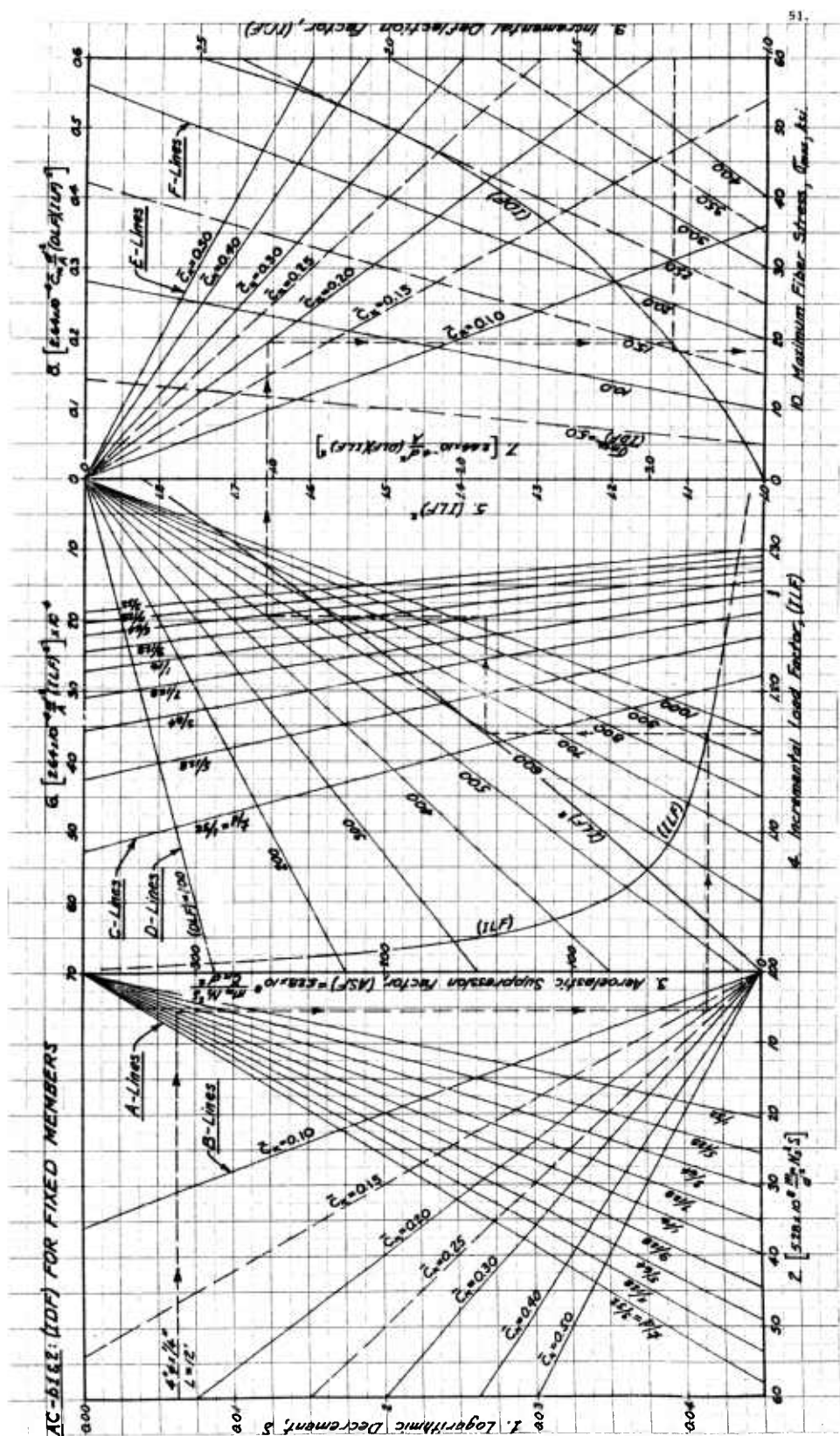
C-Lines constitute a partial solution for the second denominator term in the appropriate expression for the incremental deflection factor, (IDF), depending upon the thickness-diameter ratio of the member.

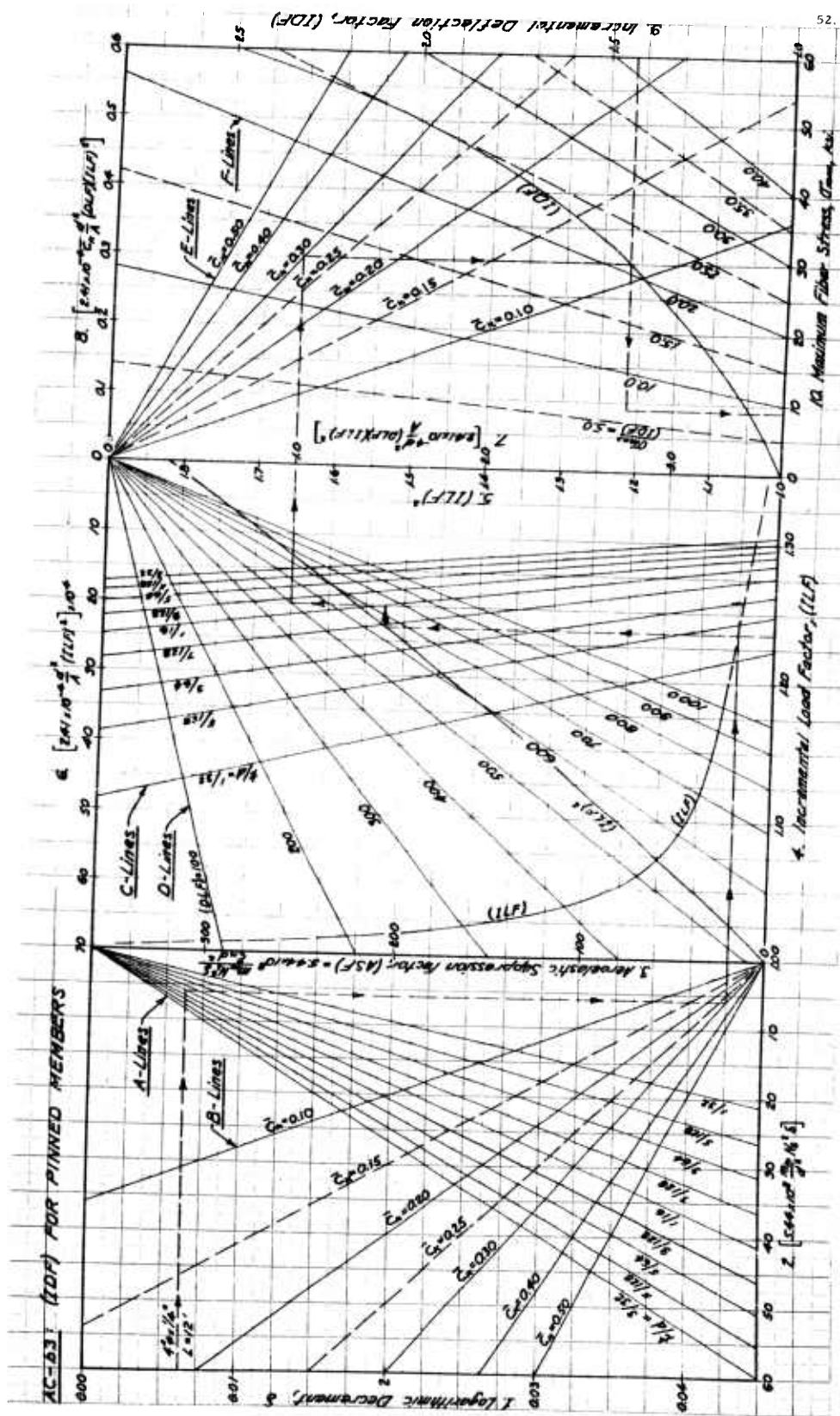
D-Lines multiply the C-Lines by various values of dynamic load factors, (DLF).

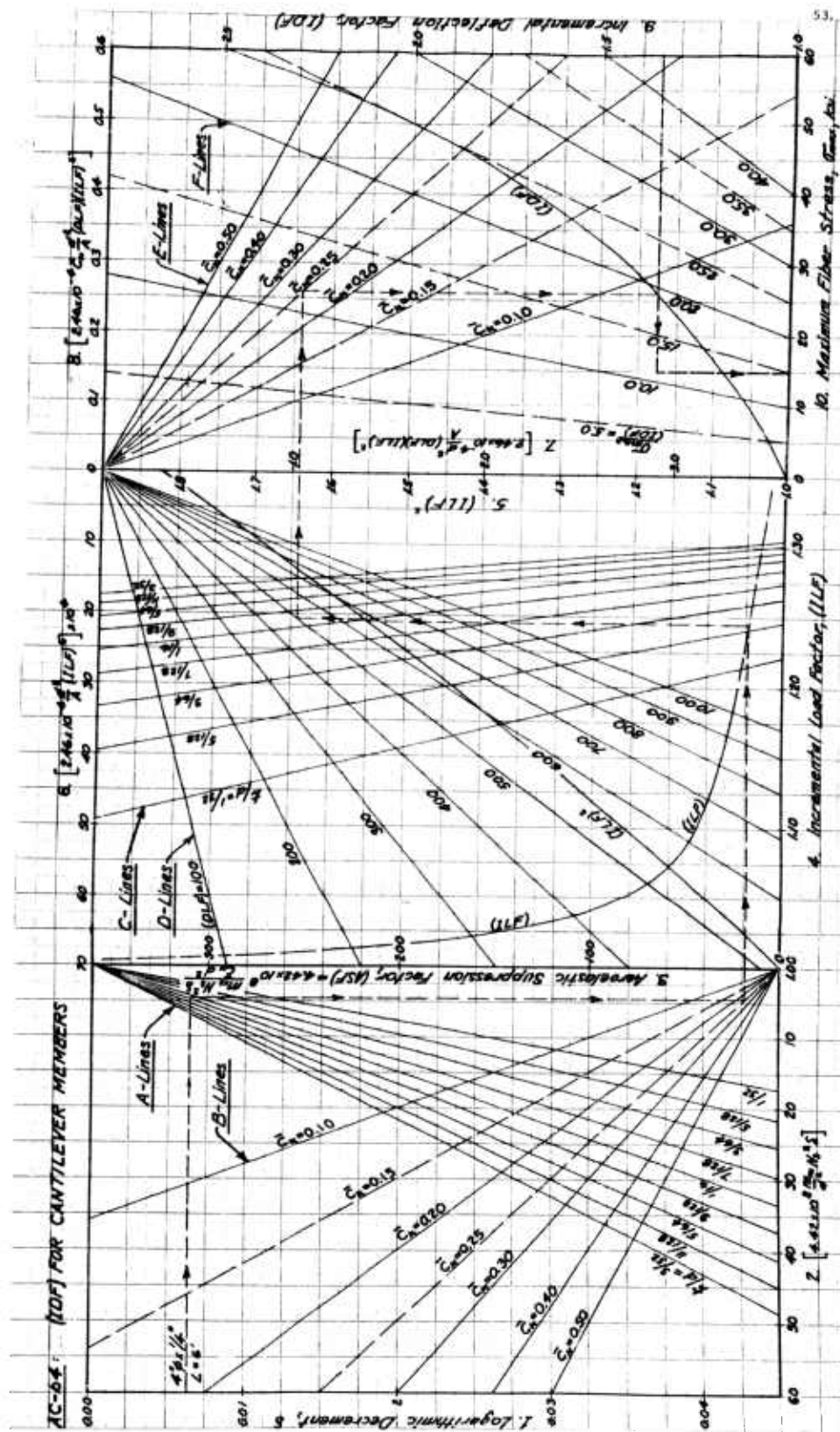
E-Lines bring in the additional effect of \bar{C}_K and give the second denominator term on scale 8. The curve for (IDF) converts scale 8 to scale 9 by means of the equation.

$$(\text{Scale } 9) = \frac{1}{1 - (\text{Scale } 8)}$$

F-Lines perform the function of multiplying the (IDF)'s by the values of $\frac{\sigma_{\max}}{(IDF)}$ (AC-a). The end results of the operation are the values of the maximum flexural stress, σ_{\max} , in kips per sq. in., given on scale 10.







(2) Procedure for Using Charts (AC-b)

The use of the second set of charts requires the same information as is necessary for the first set. The following steps delineate the procedure for using charts (AC-b):

- a. Select the chart corresponding to the support condition of the member. Enter scale 1 with the logarithmic damping decrement, δ , and draw a horizontal line to the A-Line labelled with the thickness-diameter ratio of interest.
- b. Next, draw a vertical line to intersect the B-Line for the previously-determined value of \bar{C}_K . The ordinate of this intersection is the (ASF) on scale 3.
- c. Project a horizontal line to the experimental (ILF) curve and read the value of (ILF) on scale 4 if desired.
- d. Draw a vertical line to the $(ILF)^2$ curve.
- e. The next step is to draw a horizontal line to meet the C-Line of the appropriate thickness-diameter ratio.
- f. Draw a vertical line to the D-Line of (DLF) corresponding to δ .
- g. Trace a horizontal line to the E-Line of the known \bar{C}_K .
- h. Next, draw a vertical line to the (IDF) curve and read the value of (IDF) on scale 9.
- i. Finally, project a horizontal line to the proper F-Line (or interpolated F-Line) for the value of $\frac{\sigma_{max}}{(IDF)}$ obtained previously from charts (AC-a). The value of σ_{max} on scale 9 is the maximum vibrational fiber stress for the member under consideration.

Analysis chart (AC-b1,2) is intended for use with both the case of fixed ends and the case of semi-fixed ends with $f = 2.10 f_p$. This procedure is an approximation involving very little error because of the fact that the mode shape for the semi-fixed case is almost the same as for the fully fixed case.

When many members are to be analyzed for wind-induced vibrational stresses, it is recommended that a tabular method for organizing the results be adopted. The following items should be included in the table:

Input: Size, length, condition of support, δ , and (DLF).

Output of (AC-a): f , v_{cr} , $N_{R_{cr}}$, and $\frac{\sigma_{max}}{(IDF)}$.

Output of (AC-b): (ASF), (ILF), (IDF), and σ_{max} .

c) Quantitative Examples

The following examples are analyzed graphically by the methods described, and the solutions are traced with dashed lines on the charts.

(1) Fixed Members: (4" ϕ x 1/4" x 12'-0"; DLF = 500)

(Analysis Chart (AC-a1):

Natural frequency, $f = 47.0$ cps.

Critical velocity, $v_{cr} = 56.0$ mph.

Reynolds number, $N_R = 1.75 \times 10^5$

Lift coefficient, $\bar{C}_K = 0.20$

Fiber stress, $\frac{\sigma_{max}}{(IDF)} = 14.8$ ksi

Analysis Chart (AC-b1):

$$(ASF) = 5.28 \times 10^8 \frac{m_m N_s^2 \delta}{\bar{C}_K d^2} = 28.05$$

$$(ILF) = 1.168$$

$$(IDF) = \frac{1}{1 - 2.64 \times 10^{-4} \bar{C}_K \frac{d^2}{A} (DLF) (ILF)^2} = 1.241$$

$$max = 14.80 \times 1.241 = \underline{18.37 \text{ ksi.}}$$

(2) Semi-Fixed Members: (4" ϕ x 1/4" x 12'-0"; DLF = 500)

$$(k \ell)^2 = 2.10 (k \ell)^2_{\text{pinned}}$$

Analysis Chart (AC-a2):

Natural frequency, $f = 43.5$ cps.

Critical velocity, $v_{cr} = 52.0$ mph.

Reynolds number, $N_R = 1.63 \times 10^5$

Lift coefficient, $\bar{C}_K = 0.20$

Fiber stress, $\frac{\sigma_{max}}{(IDF)} = 12.20$ ksi.

Analysis Chart (AC-b2):

$$\left. \begin{array}{l} (ASF) \\ (ILF) \\ (IDF) \end{array} \right\} \text{Assumed to be same as for fixed case.}$$

Thus,

$$\sigma_{max} = 12.20 \times 1.241 = \underline{15.14 \text{ ksi.}}$$

(3) Pinned Member: (4" ϕ x 1/4" x 12'-0"; DLF = 500)

Analysis Chart (AC-a3):

Natural frequency, $f = 20.5$ cps.

Critical velocity, $v_{cr} = 24.5$ mph.

Reynolds number, $N_R = 7.5 \times 10^4$

Lift coefficient, $\bar{C}_K = 0.30$

Fiber stress, $\frac{\sigma_{max}}{(IDF)} = 6.20$ ksi.

Analysis Chart (AC-b3):

$$(ASF) = 5.44 \times 10^8 \frac{m_m N_s^2 \delta}{\bar{C}_K d^2} = 19.25$$

$$(ILF) = 1.235$$

$$(IDF) = \frac{1}{1 - 2.41 \times 10^{-4} \bar{C}_K d^2 (DLF) (ILF)^2} = 1.422$$

Thus,

$$\sigma_{max} = 1.422 \times 6.20 = \underline{\underline{8.82 \text{ ksi}}}$$

(4) Cantilever Member: (4" ϕ x 1/4" x 6'-0"; DLF = 500)

Analysis Chart (AC-a4):

Natural frequency, $f = 29.0$ cps.

Critical velocity, $v_{cr} = 35.0$ mph.

Reynolds number, $N_R = 1.10 \times 10^5$

Lift coefficient, $\bar{C}_K = 0.25$

Fiber stress, $\frac{\sigma_{max}}{(IDF)} = 11.00$ ksi.

Analysis Chart (AC-b4):

$$(ASF) = 4.42 \times 10^8 \frac{m_m N_s^2 \delta}{\bar{C}_K d^2} = 18.85$$

$$(ILF) = 1.246$$

$$(IDF) = \frac{1}{1 - 2.46 \times 10^{-4} \bar{C}_K d^2 (DLF) (ILF)^2} = 1.35$$

Thus,

$$\sigma_{max} = 11.00 \times 1.35 = \underline{\underline{14.85 \text{ ksi}}}$$

9.4 Procedure for Design Against Lateral Vibrations

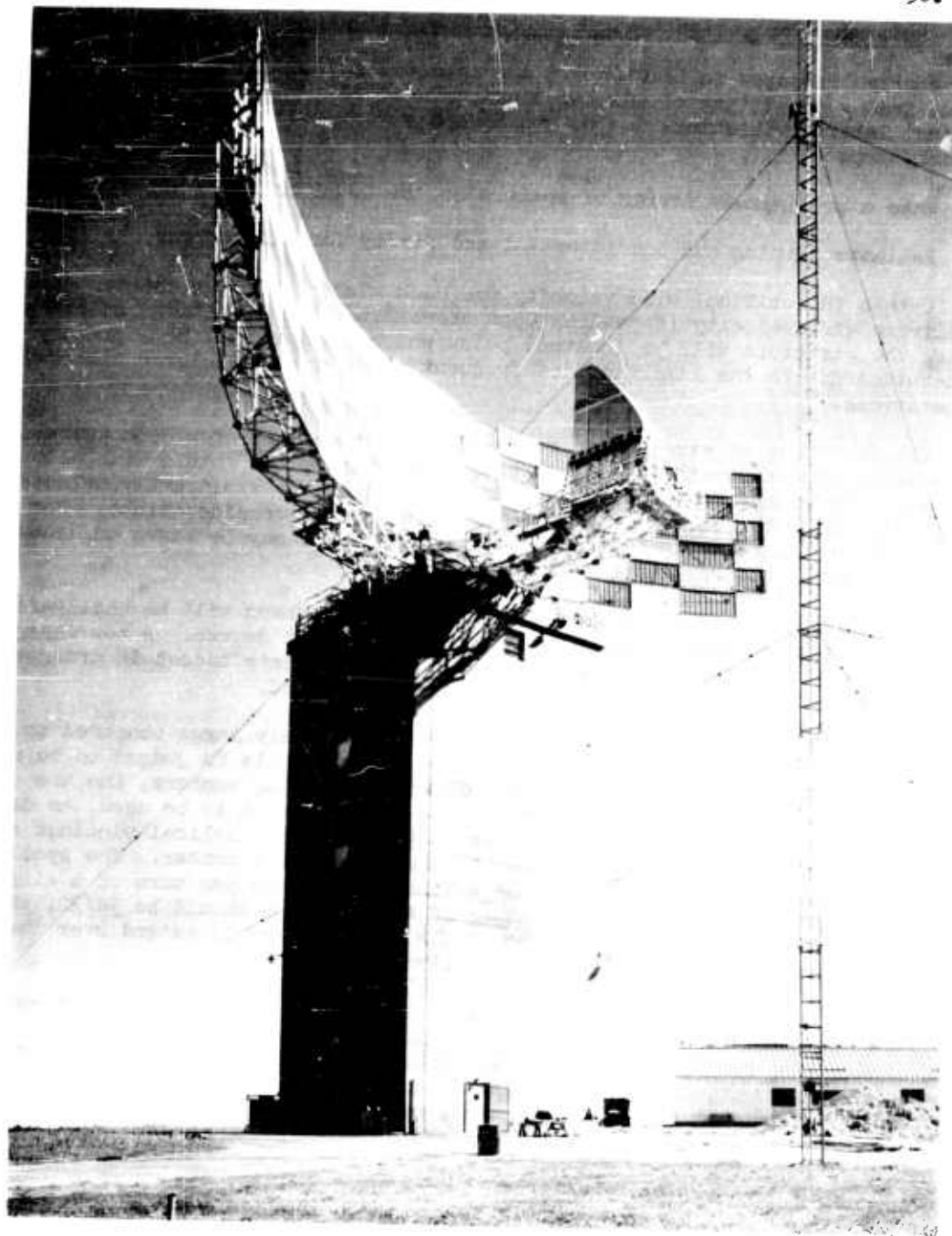
The charts presented in Section 9.3 are intended for use in the design of antenna space frames consisting of tubular aluminum members. The procedure for design against lateral vibrations due to von Kármán vortex forces is outlined in the following steps:

1. Make a preliminary design of members on the usual basis of working loads.
2. Estimate damping and conditions of end fixity for all members.
3. Obtain the critical wind velocity for each member from the charts. Select an arbitrary wind velocity (depending upon prevailing wind conditions at the site where the structure will be located) below which fatigue will be a primary consideration due to the likelihood of frequent winds causing a large number of stress repetitions.
4. Obtain values of stresses at resonance from the charts for each member. Combine these stresses with working stresses and compare the totals with allowable values. For members with critical velocities below the arbitrarily selected velocity, the allowable stress should be based on fatigue considerations. For members with higher critical velocities, the allowable stress may be based on dynamic yield strength considerations.
5. The foregoing stress analysis will show which members will be endangered by the possibility of wind-induced vibrations and to what degree. A new design should then be executed using larger members and/or intermediate braces in order to increase the natural frequencies of the members concerned.
6. If in step 5 the members are found to be excessively large compared to their working load requirements, or if the structure as a whole is judged to be unduly complex and redundant because of the addition of bracing members, the use of spoilers should be considered. The spoiler configuration to be used, as determined by the present experimental investigation, is four helical windings symmetrically spaced 90° apart with respect to the axis of the member. The spoilers should be wound at a pitch (number of cylinder diameters per turn of a single winding) of 12 diameters. The diameter of the windings should be $3d/32$, where d is the outside diameter of the member. The spoilers should extend over the central 40% of the member to which they applied.
7. Another alternative solution to the problem is the use of rolled or extruded shapes other than structural tubing. The primary disadvantage in the use of rolled sections for space frames is the inherent difficulty in making three-dimensional connections. The circular tube possesses the advantage that any pair of perpendicular axes are principal axes, and the section properties are independent of rotation about the longitudinal axis.

9.5 Analysis of Existing Structures

a) General

The charts are also useful for the purpose of making a vibration analysis of an existing structure. The procedure to be followed is the same as for design. In this case, however, member sizes cannot be changed; so only the two alternatives of adding braces or of adding spoilers are available. The latter alternative is much more desirable than the former because of (1) the ease and speed of



Photograph 9.1: 120' x 30' G.C.I. Antenna Structure

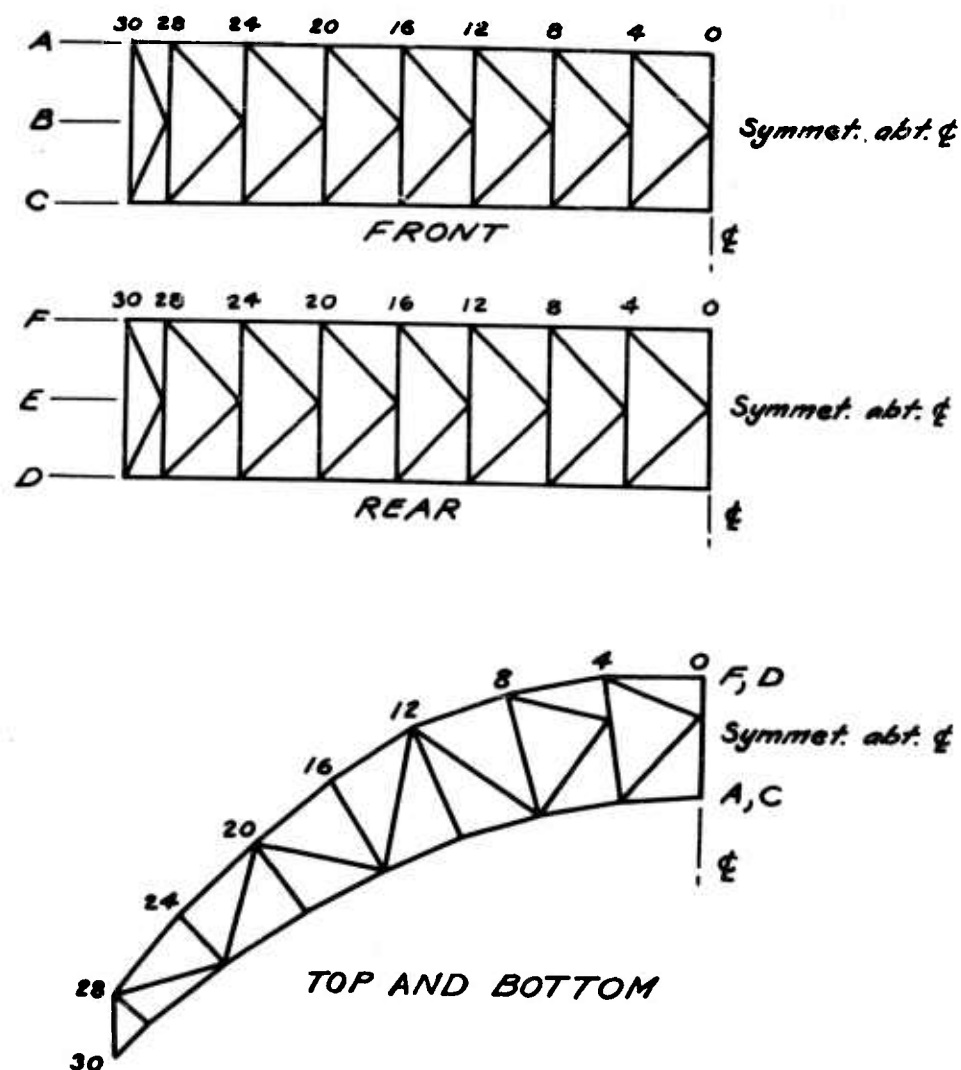


Figure 9.1: SCHEMATIC DIAGRAM OF G.C.I. ANTENNA

Table 9.1: Analysis of G. C. I. Antenna Members *

Input Information		Output of (AC-a)					σ_{\max} $\frac{(\text{IDF})}{(\text{ksi})}$	$\frac{(\text{IDF})}{(\text{ksi})}$	$\frac{(\text{ILF})}{(\text{ksi})}$	$\frac{(\text{IDF})}{(\text{ksi})}$
Members	Sizes	$\frac{f}{(\text{cps})}$	$\frac{V_{\text{cr}}}{(\text{mph})}$	$\frac{N_R}{\times 10^5}$	\bar{C}_K					
{ 28A > 24B 28C }	$3\frac{1}{4} \phi \times \frac{3}{16} \times 14.0'$	26.0	25.0	0.62	0.33	10.0	17.0	1.262	1.62	16.2
{ 30A > 28B 30C }	$2\frac{1}{4} \phi \times \frac{3}{16} \times 10.5'$	32.2	21.8	0.37	0.40	11.4	19.0	1.245	1.49	17.0
{ 20F > 16E 20D }	$1\frac{1}{2} \phi \times \frac{3}{16} \times 14.0'$	27.5	28.7	0.80	0.29	10.1	18.0	1.252	1.58	16.0
{ 24F > 20E 24D }	$3\frac{1}{4} \phi \times \frac{3}{16} \times 14.0'$	26.0	25.0	0.62	0.33	10.0	17.0	1.262	1.62	16.2
{ 28F > 24E 28D }	$3\frac{1}{4} \phi \times \frac{3}{16} \times 14.5'$	24.5	23.8	0.60	0.33	10.3	17.0	1.262	1.62	16.7
{ 30A > 28E 30C }	$2\frac{1}{2} \phi \times \frac{3}{16} \times 12.0'$	26.6	19.5	0.37	0.40	9.8	18.0	1.252	1.57	15.4
{ 12F-16A 12D-16C }	$4" \phi \times \frac{1}{2} \times 16.5'$	11.0	13.5	0.43	0.38	4.5	30.4	1.157	1.20	5.4
{ 16A-20F 16C-20D }	$3\frac{1}{2} \phi \times \frac{3}{8} \times 13.5'$	14.5	15.0	0.42	0.38	5.3	24.8	1.195	1.40	7.4
{ 20F-24A 20D-24C }	$3" \phi \times \frac{3}{8} \times 14.0'$	12.0	10.7	0.26	0.43	3.9	25.1	1.197	1.28	5.0
{ 24A-28F 24C-28D }	$3" \phi \times \frac{1}{4} \times 12.0'$	16.0	14.5	0.35	0.40	7.0	18.9	1.245	1.45	10.2

Front Diags.

Rear Diagonals

Top & Bot. Diagonals

Assumed Semi-Fixed

Assumed Pinned

* Assumed (IDF) = 500; $\delta = 0.0063$

Front Diags.

Rear Diagonals

Top & Bot. Diagonals

Assumed Semi-Fixed

Assumed Pinned

installation, (2) the low cost of material, equipment, and labor involved, and (3) the preservation of the integrity of the structural framing. The slight increase in drag and dead weight of the structure due to the addition of spoilers is inconsequential compared to the alternative of adding bracing members.

b) Example Analysis of the G.C.I. Antenna

The 120' x 30' G.C.I. Antenna is a large radar antenna constructed in 1958 at the Boston Hill site in North Andover, Massachusetts. This structure was analyzed for wind-induced vibrations in a preliminary manner by the writer (Ref. 29). The antenna is shown in Photograph 9.1, and a schematic diagram of the space frame appears in Figure 9.1. Properties and characteristics of the more flexible members of this space frame are summarized in Table 9.1. Analysis charts (AC-a) and (AC-b) are used to obtain the vibrational information and the flexural stresses which are also presented in Table 9.1.

In this antenna a system of intermediate braces was added to alleviate the vibrational stresses.

X DISCUSSION

10.1 Validity of Initial Assumptions

The basic assumptions stated in Section 5.1 were substantiated in a satisfactory manner by the results of the experiments.

Spanwise correlation of the vortex shedding mechanism appears to have been a fairly valid assumption for stationary cylinders. Otherwise, a continuous curve for C_K would not have been obtained for various size cylinders having different aspect ratios. For vibrating cylinders and members, spanwise correlation is insured to a great extent by the vibration itself. The ability of vortices to conform to the motion of flexural members is demonstrated by the ease with which higher modes of vibration are developed. In these higher modes, vortices must be shed simultaneously from opposite sides of the member along different portions of the span, and yet the flow picture readily adjusts itself to accomplish this complex feat.

The assumption that spoiler configurations optimized on stationary cylinders are optimum for vibrating cylinders has also proved to be justified. The reduction of the response amplitudes in Phase B speaks for itself in this respect. There was no opportunity to optimize spoilers on cylinders smaller than 3" ϕ because the resulting aspect ratios would have been too large for the cylinders to behave as rigid bodies in the standardized set-up of Phase A. Therefore, the optimum spoilers for larger diameters were extrapolated to the 1 1/2" ϕ and 2" ϕ members by geometric ratio. In some cases these spoilers were not too effective, but this short-coming is probably due to factors other than the method of extrapolation.

The fact that the standard \bar{C}_K curves of Phases B and C merge into each other verifies the assumption that short, spring-supported cylinders may be used to simulate the behavior of structural members which are too large to test in the wind tunnel. Since the plotted values of \bar{C}_K are independent of the self-amplification phenomenon, this result is to be expected.

Directing this project toward studying first modes of vibration for all types of members had the advantage of simplifying the laboratory instrumentation problems

as well as covering the consideration of primary interest in most structural members. However, disregarding the higher modes of vibration for very flexible members can be unconservative where the vortex-shedding problem is involved. The higher modes can cause high stresses in a member even when the \bar{C}_K is low because they are produced by substantial wind velocities, and the resulting lift forces vary as the square of the velocities.

10.2 Vibrations in Subcritical Range

This investigation shows that wind-induced vibrations in the subcritical range of Reynolds numbers can be dealt with effectively by adhering to the concept of the "standard" \bar{C}_K as a basis for all response calculations. The \bar{C}_K not only accounts for the randomness in the amplitude of C_K , but it also provides independence from the mode shape of a particular vibration and the various other factors which affect the degree of self-amplification.

10.3 Vibrations in Supercritical Range

a) Antenna Members

Since the supercritical range was of secondary interest to this project, insufficient experimental studies were made in the region of high Reynolds numbers to draw any definite conclusions regarding the stochastic response of large cylindrical structural members. In fact, there seems to be some inconsistency in the results of Phases B and C in this respect. A study directed toward this region of Reynolds numbers is necessary for the solution of the problem, but the benefits would be marginal where antenna members are concerned.

b) Large Diameter Structures

Considering cylindrical structures of large diameters, however, an investigation involving stochastic response would be of fundamental value and of current interest. The concepts outlined in Section 4.3 identify this method of approach to the problem of vibrating stacks, missiles, etc., as a valid and promising means of coping with past and present difficulties on the subject.

10.4 Discussion on Use of Spoilers

The first mode optimum spoiler design described in Section 9.4 is suitable for the suppression of vibrations except for the following reservations:

a) Spoilers are not recommended for Reynolds numbers below 1×10^4 or above 4×10^5 , since it was in this range that spoiler optimization was carried out. Fluid flow has greater ability to override protuberances at the lower Reynolds numbers. At high Reynolds numbers the lift forces on bare cylinders are quite erratic without the addition of spoilers, and Phase A tests revealed no differences in the oscillograph records for supercritical Reynolds numbers with and without spoilers.

b) Spoilers are not recommended for members with diameters smaller than 2" ϕ , or for cantilevers with L/d greater than 20. This statement is based on the fact that test members having small diameters and large non-dimensional amplitudes of vibration during bare runs demonstrated an ability to persist in fairly large amplitudes of oscillation with spoilers attached, whereas vibrations in other types of members were readily suppressed with spoilers.

- c) When it is necessary or desirable to suppress modes of vibration higher than the first mode, windings must be applied over the full length of the member under consideration rather than over only a portion of its length.

XI CONCLUSIONS AND RECOMMENDATIONS

11.1 Conclusions

a) Information Obtained from Tests

The experiments conducted in this investigation have provided a continuous curve for C_K in the range of Reynolds numbers of interest for antenna members. This curve represents the basic tool with which the problem of wind-induced vibrations may be solved.

The second essential experimental plot which has been developed is the curve for incremental load factors, (ILF), - vs - aeroelastic suppression factors, (ASF), from the member tests of Phase C. The use of (ILF)'s in conjunction with the expressions for incremental deflection factors, (IDF), permits the calculation of the degree of self-amplification for any of the types of members considered in this project. Moreover, the method can be extended to other types of members by writing appropriate expressions for (ASF) and (IDF) for the particular mode shapes involved.

Experimental plots of Strouhal numbers check well with previously published information. The accuracy of this agreement (within 5%) is deemed to be sufficient for engineering purposes. Considering all of the possibilities for experimental error involved in the laboratory tests, this discrepancy is reasonable.

b) Effectiveness of Spoilers

Spoiler tests show that a configuration of four helical windings is most effective in suppressing lift forces. A spoiler diameter of $d/16$ to $d/8$ is necessary for good suppression, and a diameter of $3d/32$ reduces the lift forces to a minimum. Although the pitch of windings is an essential property of the spoilers, the phenomenon is not particularly sensitive to the pitch. The most effective pitch in the wide range of choice ($8d$ to $16d$) was determined to be $12d$.

11.2 Recommendations

a) Design Criteria, Procedures, and Applications

The design criteria and the methods of analysis and design against vibrations described in detail in Section 9 are recommended for the solution of the problem of wind-induced vibrations in antenna members. Analysis charts contained in Section 9.3 provide complete and automatic solutions for all of the factors involved, and the complete range of practical member types and sizes is covered. These charts can also be applied to aluminum structures other than antenna space frames, of course.

b) Use of Spoilers

It is recommended that spiral spoilers of the optimum design described in Section 9.4 be used wherever this method of suppression is deemed suitable compared to the other choices available. This recommendation is subject to the reservations

enumerated in Section 10.4. Disruption of the aerodynamic forces causing vibrations represents the basic scientific approach to the problem compared to the usual engineering approach of altering the structure to avoid the difficulties. However, both approaches have their merit, and it is the responsibility of the designer to judge which method is suitable for a given situation.

11.3 Recommendations for Further Research

a) Field Tests in Atmosphere

One of the essential tools lacking in the problem of vibrations in antenna members is information concerning the structural damping. This parameter varies from one structure to another depending upon the method of fabrication, the type of field connections, and the design of support systems. A series of field tests should be conducted to obtain sufficient information on the damping characteristics of existing antenna structures so that the designer will have some basis for estimating the damping coefficients to be expected in new antennae. Without this information the designer is severely handicapped with respect to carrying out vibration analyses of his proposed structures.

Within the same series of field tests can be included a study of the response of actual antenna members to prevailing winds. This type of an investigation lacks the velocity control feature of the wind tunnel, but it possesses the advantage of reality with respect to atmospheric conditions at the site. Moreover, in those members in which vibrations are observed, the effect of adding spoilers can also be observed directly.

b) Laboratory Investigations of a Similar Nature

Experiments of a nature similar to the present investigation may be carried out to determine the following information if warranted by necessity:

- (1) The effects of axial forces on the response of various types of members may be determined. Of particular interest would be the manner in which axial forces determine the resonant velocity with respect to Reynolds numbers and the manner in which the axial forces affect the self-amplification phenomenon.
- (2) Other types of members may be studied. One important series of end-supported members is that in which fixities are not the same at both ends.
- (3) Higher modes of vibration may be studied to ascertain the relative importance of the various modes with respect to the fiber stresses developed in the members.

c) Laboratory Investigations of a Different Nature

There are two experiments of a different nature from this investigation which should, and without doubt will, be performed at some time in the near future.

- (1) A series of tests with elastically-supported cylinders may be conducted in a water channel in order to obtain a continuous curve for \bar{C}_K in the range of Reynolds numbers below 10^4 .
- (2) Studies similar to Y. C. Fung's experiments on a large diameter stationary cylinder should be carried out using large, light-weight spring-supported cylinders in order to obtain information on the stochastic response of important cylindrical structures.

BIBLIOGRAPHY

1. Biggs, J.M., Dahl, N.C., and Shank, M.E., "Report on 28 ft. Kennedy Paraboloids," M.I.T. Lincoln Laboratory, March 18, 1955.
2. Bingham, H.H., Weimer, D.K., and Griffith, W., "The Cylinder and Semicylinder in Subsonic Flow," Princeton Univ. Dept. of Physics, Tech. Report II-13, July, 1952.
3. Bridgman, P.W., "Dimensional Analysis," Yale University Press, New Haven, 1931.
4. Delaney, N.K., and Sorensen, N.E., "Low Speed Drag of Cylinders of Various Shapes," N.A.C.A. T.N. 3038, Nov., 1953.
5. Den Hartog, J.P., "Mechanical Vibrations," McGraw-Hill, New York, 1947.
6. Dickey, W.L., and Woodruff, G.B., "The Vibrations of Steel Stacks," Trans. A.S.C.E., 121:1054, 1956.
7. Dockstader, E.A., Swiger, W.F., and Ireland, E., "Resonant Vibrations of Steel Stacks," Trans. A.S.C.E., 121:1088, 1956.
8. Etkin, B., Korbacher, G.K., and Keefe, R.T., "Acoustic Radiation from a Stationary Cylinder in a Fluid Stream (Aolian Tones)," Univ. of Toronto Institute of Aerophysics, Report No. 39, May, 1956.
9. Fage, A., and Warsap, J.W., "The Effects of Turbulence and Surface Roughness on the Drag of a Circular Cylinder," British A.R.C., R. and M. No. 1283, Oct., 1929.
10. Fung, Y.C., "An Introduction to the Theory of Aeroelasticity," John Wiley and Sons, New York, 1955.
11. Fung, Y.C., "Fluctuating Lift and Drag Acting on a Cylinder in a Flow at Supercritical Reynolds Number," Shock and Vibration Bull. No. 26, Part II, published by the U.S. Naval Research Laboratory, Wash., D.C., Dec., 1958.
12. Goldman, R., "The Generation and Suppression of von Kármán Vortex Forces," Eng. Report No. 8984, Martin Co., Baltimore, Maryland, 1957.
13. von Kármán, Th., and Rubach, H., "Über den Mechanismus des Flüssigkeits and Luftwiderstandes," Phys. Zeits., Bd. 13, Heft 2, Jan. 15, 1912. (Translated by Jack Lotsif, Cornell Aeronautical Laboratory, Oct., 1947.)
14. McGregor, D.M., "An Experimental Investigation of the Oscillating Pressures on a Circular Cylinder in a Fluid Stream," Univ. of Toronto Institute of Aerophysics, Tech. Note No. 14, June, 1957.
15. Milne-Thomson, L.M., "Theoretical Hydrodynamics," MacMillan, New York, 1955.
16. Penzien, J., "Wind Induced Vibration of Cylindrical Structures," Proc. A.S.C.E., EM-1, Paper 1141, Vol. 83, Jan., 1957.
17. Price, P., "Suppression of the Fluid-Induced Vibrations of Circular Cylinders," Proc. A.S.C.E., EM-3, Paper 1030, Vol. 82, July, 1956.
18. Relf, E.F., and Simmons, L.F.G., "Frequency of Eddies Generated by Motion of a Cylinder through a Fluid," British A.R.C., R. and M. 917, 1924.

19. Reudy, R., "Vibrations of Power Lines in a Steady Wind," Canadian Journal of Research, Oct., 1935.
20. Roshko, A., "On the Development of Turbulent Wakes from Vortex Streets," N.A.C.A. Technical Notes 2913, 1953.
21. Schwabe, M., Ingenieur-Archiv 6:34-50, 1935.
22. Scruton, C., "Wind-Excited Oscillations of Tall Stacks," The Engineer, London, 199:806, 1955.
23. Scruton, C., and Walshe, D.E.J., "A Means for Avoiding Wind-Excited Oscillations of Structures with Circular or Nearly Circular Cross-Section," N.P.L. Aero. 335, Oct., 1957.
24. Steinman, D.B., "Problems of Aerodynamic and Hydrodynamic Stability," Proceedings of the Third Hydraulics Conference, Univ. of Iowa Studies in Engineering, Bull. 31, 1946.
25. Streeter, V.L., "Fluid Dynamics," McGraw-Hill, New York, 1948.
26. Strouhal, V., "Über eine besondere Art der Tonerregung," Annalen der Physik und Chemie, Bd. 5, Heft 10, Oct., 1878, pp. 216-251.
27. Thomson, W.T., and Barton, M.V., "The Response of Mechanical Systems to Random Excitation," Journal of Applied Mechanics, 24:248-251, 1957.
28. Timoshenko, S., "Vibration Problems in Engineering," D. Van Nostrand Co., New York, 3rd Ed., 1955.
29. Weaver, William Jr., "Investigation of Vibration of Tubular Members in 120' x 30' G.C.I. Antenna Structure," M.I.T. Lincoln Laboratory Group Report 75-2, August 15, 1958.
30. Weaver, William Jr., "Preliminary Wind Tunnel Test on Effect of Spiral Spoilers in Reducing Wind-Induced Vibrations of Cylindrical Structural Members," M.I.T. Lincoln Laboratory Group Report 75-3, August 19, 1958.
31. Weaver, William Jr., "Experimental Investigation of Wind-Induced Vibrations in Antenna Members," Sc. D. Thesis, Dept. of Civil and Sanitary Engineering, M.I.T., September, 1959.

APPENDIX A

Phase A Test Results

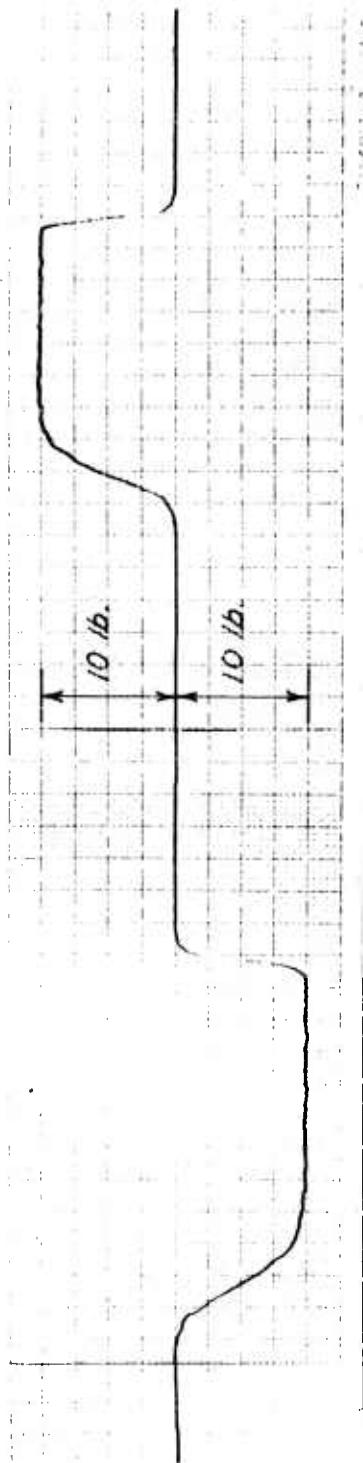


Figure A-1: Transducer Calibration---Sanborn Oscillograph
10# ea. way at x20 attenuation = 20 mm amplitude.

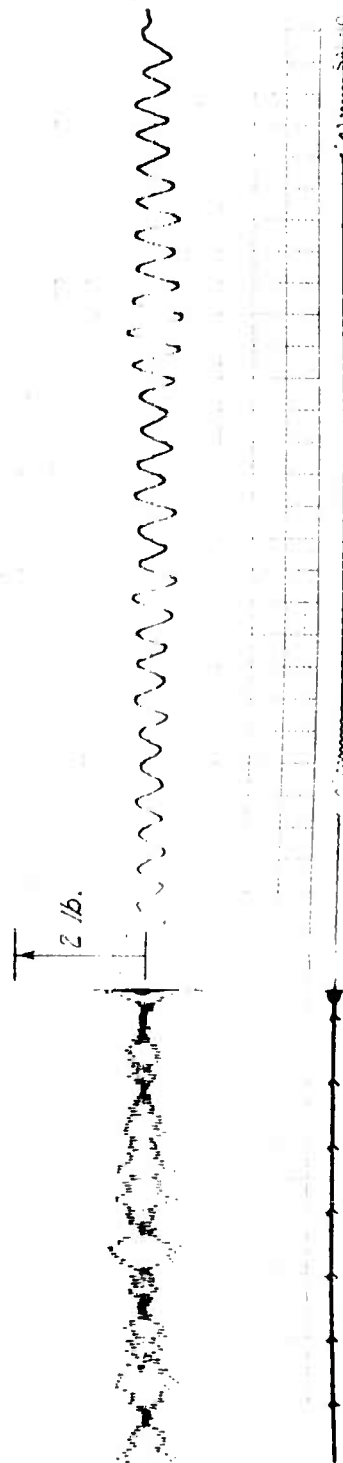


Figure A-2: Example Sanborn Oscillograph Record for Stationary 5" Bare Cylinder (Subcr. N_R)
Paper speeds 10 and 100 mm per sec.; $v = 30.0$ mph; $F_k = 1.3\#$;
 $C_k = 0.303$; $f_v = 20.0$ cps; $N_s = 0.190$; $N_R = 1.17 \times 10^4$.

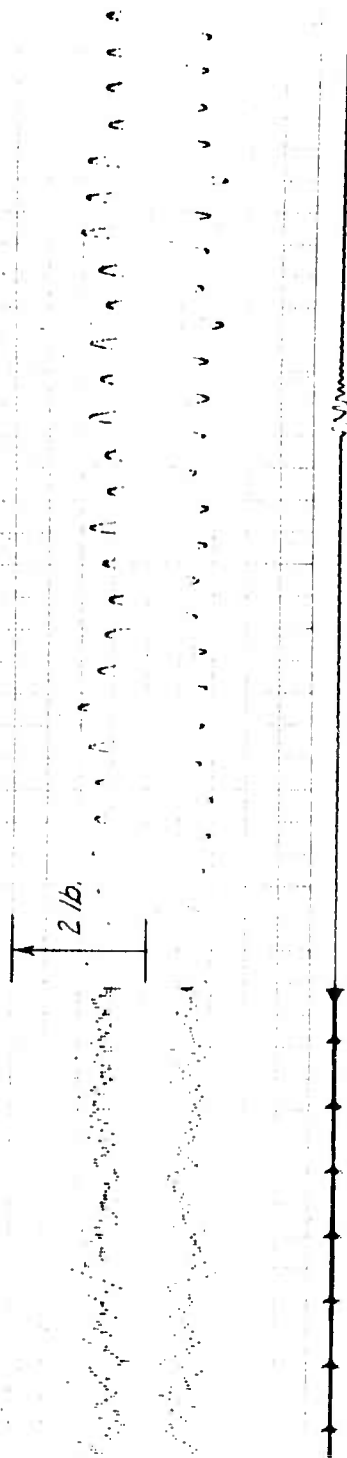


Figure A-3: Example Sanborn Oscillograph Record for Stationary 5" ϕ Cylinder with 8 Windings
 Paper speeds 10 and 100 mm per sec.; $v = 30.0$ mph; $F_k = 2.4\#$;
 $C_k = 0.519$; $f_v = 18.0$; $N_s = 0.184$; $N_R = 1.26 \times 10^5$.

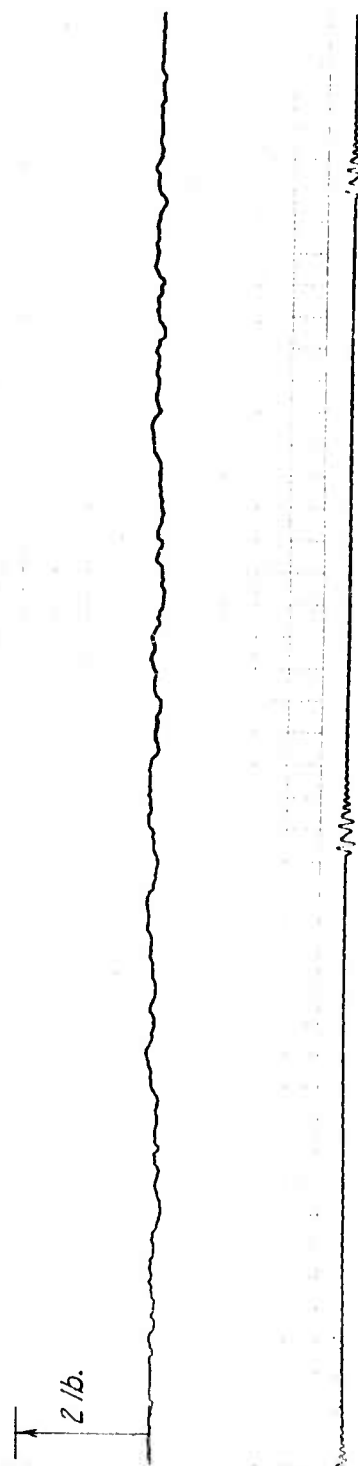


Figure A-4: Example Sanborn Oscillograph Record for Stationary 5" ϕ Cylinder with Spoilers
 Paper speed 100 mm per sec.; $v = 30.0$ mph; $F_k = 0.15\#$; $C_k = 0.035$;
 $N_R = 1.17 \times 10^5$.

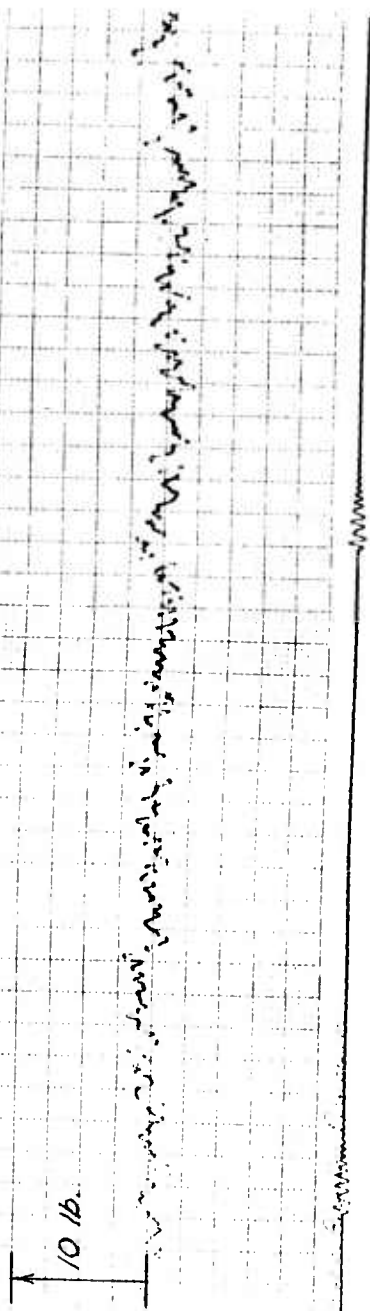


Figure A-5: Example Sanborn Oscillograph Record for Stationary 10" ϕ Bare Cylinder (Super. N_R)
 Paper speed 100 mm per sec.; $v = 73.9$ mph; Atten. x20; $N_R = 5.77 \times 10^5$.

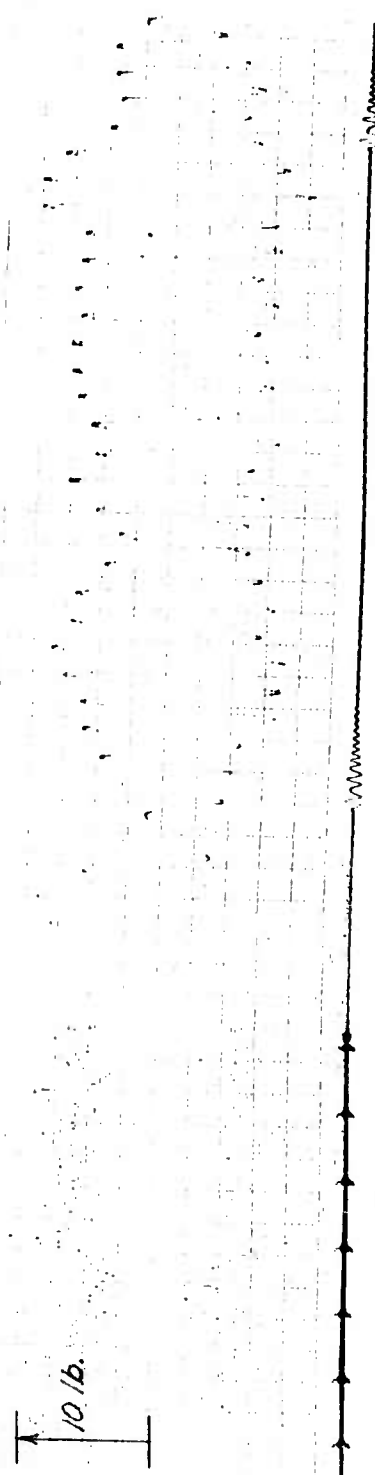


Figure A-6: Example Sanborn Oscillograph Record for Stationary 10" ϕ Cylinder with 16 Windings
 Paper speeds 10 and 100 mm per sec.; $v = 73.9$ mph; Atten. x20; $F_R = 21.0\#$;
 $C_R = 0.381$; $f_v = 24.0$ cps; $N_s = 0.193$; $N_R = 6.06 \times 10^5$.

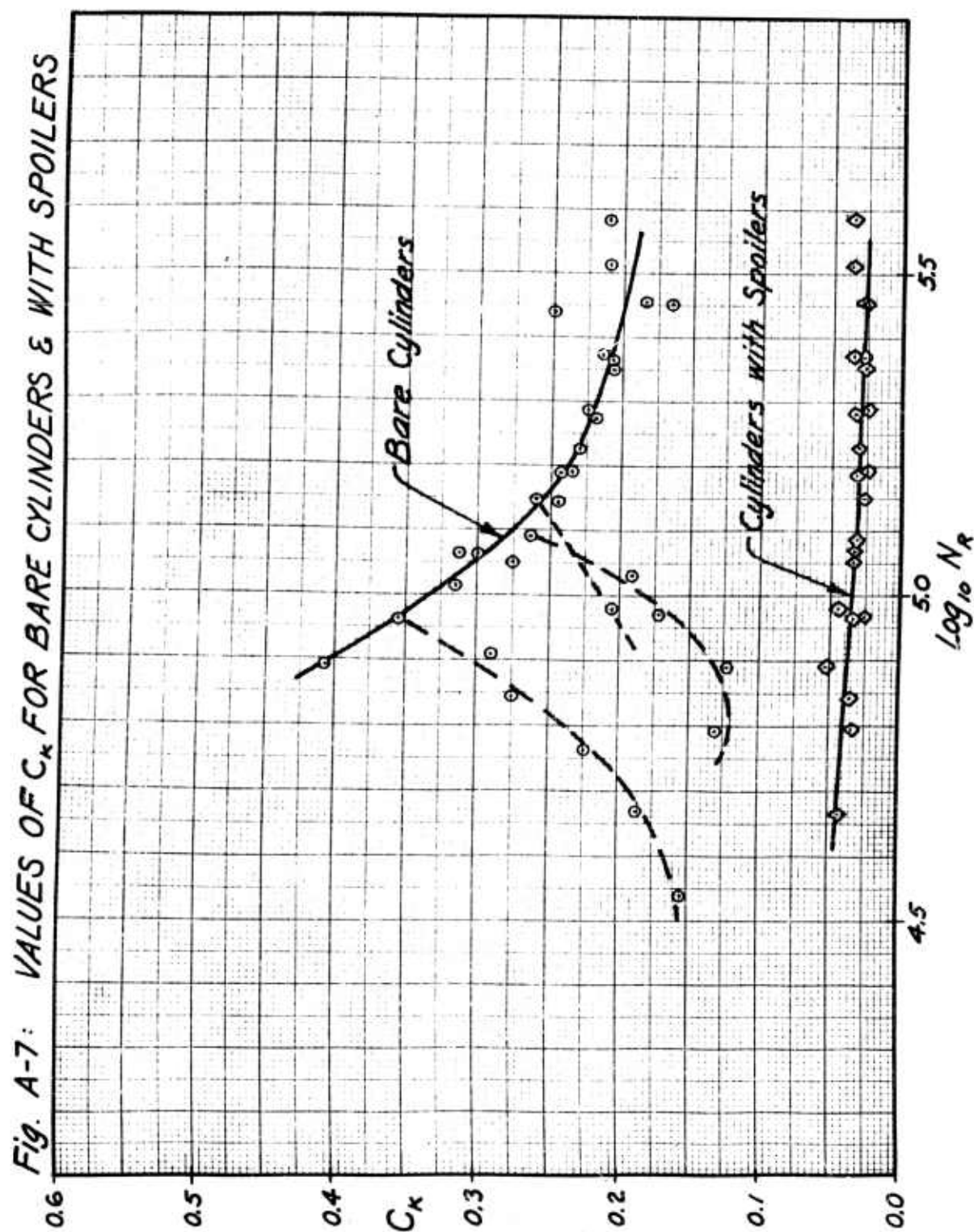
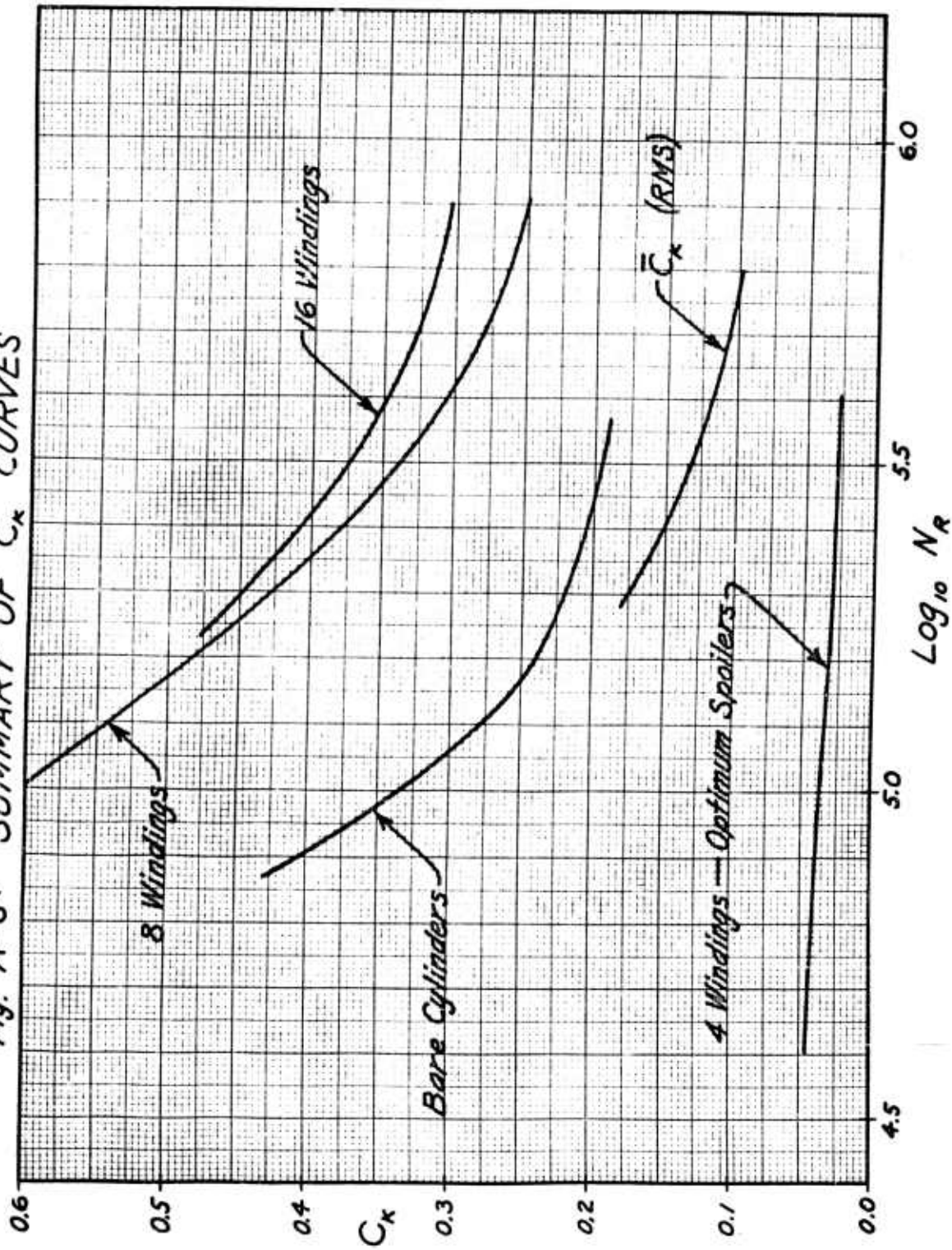


Fig. A-8: SUMMARY OF C_K CURVES

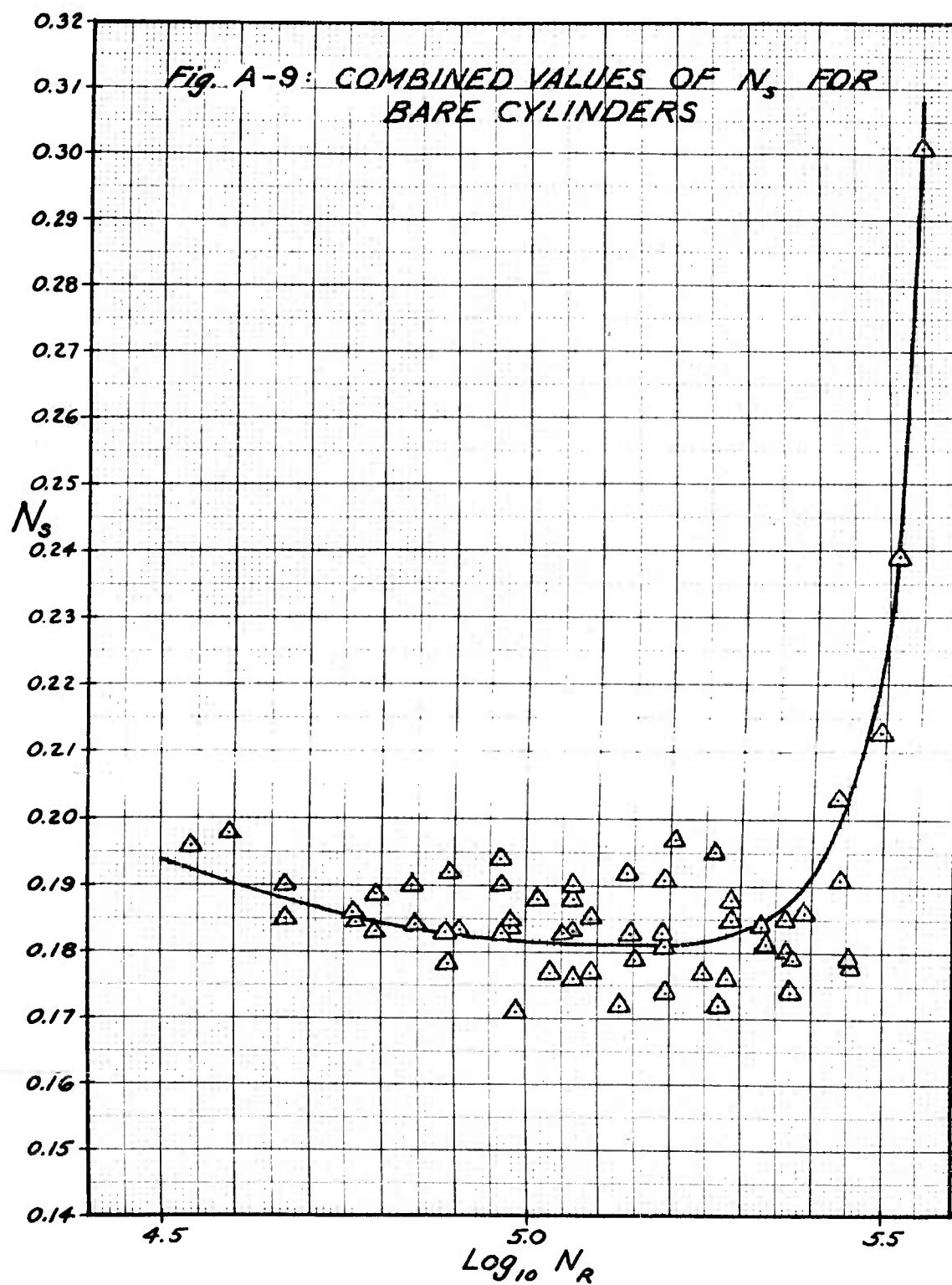


Fig. A-10: VALUES OF N_s FOR CYLINDERS WITH 8 AND 16 WINDINGS

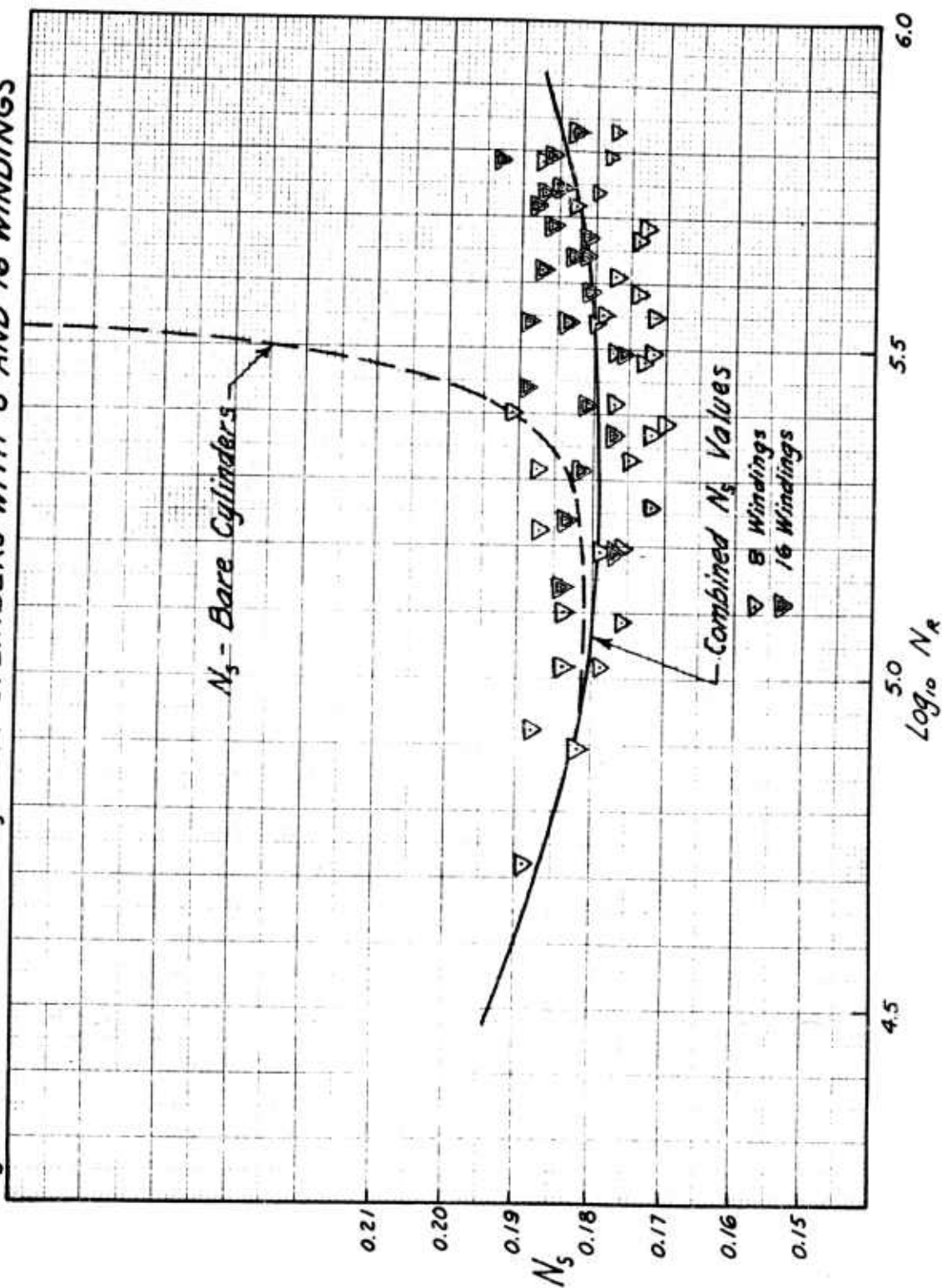
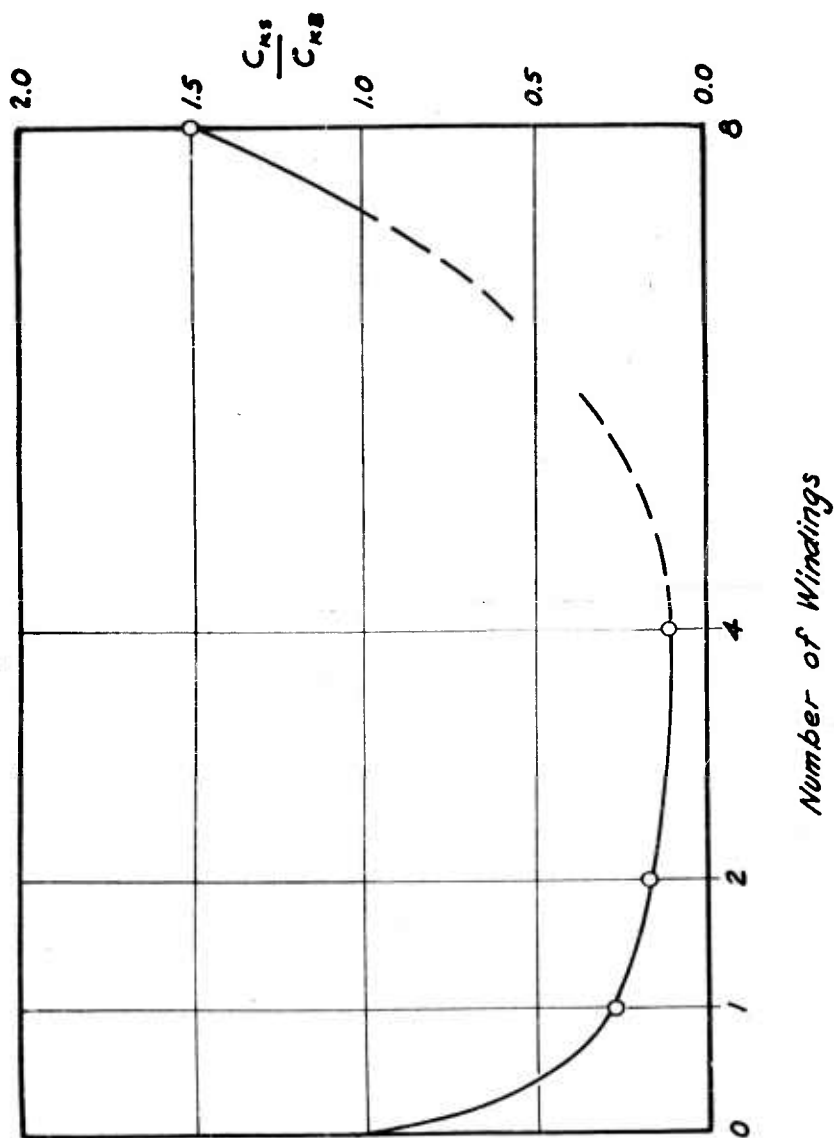
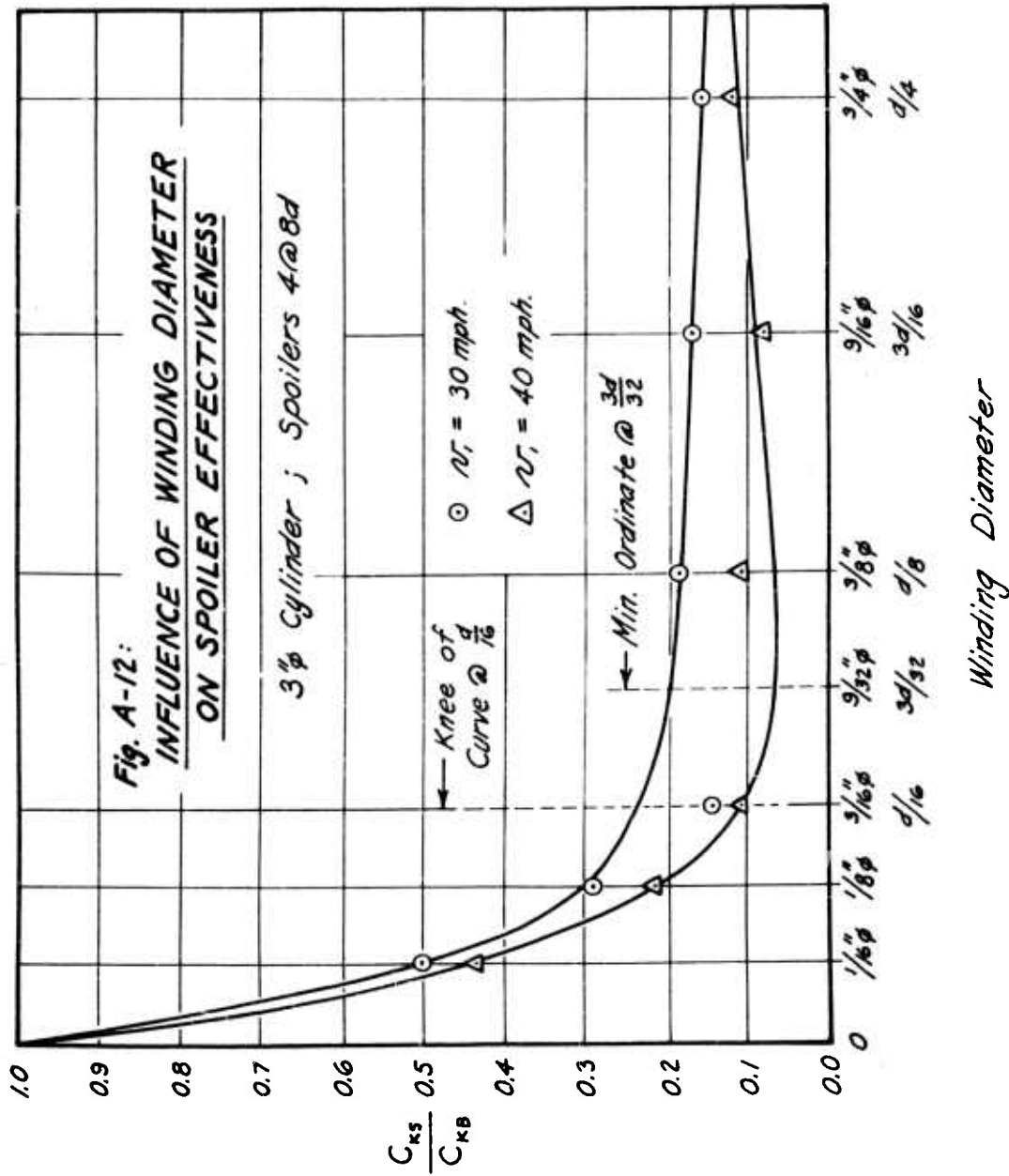
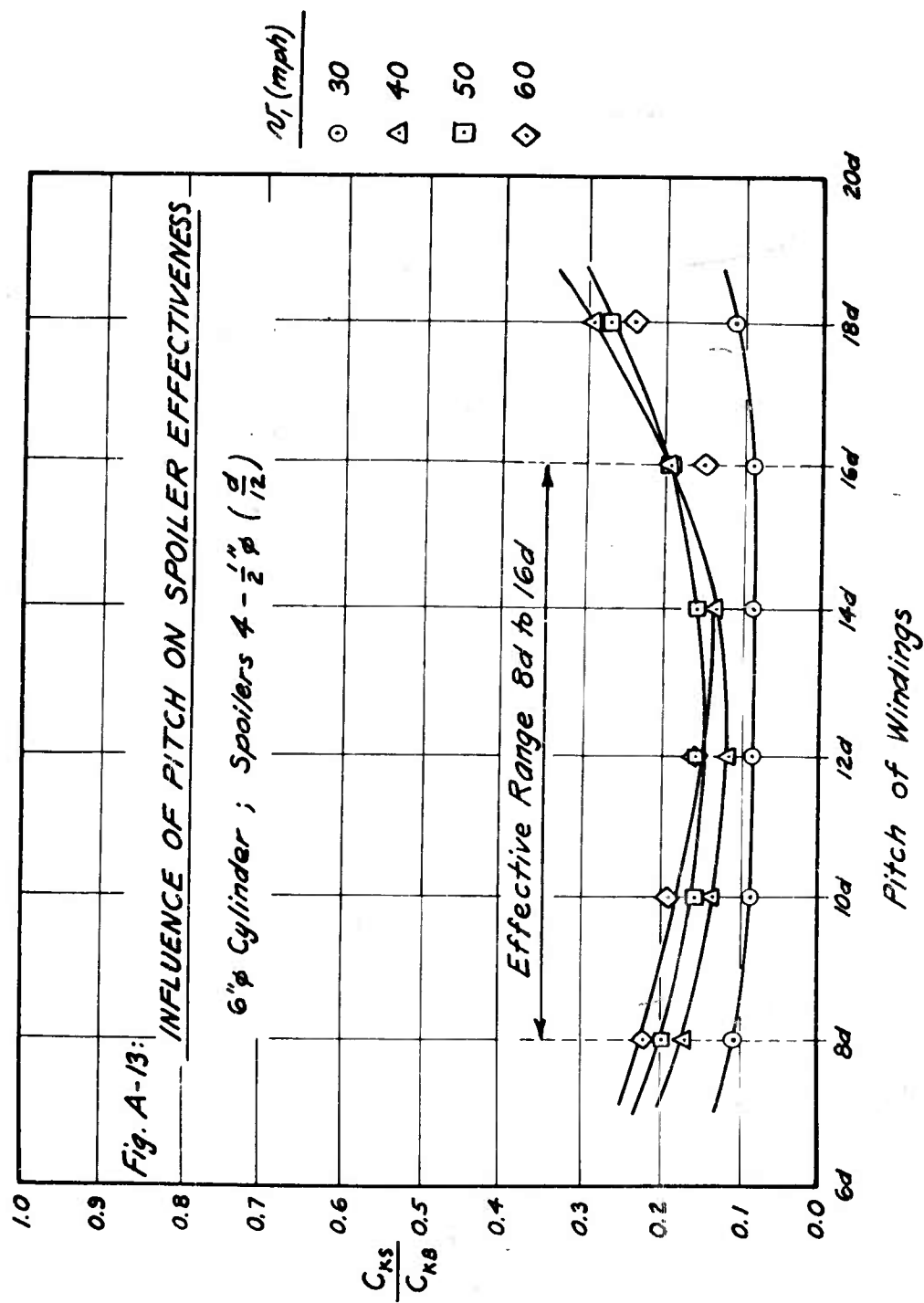


Fig. A-11: INFLUENCE OF NUMBER OF WINDINGS
ON SPOILER EFFECTIVENESS

3" ϕ Cylinder ; Spoilers $\frac{3d}{16}$ @ $14d$; $U = 40$ mph.







APPENDIX B

Phase B Test Results

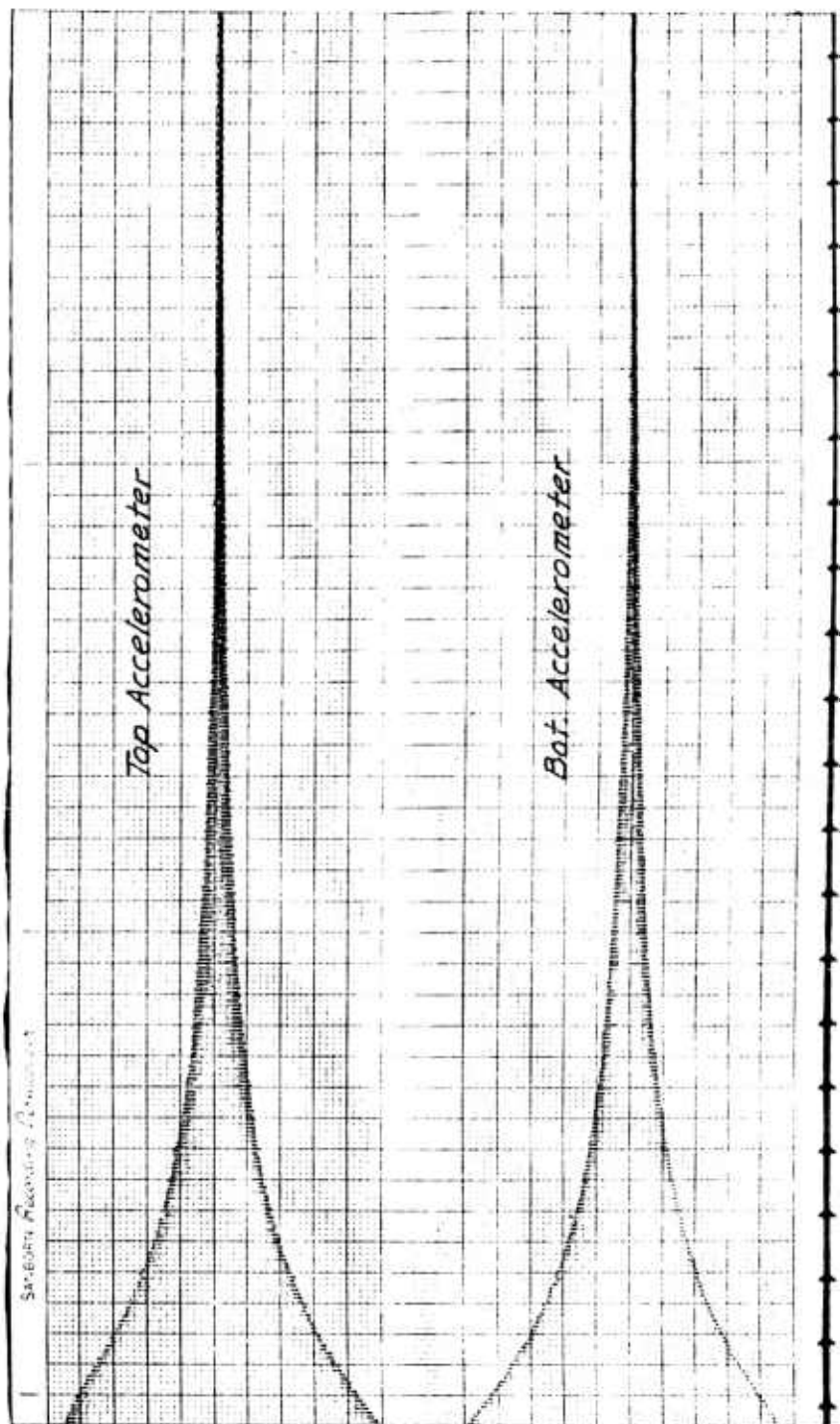


Figure B-1: Example Sanborn Oscillograph Record of Decay Curve for 6" ϕ Spring-Supported Cyl.
 Paper speed 10 mm per sec.; Atten x1; $\delta = 0.022$; $k_c = 533 \text{ \#/in}$; $f_c = 15.05 \text{ cps}$

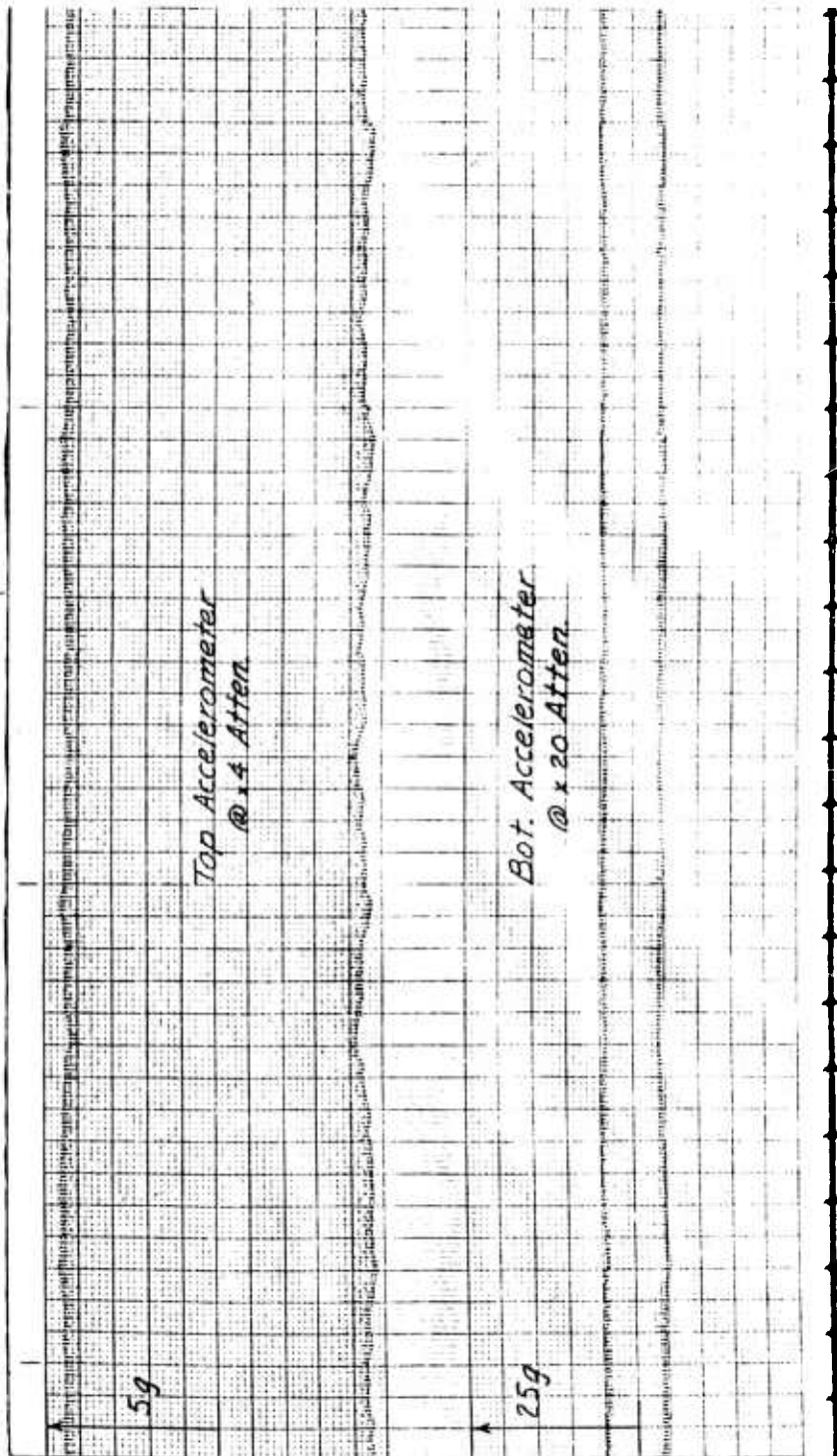


Figure B-2: Example Sanborn Oscillograph Record for 6" Spring-Supported Bare Cylinder
Oscillating at Maximum Amplitude

Paper speed 10 mm per sec.; Atten. $\times 4$ and $\times 20$; $\delta = 0.022$; $k_e = 533 \text{ \#/in}$;
 $f_c = 15.05 \text{ cps}$; $v_p = 29.8 \text{ mph}$; $a_e = 5.00g$; $NDD = 0.036$.

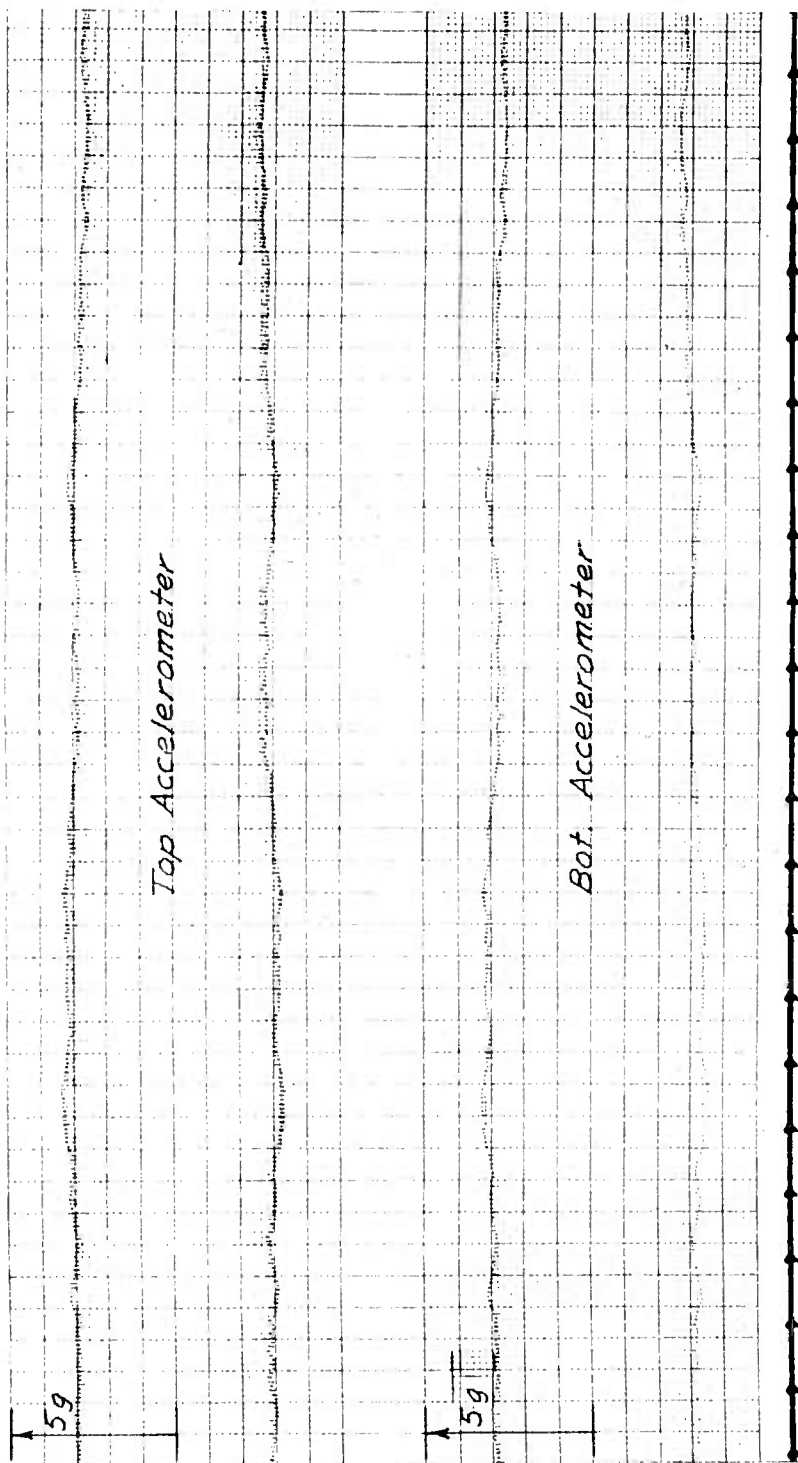


Figure B-3: Example Sanborn Oscillograph Record for 6" ϕ Spring-Supported Cylinder with

8 Windings 3/16" ϕ at 12d Oscillating at Maximum Amplitude

Paper speed 10 mm per sec.; Atten. x_{14} ; $\delta = 0.029$; $k_c = 533$ #/in; $f_c = 15.05$ cps
 $v_p = 32.4$ mph; $a_c = 3.40g$; NDD = 0.0231.

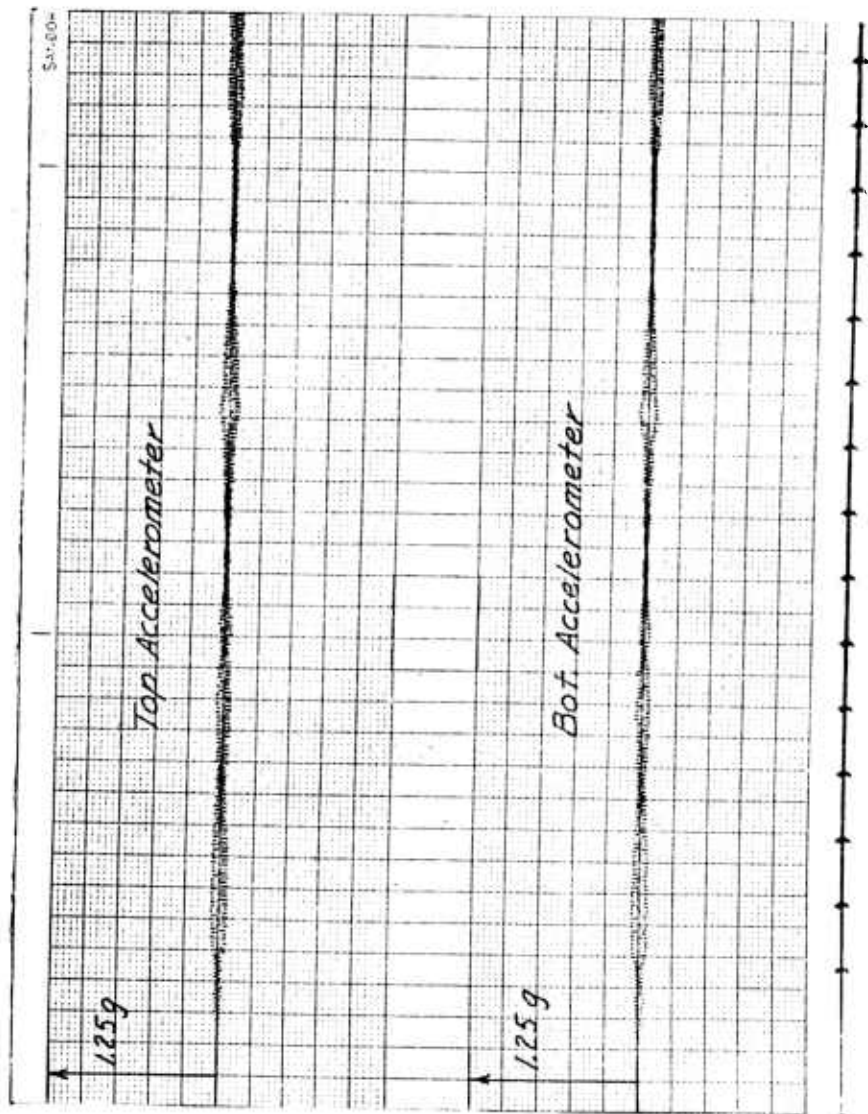


Figure B-4: Example Sanborn Oscillograph Record for 6" ϕ Spring-Supported Cylinder with Spoilers, 4-3/8" ϕ at 12d, Oscillating at Maximum Amplitude
 Paper speed 10 mm per sec.; Atten. x_1 ; $\delta = 0.022$; $k_c = 533$ #/in; $f_c = 15.05$ cps; $v = 31.3$ mph; $a_c = 0.07g$; NDD = 0.0005.

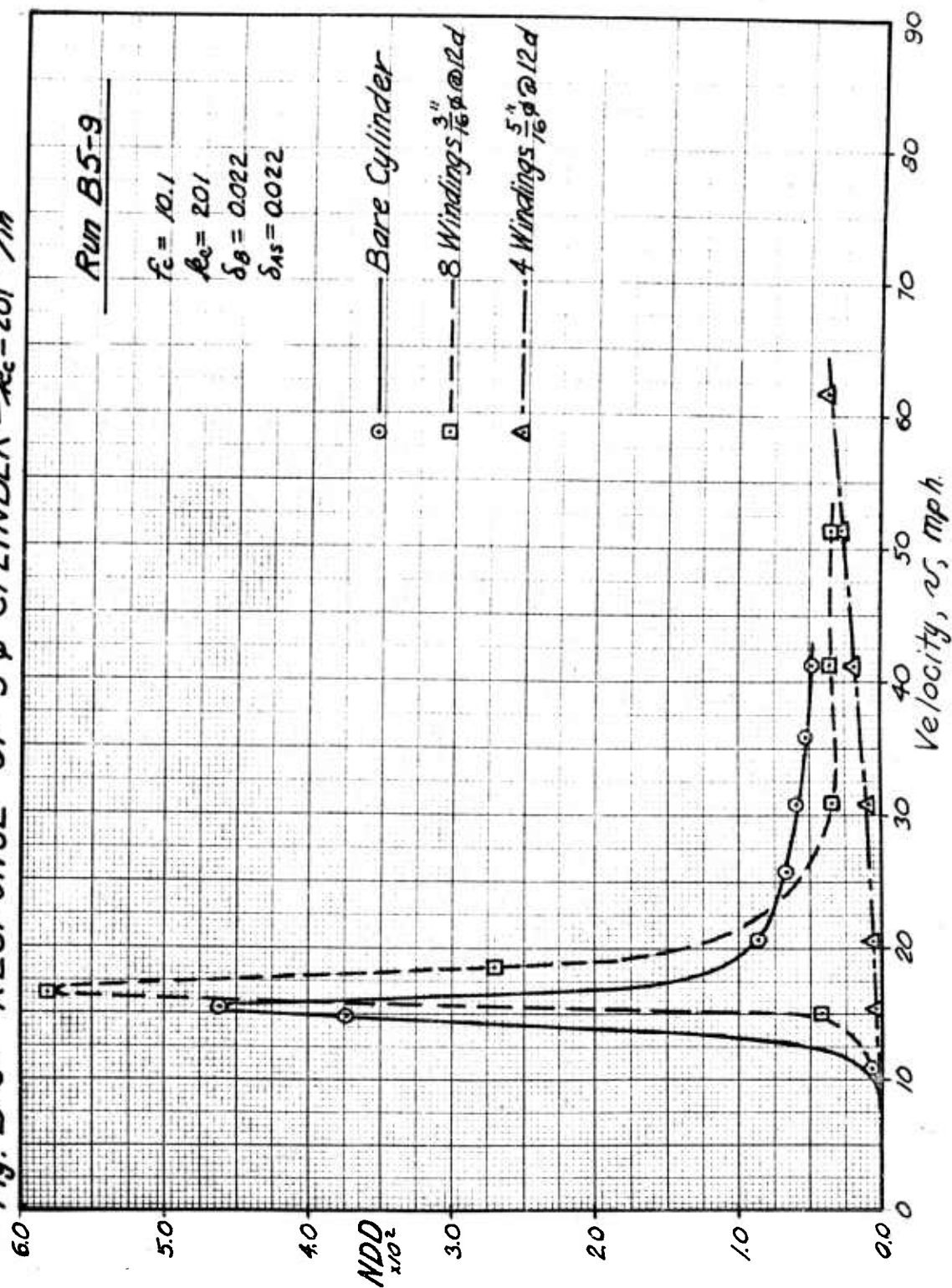
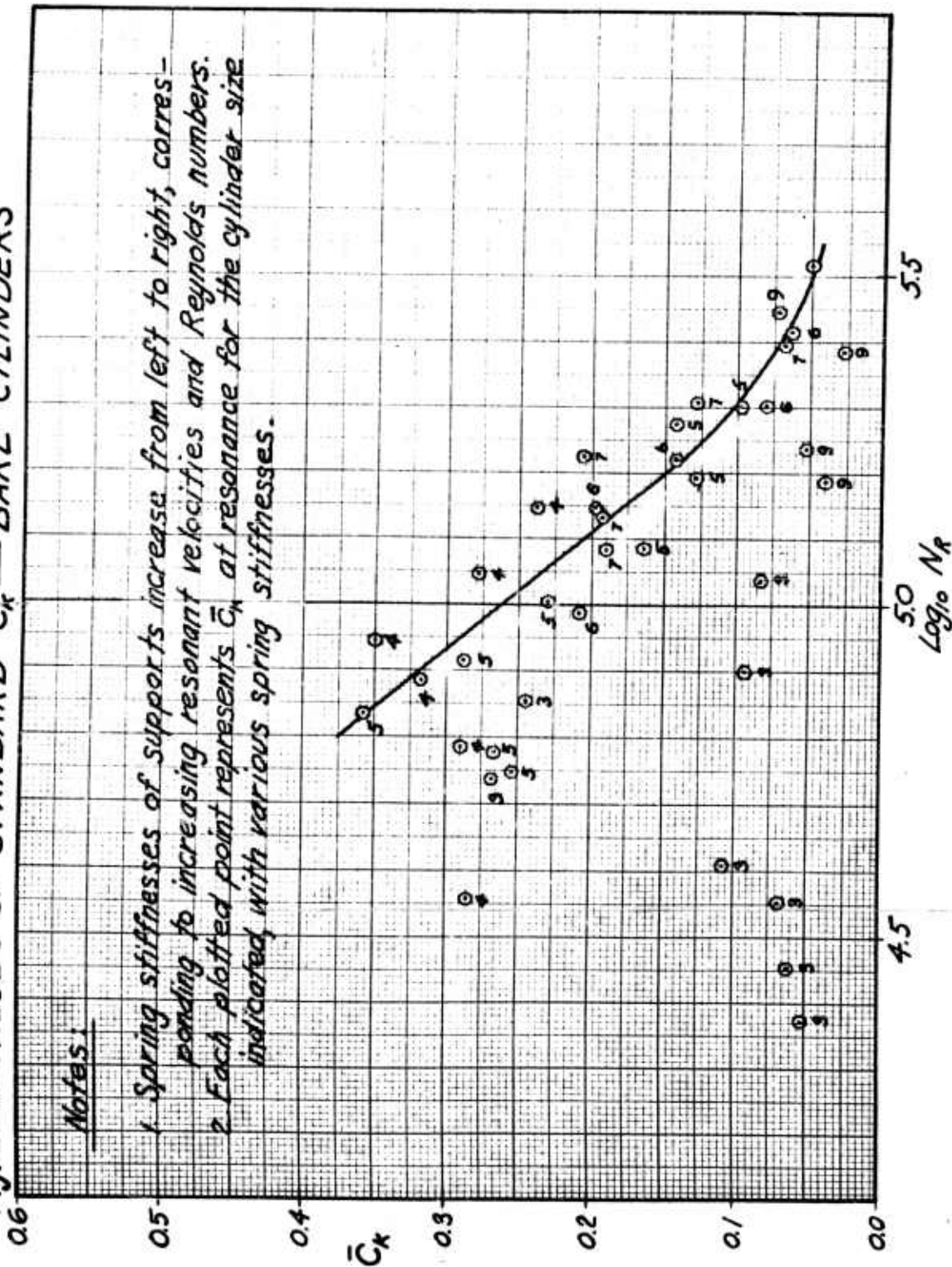
Fig. B-5: RESPONSE OF 5" CYLINDER - $R_c = 201 \text{ lb/in}$ 

Fig. B-6: VALUES OF STANDARD \bar{C}_K — BARE CYLINDERS



VALUES OF STANDARD \bar{C}_K — CYLS. WITH NUMEROUS WINDINGS

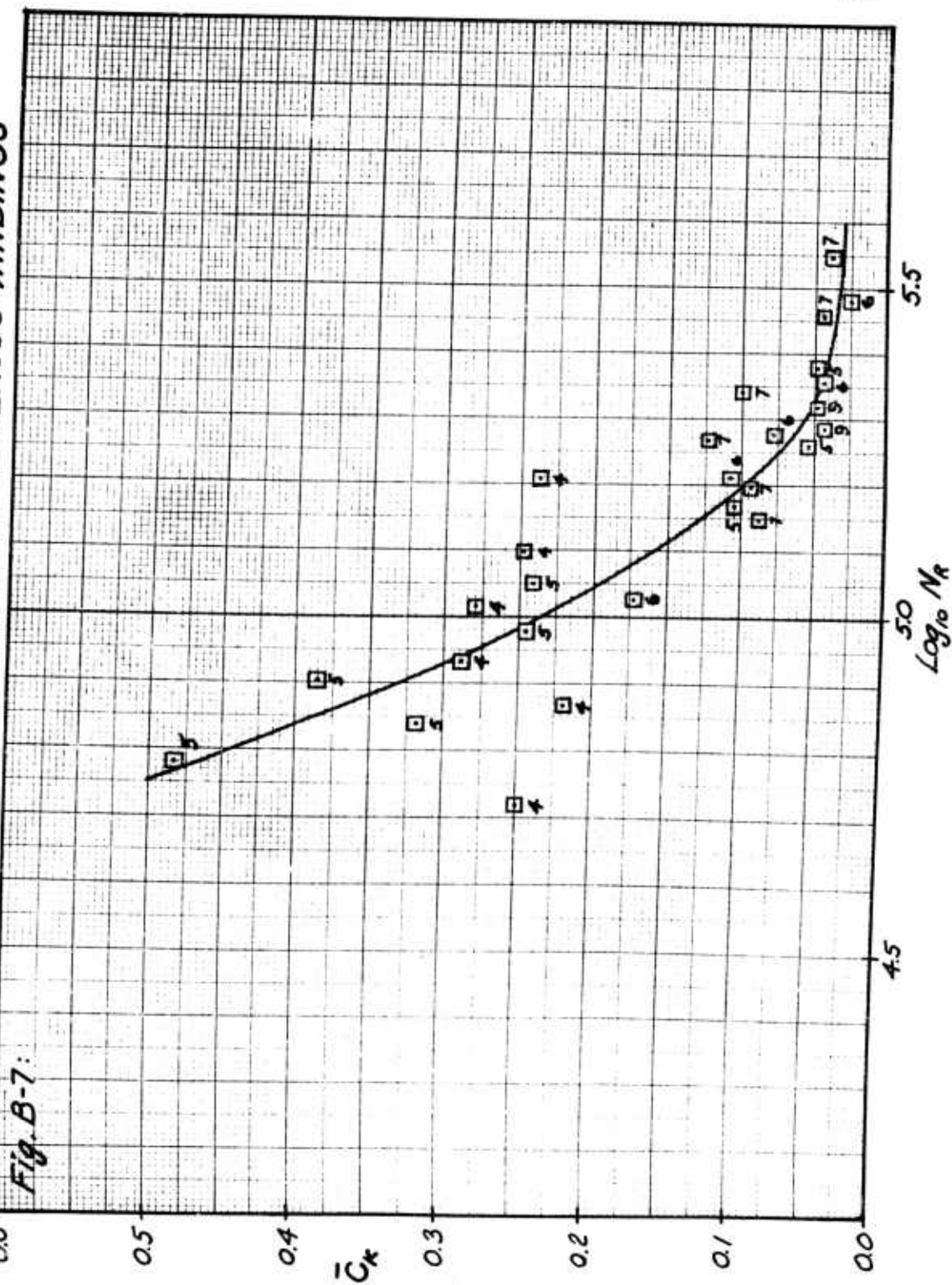


Fig. B-8: VALUES OF N_s — BARE CYLINDERS

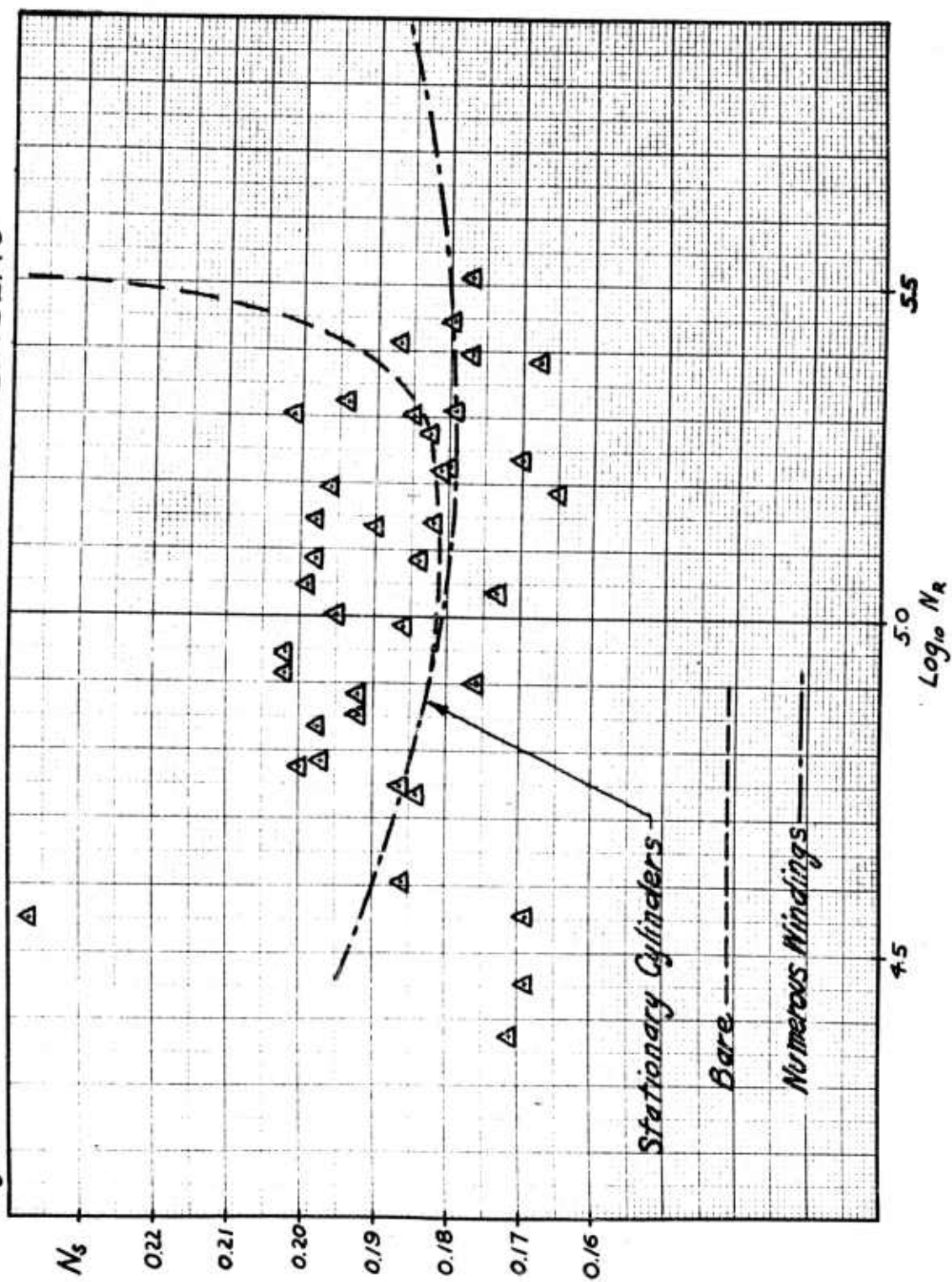
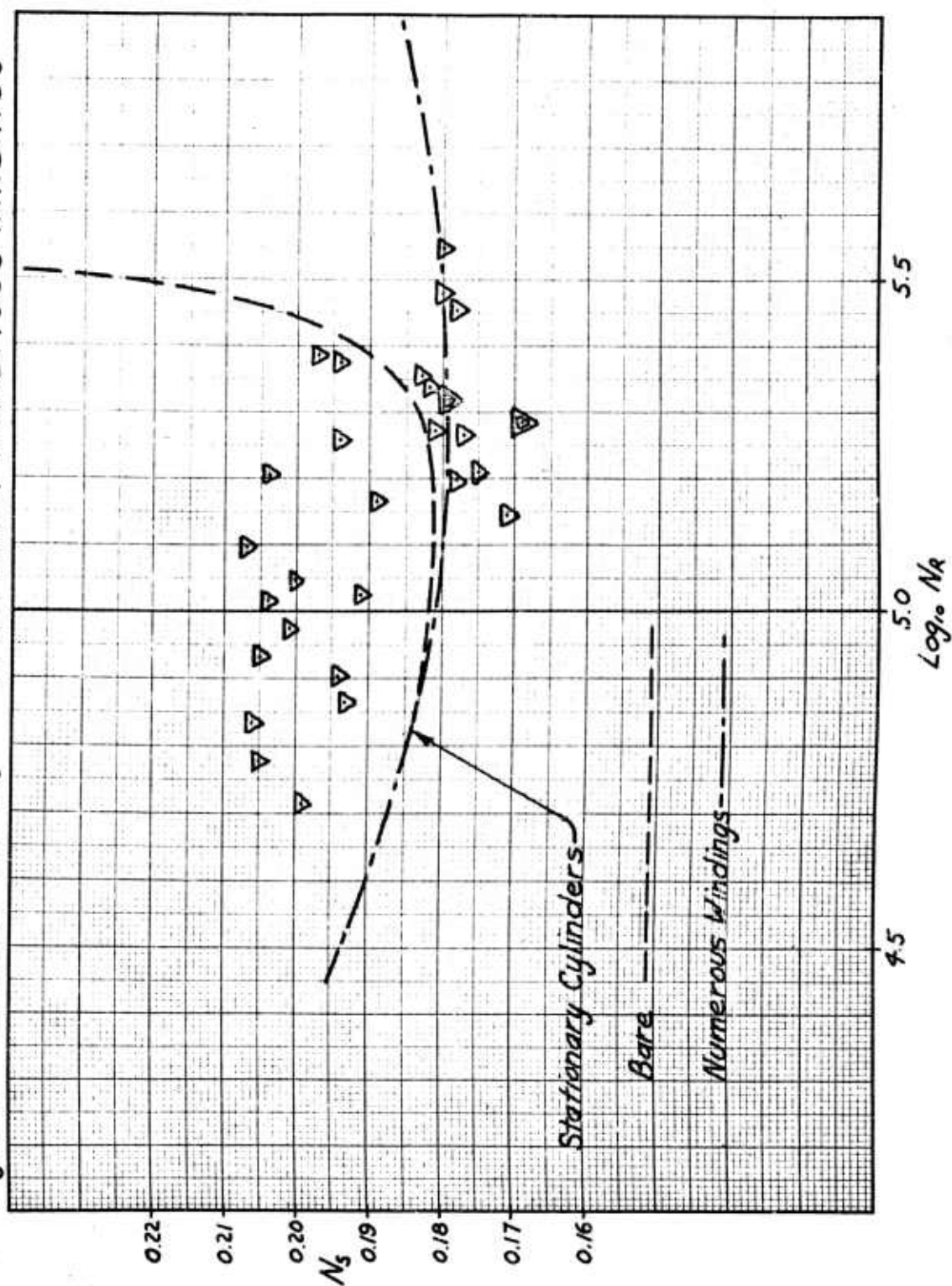


Fig. B-9: VALUES OF N_s — CYLS. WITH NUMEROUS WINDINGS



APPENDIX C

Phase C Test Results

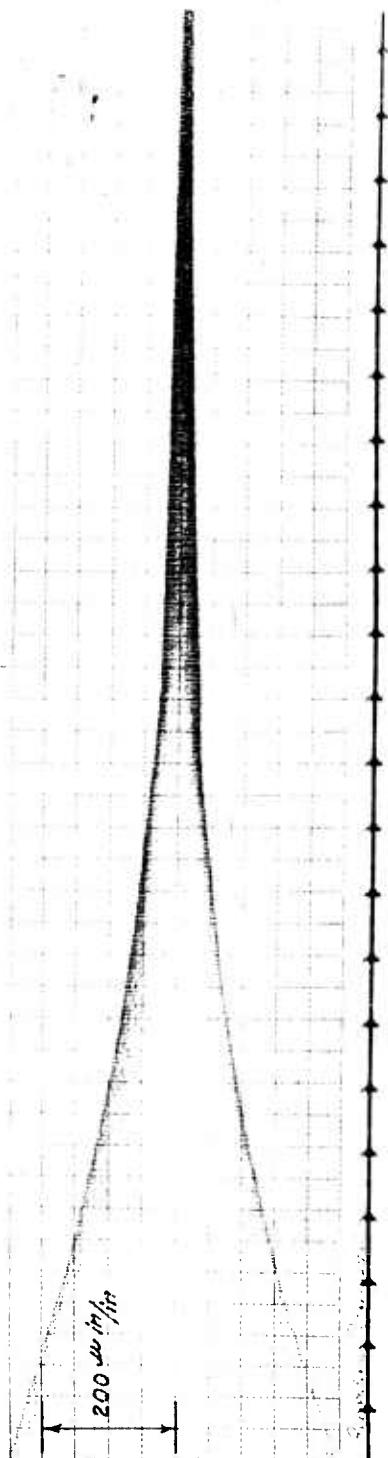


Figure C-1: Example Sanborn Oscillograph Record of Decay Curve for Member M4b1
 Paper speed 10 mm per sec.; Atten. x4; $\delta = 0.013$; $f_s = 20.0$ cps.

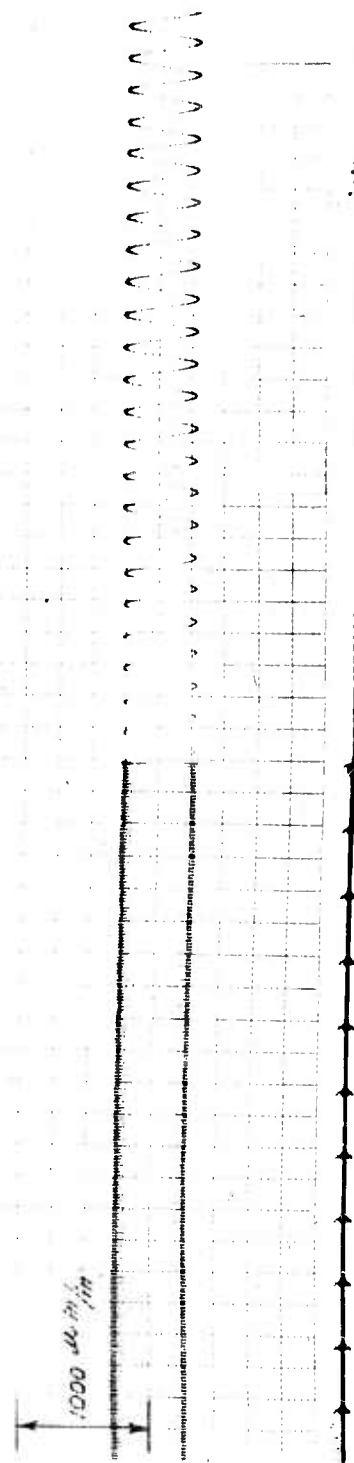


Figure C-2: Example Sanborn Oscillograph Record for M4b1 (Bare) Vibrating at Max. Amplitude
 Paper speeds 10 and 100 mm per sec.; Atten. x20; $\delta = 0.013$; $f_s = 20.0$ cps;
 $v_p = 13.21$ mph; $\epsilon_{62} = 300 \mu$ in/in; NDD = 0.134.

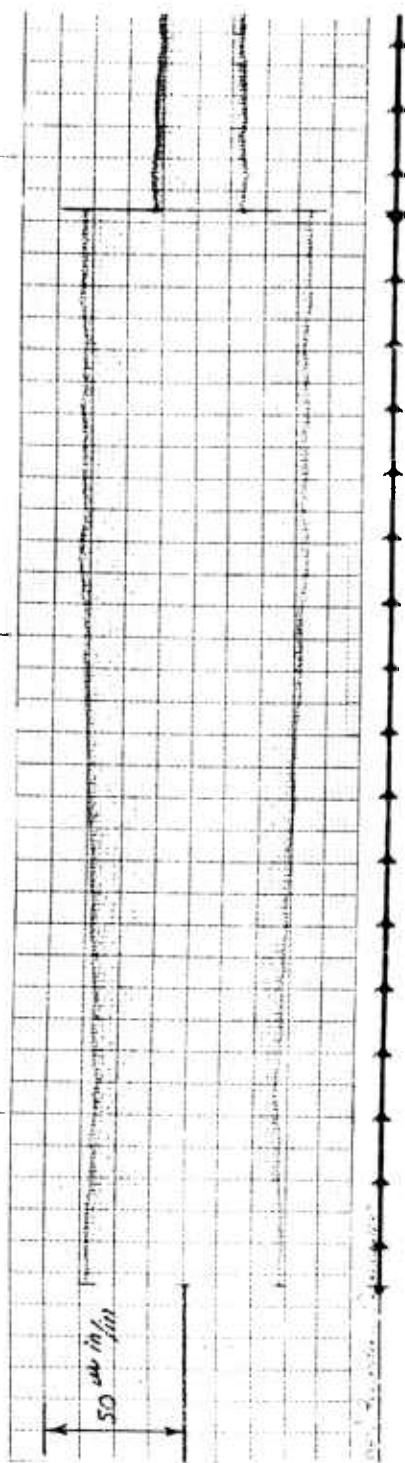


Figure C-3: Example Sanborn Oscillograph Record for Member M_{4b1} (with Spoilers 4-3/16"δ at 10d over 100% of its Length) Vibrating at Maximum Amplitude
 Paper speed 10 mm per sec.; Atten. x1; δ = 0.013; f₁ = 20.0 cps; NDD = 0.017

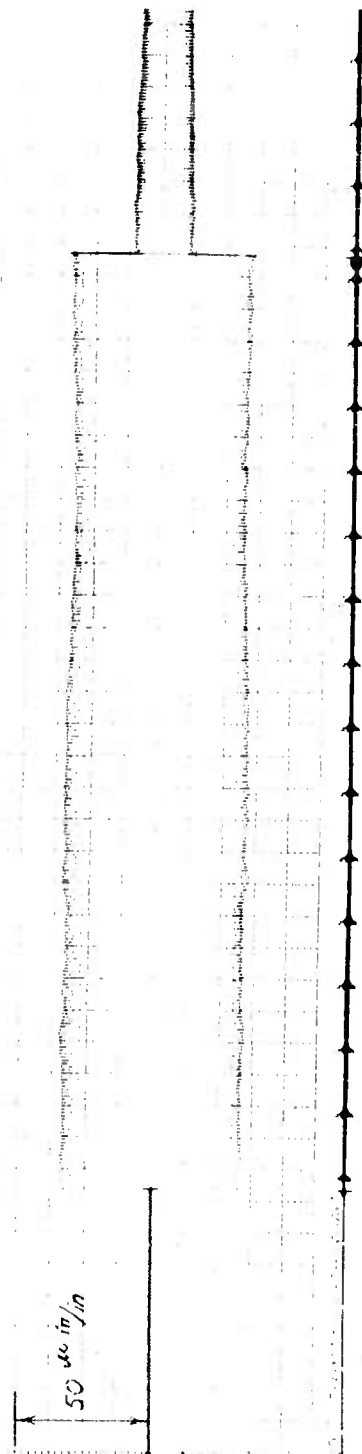


Figure C-4: Example Sanborn Oscillograph Record for Member M_{4b1} (with Spoilers 4-3/16"δ at 10d over 40% of its Length) Vibrating at Maximum Amplitude
 Paper speed 10 mm per sec.; Atten. x1; δ = 0.013; f₁ = 20.0 cps; NDD = 0.017

Fig. C-5: RESPONSE OF MEMBER M2C

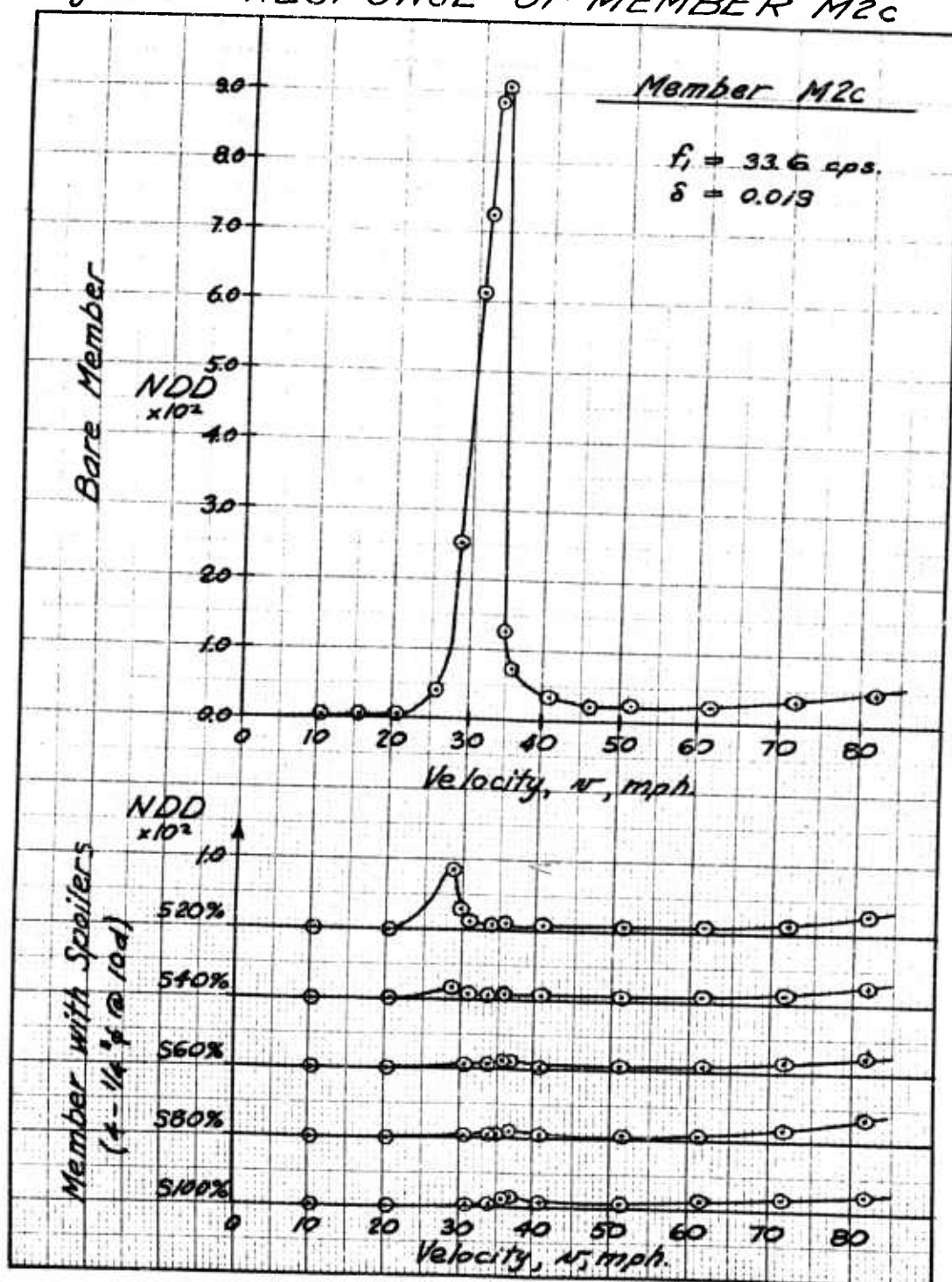


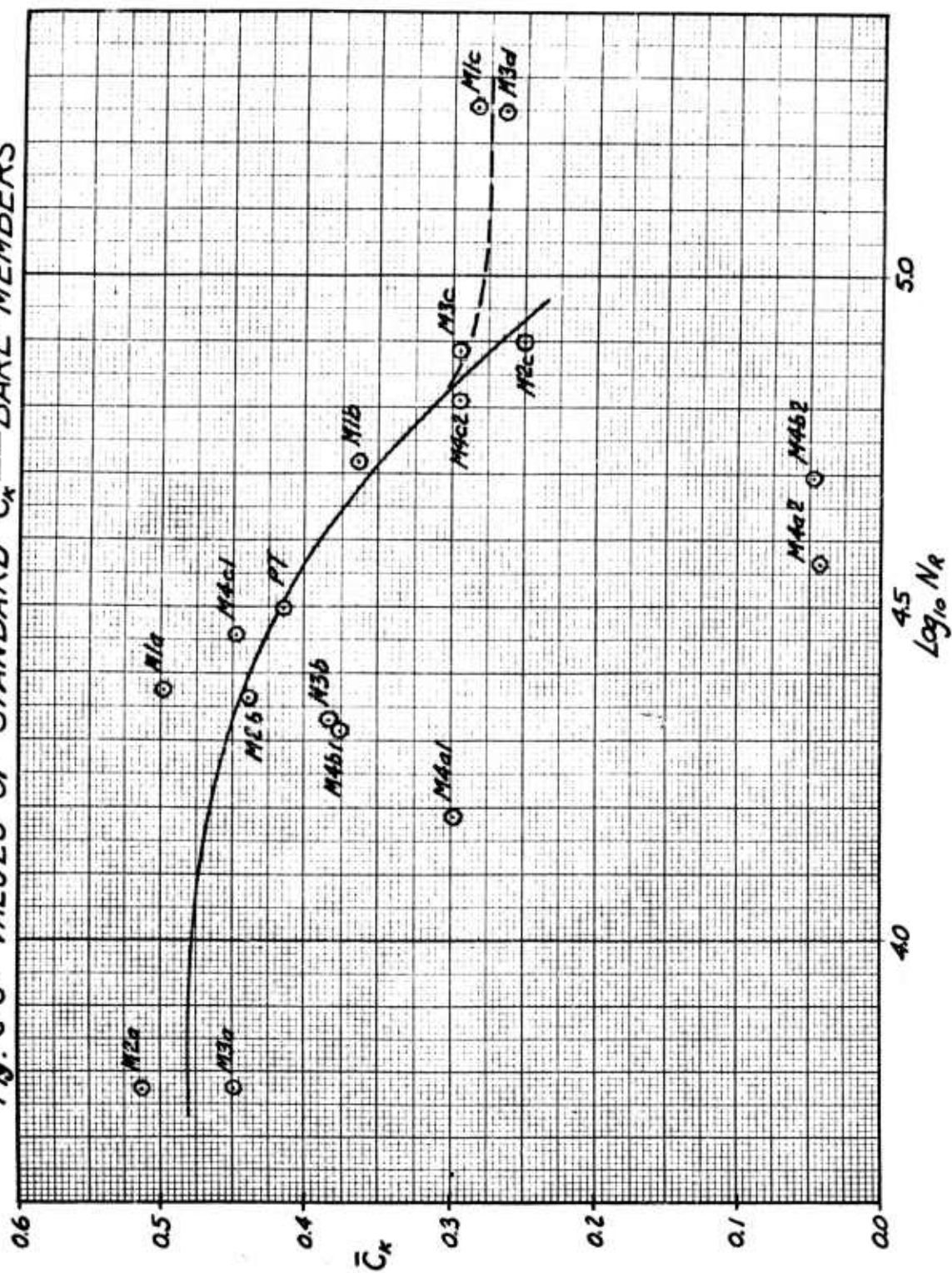
Fig. C-6: VALUES OF STANDARD \bar{C}_x — BARE MEMBERS

Fig. C-7: VALUES OF N_s FOR FIRST MODE - PHASE C

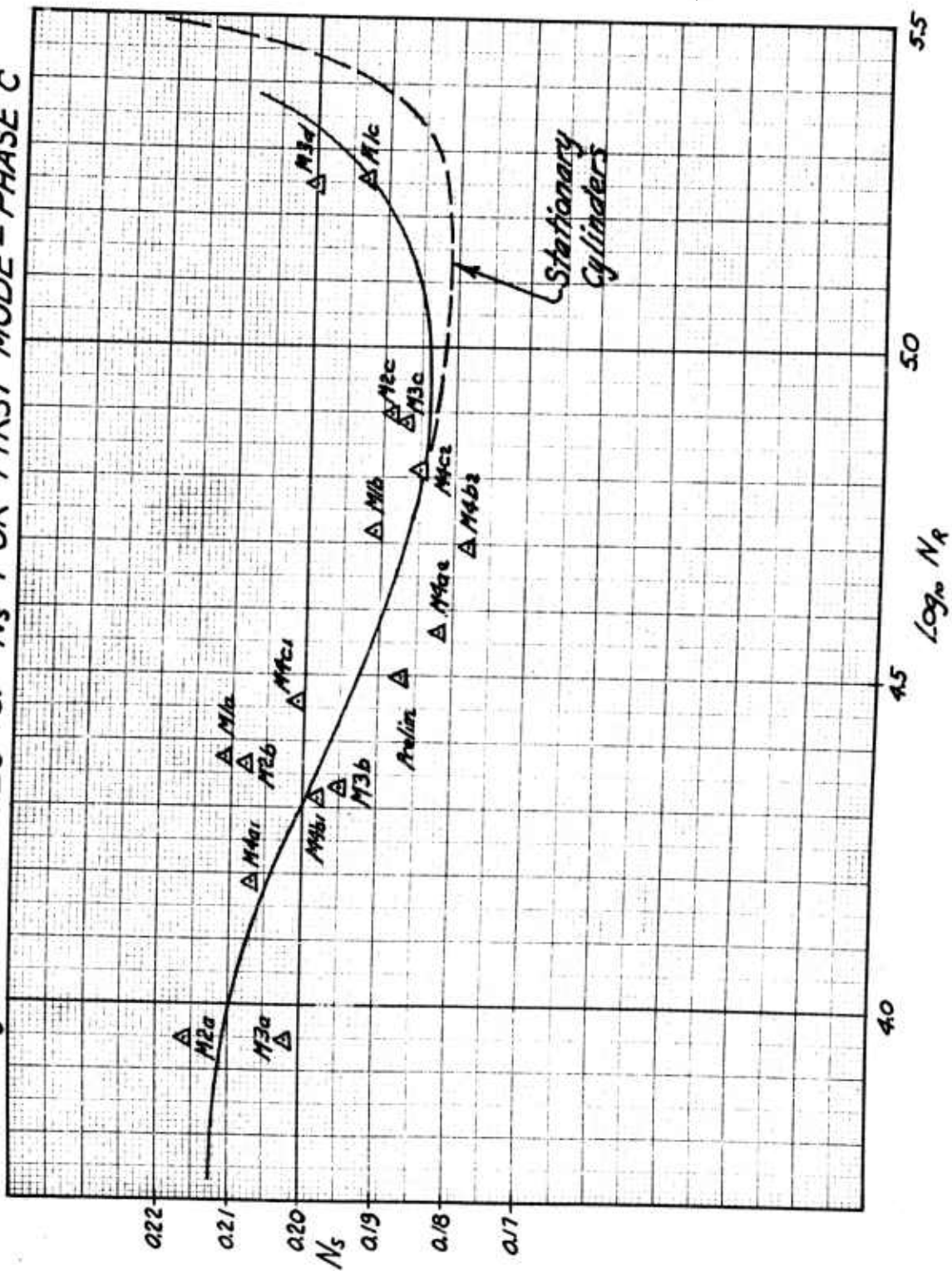


Fig. C-8: (ILF) FOR VIBRATING MEMBERS

